ISTANBUL TECHNICAL UNIVERSITY ★ GRADUATE SCHOOL OF SCIENCE ENGINEERING AND TECHNOLOGY

STRUCTURAL INVESTIGATION OF MASONRY STONE ARCH BRIDGES

M.Sc. THESIS

Ayşegül DEMİR

Department of Civil Engineering

Structural Engineering Programme

AUGUST 2016

ISTANBUL TECHNICAL UNIVERSITY ★ GRADUATE SCHOOL OF SCIENCE ENGINEERING AND TECHNOLOGY

STRUCTURAL INVESTIGATION OF MASONRY STONE ARCH BRIDGES

M.Sc. THESIS

Ayşegül DEMİR
(501131056)

Department of Civil Engineering

Structural Engineering Programme

Thesis Advisor: Assos.Prof. Dr. Kasım Armağan Korkmaz
Thesis Co-Advisor: Assist. Prof. Dr. Yaşar Hanifi GEDİK

AUGUST 2016

İSTANBUL TEKNİK ÜNİVERSİTESİ ★ FEN BİLİMLERİ ENSTİTÜSÜ

TARİHİ YIĞMA TAŞ KEMER KÖPRÜLERİN YAPISAL DAVRANIŞLARININ İNCELENMESİ

YÜKSEK LİSANS TEZİ

Ayşegül DEMİR
(501131056)

İnşaat Mühendisliği Anabilim Dalı

Yapı Mühendisliği Programı

Tez Danışmanı: Doç. Dr. Kasım Armağan KORKMAZ
Eş Danışman: Yard. Doç. Dr. Yaşar Hanifi GEDİK

AĞUSTOS 2016

Ayşegül Demir, a M.Sc. student of ITU Graduate School of Science Engineering and Technology student ID 501131056 successfully defended the thesis/dissertation entitled "STRUCTURAL INVESTIGATION OF MASONRY STONE ARCH BRIDGES", which she prepared after fulfilling the requirements specified in the associated legislations, before the jury whose signatures are below.

Thesis Advisor :	**Assoc. Prof. Dr. Kasım Armağan KORKMAZ** İstanbul Technical University	.....
Co-advisor :	**Asst. Prof. Dr. Yaşar Hanifi GEDİK** İstanbul Technical University	.....
Jury Members :	**Prof. Dr. Erdal Şafak** Boğaziçi University	.....
	Assoc. Prof. Dr. Abdurrahman Şahin Yıldız Technical University	.....
	Asst. Prof. Oğuz Güneş Istanbul Technical University	.....

Date of Submission : 02 May 2016
Date of Defense : 01 August 2016

To my family and my better half,

FOREWORD

I would like to express my gratitude to Assoc. Prof. Kasim Armağan KORKMAZ and Assist. Prof. Yasar Hanifi GEDİK for their supervision and advice during my master studies.

Thanks are also extended to Assist. Prof. Oğuz GUNES for his help, which made this study possible.

This study has been carried out with the financial help of the 114M305 project which is conducted associate of The Scientific and Technological Research Council of Turkey (TUBITAK) and General Directorate of Highways (KGM) for which the author expresses its gratitude.

A special thanks to my better half Muhammed Ataullah Dilsiz who shared with me all days and nights. He always supported me in the moments when there are the most difficult and snafu situations. I can not express how I feel gratitude towards him with words.

I would like to thank all of my friends who supported me in writing, and encourage me to go one-step further to make my goal real.

Finally, thanks to my family and my cousin Sinan Özkaya for providing me with limitless support and continuous encouragement throughout my study. I would not have sustained my life without my mother prayer for me. This thesis would not have carried out without them. Thank you so much.

August 2016 Ayşegül DEMİR

TABLE OF CONTENTS

Page

ABBREVIATIONS

DEM : Discrete Element Method
GPR : Ground Probing Radar
FE : Finite Element
FEM : Finite Element Method
KGM **:** General Directorate of Highways (Karayolları Genel Müdürlüğü)
PEER : Pasific Earthquake Engineering Research

SYMBOLS

u,v	**:** Displacement Vector Components (mm)
g	**:** Accelaration of Gravity
ρ	**:** Density
F	**:** Frequency, Hz
T	**:** Natural Period, Second
P	: Point Load
Mp	: Plastic Moment
x	: Position of P
ξ, η, ζ	: Isoparametric Coordinates
A(T)	: The Spectral Acceleration Coefficient,
A0	**:** Effective Ground Acceleration Coefficient
I	**:** Building importance factor
Sae (T)	**:** Elastic Spectral Acceleration
S(T)	**:** The Spectrum Coefficient
SXX	**:** Normal Stress in X direction
SYY	**:** Normal Stress in Y direction
SZZ	**:** Normal Stress in Z direction
SXY	**:** Shear Stress in XY direction
SYZ	**:** Shear Stress in YZ direction
SZX	**:** Shear Stress in ZX direction
$\mathbf{f_c}$	**:** Compression Strength
$\mathbf{f_t}$	**:** Tensile Strength

LIST OF TABLES

Page

LIST OF FIGURES

Page

STRUCTURAL INVESTIGATION OF MASONRY STONE ARCH BRIDGES

SUMMARY

Turkey, with its ancient civilization history, has an invaluable inventory of structural heritages inherited from the past eras. Existing structural reserves include historic mosques, bridges, churches, viaducts, palaces, traditional baths, schools and residential houses etc. Historical bridges have an important part within these heritages in Turkey, and the structural system type is mostly stone arch masonry.

Protection of historic masonry bridges and their transition to next generations are priority national and international goals. Historical masonry bridges, which are mostly located far from urban areas, typically do not undergo sufficient maintenance and repair. Recently, greater emphasis has been placed on maintaining the integrity of existing stone masonry bridges as important heritage structures. Numerous restoration projects have been undertaken by the General Directorate of Turkish Highways (KGM) to preserve and protect historic bridges.

There are many studies in literature about modeling and structural evaluation of stone arch bridges. Analysis and performance evaluation of historic stone arch bridges can be performed using simplified analytical approaches as well as numerical approaches using computer technology. In the latter, important aspects of modeling are the determination of the materials properties and selection of a suitable modeling approach that is sufficiently accurate yet computationally inexpensive. There are two ways to assess these type of bridges; (a) simple and rapid assessment method which use linear elastic and isotropic material model basis, (b) complex and detailed methods which use nonlinear models that take into account the behavior of the material.

In this study, four historic stone arch bridges Dicle (On Gozlu), Malabadi, Papaz and Sinanlı-Alpullu, which were constructed in different periods and have different geometric properties such as span, rise, and length, were selected for evaluation of structural behavior.

The followed approach included performing analyses using two different modeling approaches. 3D FE models of the bridges were created using FX+ DIANA software using two different mesh sizes for each bridge. Linear static analysis, modal analysis and response spectrum analysis were carried out for both models involving different mesh sizes. The Specification for Buildings to be Built in Seismic Zones (Turkish seismic code, 2007) was used to perform structural response spectrum analysis under various load combinations. The obtained results for both models with two mesh sizes, which are referred to as fine and coarse meshes, were compared and discussed for selected bridges. Considering computation time and obtained minor differences between results of fine and coarse meshes models, coarse mesh was used to perform complex and detailed nonlinear static and dynamic analyses.

Nonlinear static analyses of the studied bridges were performed using the incremental lateral force method for coarse mesh models. According to the first mode shape, which had the maximum mass participating ratio, gradually increased lateral force was applied to the bridges until capacity is reached. The obtained results, in the form of base shear force/weight (V/W) ratio corresponding to the drift ratio (d/h), were discussed in relation to the geometric characteristics. It was concluded that, span, rise and thickness of the arch is directly related with the ultimate drift capacity of the studied bridges.

In the nonlinear dynamic analyses, ten earthquake ground motion records for site class A were used in the analysis of the studied bridges. Maximum base shear corresponding to the maximum displacement under ten ground motion records were assessed for each selected bridge. The performance of the bridges was discussed according to the base shear force/weight (V/W) ratio corresponding to the drift (d/h) ratio. Duzce, 1999 (Turkey) earthquake motion with a peak ground acceleration in the selected 10 ground motion records, cause the maximum displacement for each bridge. It was observed that for Duzce, 1999 (Turkey) ground motion, the capacity of Sinanlı-Alpullu Bridge was exceeded. In the case of nonsymmetrical geometry, the pushover analysis results.

TARİHİ YIĞMA KEMERLİ KÖPRÜLERİN YAPISAL DAVRANIŞLARININ İNCELENMESİ

ÖZET

Tarihi yapılar, kültürel mirasımızın büyük bir çoğunluğunu oluşturmaktadır. Tarihi yapılar için mevcut yapı stoku tarihi camiler, köprüler, kiliseler, saraylar, tarihi hamamlar, okullar ve konutlardan oluşmaktadır. Tarihi köprüler ise bu eserler içerisinde önemli bir yere sahiptir ve bunların büyük bir çoğunluğu taş yığma kemerli köprüdür. Bu eserlerin bir kısmı günümüze kadar ulaşamamış olsa da önemli bir kısmı varlığını sürdürmektedir.

Oldukça zengin olan tarihi yığma köprü mirasımızın korunarak gelecek nesillere aktarılması ulusal ve uluslararası öncelikli hedefler arasındadır. Tarihi yığma köprüler çoğunlukla şehir merkezlerinden uzakta kalmış eserler oldukları için yeterli bakım ve onarım görememiştir. Son zamanlarda bu yapıların önemlerine dikkat çekilerek, çok sayıda restorasyon projesi Karayolları Genel Müdürlüğü tarafından yürütülmüştür.

Ülkemizdeki tarihi yığma köprülerin büyük bir bölümü taş kemer köprü olarak inşa edilmiştir ve ilgili literatürde, bunların yapısal olarak değerlendirmeleri amacıyla modellenmesi ve analizi ile ilgili yapılmış birçok çalışma mevcuttur. Tarihi taş köprülerin performans analizleri basitleştirilmiş analitik yöntemlerle yapılabileceği gibi, bilgisayar teknolojisi yardımı ile sayısal yöntemlerle de yapılabilir. Doğru sonuç alınabilen ve hesaplaması masraflı olmayan doğru model yaklaşımın seçilmesi ve malzeme özelliklerine karar verilmesi, modelleme aşamasının önemli adımlarıdır. Basit ve hızlı değerlendirme yöntemleri genellikle doğrusal elastik ve izotropik malzeme modelini esas alırken; karmaşık ve ayrıntılı yöntemler, malzemenin doğrusal olmayan elastik ötesi davranışını dikkate alan modeller kullanmaktadır.

Tarihi köprülerin yapısal analizi tarih boyunca geliştirilen birçok yöntem kullanılarak yapılmış ve değerlendirilmiştir. Geliştirilen sayısal yöntemlerden biri olan sonlu elemanlar yöntemi, tarihi yapıların yapısal analizinde oldukça yaygın bir şekilde kullanılmaktadır. Sonlu elemanlar sayısal yönteminde 3 farklı modelleme yaklaşımı mevcuttur. Bu yöntemler sırasıyla mikro modelleme, basitleştirilmiş mikro modelleme ve makro modellemedir.

Bu çalışmada, sonlu elemanlar yöntemi ile makro modelleme yaklaşımı kullanılarak Artuklu ve Osmanlı dönemlerine tarihlenen, açıklık, yükseklik ve uzunluk gibi farklı geometrik özelliklere sahip Dicle (On Gozlu) köprüsü, Malabadi köprüsü, Papaz köprüsü ve Sinanlı-Alpullu köprüsü modellenmiştir. Çalışmada farklı boyutlarda ağ örgüsü ile tasarlanmış köprü modellerinin sonuçlar üzerindeki etkisini anlamak, köprü geometrik özelliklerinin köprülerin kapasitesi üzerindeki etkisini anlamak, ve doğrusal olmayan analiz yöntemlerinden gerçekçi olan yaklaşımı belirlemek hedeflenmiştir. Bu

hedefler doğrultusunda da sonlu elemanlar yönteminin kullanımına imkan sunan FX+ DIANA programı kullanılmıştır.

Çalışma 3 aşamadan meydana gelmektedir. Birinci aşamada seçilen köprü modelleri FX+ DIANA programında sonlu elemanlar yöntemi ile her bir köprü için farklı ağ boyutlarına sahip iki model hazırlanmıştır. Yapının doğrusal analizinde, doğrusal statik, modal ve tepki spektrum analizleri yapılmıştır. Tepki spektrum analizi için Deprem Bölgelerinde Yapılacak Binalar Hakkında Yönetmelik esas alınarak deprem yükleri tanımlanmıştır. Farklı yük kombinasyonları altında iki farklı ağ örgüsüne sahip modellerin 4 köprü için de analizi gerçekleştirilmiştir.

Ağ boyutunu değiştirerek, azaltılan eleman sayısıyla işlem yaptığımızda elde edilen doğrusal sonuçlar ile fazla eleman sayısına sahip modeller için elde edilen sayısal sonuçlar tartışılmıştır. Bu karşılaştırma yapılırken lokal gerilme değerleri sonuçlardan çıkartılmıştır. Sonrasında elde edilen normal gerilme ve kayma gerilmesi değerleri arasındaki farklar karşılaştırılmış ve tartışılmıştır. Bu karşılaştırma sonucunda, kullanılan 2 farklı ağ modeli içerisinden zaman kaybını aza indirgeyerek aynı zamanda da analiz sonuçlarında da detaylı ağ modelinden farklı sonuç vermeyen kaba ağ boyutlu modelle, seçilen tarihi taş kemerli köprülerin doğrusal olmayan malzeme yaklaşımı ile statik ve dinamik analizleri yapılmıştır.

İkinci aşamada doğrusal olmayan statik analiz artımsal eşdeğer deprem yükü yöntemi ile kaba ağ boyutuna sahip model seçilen tüm köprüler için yapılmıştır. Kütle katılım oranı en fazla olan birinci titreşim mod şekline göre, köprülerin taşıma kapasitesi sınırları esas alınarak, seçilen köprülerin davranışları adım adım arttırılan eşdeğer deprem yüklerinin etkisi altında incelenmiştir. Elde edilen sonuçlar, taban kesme kuvveti/ağırlık (V/W) oranına karşılık gelen deplasman limitleri (d/h), köprü geometrik özelliklerine bakılarak karşılaştırılmıştır. Kemer açıklığı, yüksekliği ve kalınlığı gibi köprü geometrik özelliklerinin, seçilen köprüler üzerinde uygulanan doğrusal olmayan statik itme analizleri ile elde edilen köprü deplasman sınır değerleri ile doğru orantılı olduğu sonucuna varılmıştır.

Üçüncü aşamada ise, A sınıfına ait 10 ayrı mevcut deprem yer hareket kayıtları ile, seçilen köprülerin zaman tanım alanında doğrusal olmayan dinamik analizleri yapılmıştır. Her bir deprem kaydı için ayrı ayrı maksimum yer değiştirmeye karşılık maksimum taban kesme kuvveti elde edilmiştir. Aynı zamanda, seçilen köprülerin yükseklik ve ağırlıkları da dikkate alınarak, taban kesme kuvveti/ağırlık oranlarına karşılık gelen deplasman limitleri (d/h) tartışılmıştır.

Kullanılan 10 deprem kaydından en büyük yer ivmesine sahip Duzce depreminin, her köprü için de en fazla deplasmana sebep olduğu ortaya konulmuştur. Doğrusal olmayan analizde verilen çekme ve basınç dayanımları kullanılan 10 deprem verisi için de aşılmamış olup, yalnızca Sinanlı-Alpullu köprüsü için Düzce depremi analizinde 13.4 saniyede analiz durmuştur. Sinanlı- Alpullu köprüsünün düzce gibi bir deprem etkisi altında büyük hasar görerek yıkılabileceği sonucuna varılmıştır.

Doğrusal olmayan dinamik analizlerden elde edilen sonuçlar ile doğrusal olmayan statik analiz sonuçları karşılaştırıldığında, elde edilen grafiklerin birbiri ile tam olarak örtüşmediği sonucuna varılmıştır. Özellikle köprü geometrisindeki boylamsal ve enlemsel farklılıklar, simetrik olmama durumu söz konusu ise, doğrusal olmayan statik analiz sonuçları zaman tanım alanında dinamik analiz sonuçlarından uzaklaşılmaktadır. Doğrusal olmayan statik analizde kullanılan mod şeklinin ve kütle katılım oranlarının yığma yapıların yapısal analizinden elde edilen sonuçlar üzerindeki etkisi azımsanmayacak kadar önemlidir. Geometrideki farklılıklar köprü mod

şekillerini etkilemiş ve doğrusal olmayan zaman tanım alanında analiz sonuçlarından uzaklaşılmıştır. Fakat, geometrisi daha simetrik ve doğrusal olmayan statik analizde ele alınan 1. Mod katılım oranı daha fazla olan Papaz Köprüsü için doğrusal olmayan her iki analiz sonuçları arasında bulunan farklılık oldukça azdır. Doğrusal olmayan statik analizlerde kullanılan mod sayıları arttırılarak, analizlerin farklı mod birleşimleri ile yapılması daha gerçekçi sonuçlar elde etmemizi sağlayacaktır.

1. INTRODUCTION

1.1 General Overview

Historic structures are important to understand the civilizations and their social and economic progress. Because of their vulnerability, all external conditions such as weather, earthquake, and vandalism can damage historic structures in part or as a whole. Recently, heritage structures are paid greater attention due to their historic significance. Protection, conservation and maintenance procedures are becoming essential to ensure that possible intervention actions are 'minimal, compatible, and reversible'. Analysis, strengthening and repair are very important steps for these structures. It is often a challenge for the practicing engineering to find the best approach to understand the structural behavior of historical structures in order to take precaution against existing or possible structural problems.

Assessment and evaluation of historic structures as a basis for proper remedial actions require consideration of certain important parameters. Especially during the structural assessment procedures, the material properties of the structures and existing damage conditions should be taken into account. Seismic zone and soil conditions are other important factors in structural analysis, which need to be considered to understand structural behavior of historic structures accurately. However, analyses of historical structures are complex due to the lack of knowledge about their materials and geometrical properties. There are different approaches to determine these parameters. Although, some of the in situ tests are an easy way to understand geometry and materials of structure, there are some rules and regulations related with the historical structures that restrict the destructive methods (International Council on Monuments and Sites, 1964). Therefore, these structures should be investigated without inflicting any damages.

Existing heritage structures in Turkey include historic mosques, bridges, churches, viaducts, palaces, traditional baths and many others where historical bridges constitute an important part due to their significance in transportation. The structural type of

historic bridges is mostly stone arch masonry (KGM, 2015). The Turkish Directorate of Highways (KGM) is responsible for renovation and restoration of historical bridges besides the inventory and localization of historical bridges. While registered bridges are 1376 by 2008, with new records, it is currently at around 1900 for 2015 records (KGM). KGM Historical Bridge Department has been renovating many bridges, but there are numerous bridges still waiting for renovation, repair, retrofit or restoration.

1.2 Objective and Scope

In this thesis, four different masonry stone arc bridges were selected for investigation. The main objectives of the study are:

- to investigate the influence of modelling approach on the analysis results,
- to investigate the significance of geometric properties on the load capacity of bridges,
- to ascertain a realistic approach for nonlinear analyses of stone masonry arch bridges.

With the obtained results, it is intended to find out main structural problems and deficiencies in masonry arch bridges.

1.3 Procedure

The studies were carried out in three steps. In the first step, Finite Element (FE) models of the studied bridges were built using coarse and fine meshes to understand their structural behavior and load capacity. Selected bridges were Dicle, Malabadi, Papaz and Sinanlı-Alpullu stone arch bridges which are located in Turkey, constructed in 11^{th}, 12^{th}, 16^{th} and 16^{th} centuries, respectively. Dicle and Malabadi Bridges constructed in Artuqids period were rehabilitated recently. Papaz and Sinanlı were built in the Ottoman period.

In the second step, in light of the results obtained in the first stage, the mesh typology was selected as coarse mesh. Nonlinear static analyses were carried out for the four bridges using coarse mesh models. Cracking patterns and displacements were determined to evaluate structural behavior. Selected bridges have different geometric

properties. Same nonlinear material model was used in the analyses of selected bridges to discuss the geometric properties effectiveness on obtained results.

Finally, in the nonlinear dynamic analysis, ten earthquake ground motion records for site class A were applied as ground motion to the studied bridges. Maximum base shear corresponding to the maximum displacement under ten ground motion records were assessed for each bridge. The performance of the bridges was discussed according to the base shear force/weight (V/W) ratio corresponding to the drift (d/h) ratio.

1.4 Organization of Thesis

Chapter 1 gives a general introduction about masonry stone arch bridges as well as the thesis objectives and aims. Chapter 2 summarizes thesis literature review, which relates with numerical and experimental assessment methods for the structural behavior of masonry bridges. Chapter 3 discusses the improvement of numerical analysis methods, and describes FE method by using DIANA software. In Chapter 4, selected bridges have been introduced with their geometric properties and material properties, and the FE models with fine and coarse meshes of selected bridges were given in this section. The predicted results from the FE are compared with each other in Chapter 5. In the last chapter, all findings are discussed and the suggestions for the further research are given.

2. LITERATURE REVIEW

Masonry stone arches have been used to build different kind of structures such as churches, mosques for centuries. Historical bridges also were built with masonry stone arches. Possible structural problems and deficiencies on the historical bridges can be investigated to protect them for next generations. There are many methods such as numerical and analytical. In this part, to understand the masonry arch structures and their assessment methods properly, some research was deeply investigated.

Kishi et al. (2016) found out a simple solution to understand dynamic behavior of multi span masonry arch bridges. They assessed two types of bridges; one of them was single span arch bridge and the other one was multi span arch bridge. Single span bridge was modelled by using FE with auto mesh tool, while multi span arch bridge was analyzed with frame structure model. The comparison between the results obtained from models showed the applicability of the auto mesh, which is easy way to assess dynamic response of the bridge. Distribution was mainly localized in piers that led to collapse in an earthquake. According to this research, piers were the most critical regions with regard yielding distribution considering the results of both single and multi-span arch bridges.

Jun et al. (2015) worked on a single span stone arch bridge, which was scaled in 1:10. The bridge model was tested to determine ultimate load bearing capacity and maximum displacement of the bridge, until reach up to the collapse mechanism. This research also tracked the development of the crack patterns during the loading process. The bridge was also assessed under Heyman theoretical approach (thrust line method) to figure out the similarity between theoretic and experimental assessment methods. The results of both methods showed agreement with each other.

Bergamo et al. (2015) performed destructive and non-destructive in situ tests on masonry arch bridge. The research aimed to show advantages and disadvantages of in situ test. They carried out FE analysis with three different modeling approaches. As a result, they found; the georadar analysis which is a non-destructive method used to model arch bridge was useful method to investigates bridge and vibrational test, flat

jack test and static penetration test were not only useful to investigate damage causes but also useful to calibrate the FE.

Srinivas et al. (2014) conducted experiments on an arch bridge to evaluate the performance of the bridge under incremental axle loads; meanwhile the numerical model was created in ANYSIS software. It was clearly seen that, the results of numerical FE model, which was validated with the static test results obtained experiments, were in good agreement with the results of the experiment. Also, this research provided an approach to measure strains in the piers.

Raj et al. (2014) studied the structural behavior of masonry arch bridge by using ATENA software in order to understand structural behavior and predict the failure of a brick masonry arch under different kind of loads. As a result, stress distribution under these loads and ultimate load bearing capacity of the bridge were evaluated.

Nagarajan et al. (2014) carried out experiments to investigate the material properties of brick masonry with different mortar ratio. These experiments helped to get knowledge about differences between individual and composite behavior of brick masonry. This research gave recommendation abut Young's modulus, Stress-strain values and the flexural strength of bridge for brick masonry.

Nobile and Bartolomeo (2014) evaluated selected analytical methods: i) Thrust Line Analysis Method; ii) Mechanism Method; iii) FE Method. According to the paper, FE Method can assess the structure from different way sophisticatedly. This study explains these assessment methods in detail by discussing their positive and negative sides.

Xul et al. (2013) worked on a collapsed stone arch bridge by simulating 3D FE model and performing a nonlinear analysis on the bridge. They figured out the potential starting point of the collapse mechanism. This research described the importance of different components of the stone arch bridge. Then, the most critical regions of the bridge obtained from existing collapsed bridge were identified. The results of the simulated progressive-collapse process were compatible with the behavior of the existing collapsed bridge.

Costa et al. (2013) conducted research on both dynamic tests and numerical assessment with FE method. After, the results of dynamic tests were discussed to identify modal parameters of the bridge. Comparison between numerical and experimental

frequencies and mode shapes helped to modify the FE changing parameters such as material properties and boundary conditions.

Behnamfar and Afshari (2013) discussed the efficiency of FE Method and Discrete Element Model (DEM) in linear and nonlinear material. Both approaches made good prediction about the behavior of the bridge in linear region. However, DEM results showed similarities with experimental findings in nonlinear region. They discussed the efficiency of mesh set optimization.

Korkmaz et al. (2013) analyzed Timisvat Bridge with FEM by using SAP2000 software. Ten different earthquake acceleration records were used for time history analysis. Seismic record and SAP2000 results were in a good agreement. The highest earthquake acceleration record gave the highest results.

Scheibmeir (2012) studied on the influence of different constitutive material laws and non-elastic parameters of masonry on the seismic performance level which was carried out with DIANA FE software. Nonlinear static analysis (pushover) and nonlinear dynamic analysis were conducted to acquire the aim of study. Nonlinear dynamic analysis was applied to decide performance point of the bridge.

Tecchio et al. (2012) discussed seismic retrofit of three historical masonry arch bridges. A seismic assessment was conducted with static analysis in non-linear by using 3D FEM on arch bridge. It was also applied some in situ tests to understand material properties of bridges. This research was concluded with suggestion of appropriate decision for intervention techniques which was implemented according to rise of the load bearing capacity.

The numerical analysis for Viaduc de Saint Ouen was performed by using a continuous FEM in the ANSYS software by Stablon et al. (2011). Numerical damage model was created and applied in FE Method. Core samples were also taken from bridges to get material properties. It was indicated that the first crack occurs under the loading point. As a result, this research assessed the failure behavior of the bridge considering the realistic damage pattern.

Lubowiecka et al., (2011) studied a general method to assess masonry structures with a complex geometry and unknown material properties. It was brought some nondestructive methods together such as digital close range photogrammetry, ground-probing radar (GPR) and FE Method to analyze a Carnedela masonry bridge. Taken

information from photogrammetry and radar was used as a source of 3D model. After, it was used for structural analysis process in FE Method. According to the findings, digital close range photogrammetry is useful to document the historic bridge; GPR test is useful to understand inner material properties of bridge. If these two methods come together, the structural analysis with FEM gets easy.

Cai (2011) studied the structural behavior of masonry arch bridges by using firstly Limit analysis to stimulate the bridge using RING 1.5 then FE model with DIANA software taking account nonlinear behavior of masonry and infill. In addition, experiment was conducted on masonry arch bridge in laboratory to get results of material properties. In analysis procedure, plane stress model and 3D model were analyzed to understand the effect of the infill material. These analyses were also compared with experiment results. Moreover, in plane stress model, it was used steel brace elements, and assessed the effect of the ultimate load bearing capacity. As a result, three dimensional model has more stiffness comparing to the plane stress model. However, 3D model is more complex to prepare and analyze.

Sayin et al. (2011) carried out linear and non-linear dynamic analyses on Uzunok Bridge by using macro model approach. Bridge was modelled as a 3D model with the FEM, and displacements in linear and nonlinear analyses were compared. By means of the results of this research, the characteristic of earthquake ground motion affects vibrational motion, which has significance on damage distribution on bridges.

Holmstrom (2010) discussed the different methods to calculate load bearing capacity. RINGx2.0 and Archie-M commercial programs were chosen for parametric study which was performed to identify material parameters for both long span and short span bridges. It was concluded: the fill height was the most effective parameter on the load capacity; the angle of friction for the backfill material played a significant role in RING2.0 for the short span bridge and Archie-M gives a lower load capacity than RING2.0 for the tested cases.

Sevim et al. (2010) conducted dynamic in situ tests and linear FE analysis on Mikron arch bridge. Comparison of the results of dynamic and numerical analyses was used to adjust FEM changing boundary conditions. This adjustment was done to coincide the analytical predictions with ambient vibration test results. The calibrated linear FE

model extended non-linear model. Results of calibrated FE model and nonlinear analysis matched reasonably with results of the experiment.

Bayraktar et al. (2010) performed numerical analysis by using FEM in the ANSYS software and also carried out ambient vibration test on Ottoman masonry arch bridge. It was aimed to minimize the differences between FEM and test results changing boundary conditions. As a result, the mode shapes of the bridge in both analyses were same, but there were little differences in frequency of modes. Changing of the boundary conditions led to decrease of differences from 18% to 7%.

Cappini et al. (2010) studied on multi span stone masonry bridge experimentally and numerically. In situ tests were carried out to analyze static and dynamic behavior of bridge. In addition, "Gilbert" and FEM approaches were used as a numeric assessment method. The material properties were obtained from experimental flat-jack test to use in numeric analyses. According to the experimental investigations and numerical analysis, this research suggested intervention methods for the bridge of Ribellasca.

Lourenco et al. (2010) assessed the static and dynamic performance of stone masonry arches in three different ways: experiment on single span prototype bridge, advanced non-linear analysis by using DIANA and simplified methods by using RING software. As a result of the experiment, the deformation and force graph was obtained. The influence of joint interface properties was addressed. It was concluded that the joint stiffness parameters affect the results of the numerical analysis. Therefore, the calibration of the numeric model was done by using results of experiment of the arch with dry joint and mortar joint.

Dulinska (2010) conducted FE models for two different bridges. The models have all part of structure such as spandrels, arch, fill and soil. Experiments were conducted on bridges not only to determine natural frequencies of the bridge but also to determine the damping. Consequently, the frequencies obtained from FEM were in a good agreement with frequencies obtained from experiment. The obtained value for damping was good agreement with literature.

Invernizzi et al. (2010) interpreted numerically the damage evolution by using nonlinear FE analysis with the help of DIANA commercial software. The important part of this research was that the definition of interface parameter at the pier for evaluation of the actual contact area. Scaled masonry bridge model was built in

laboratory for the experimental analysis of the pier abrasion. The structural behavior of the bridge was recorded under different settlement. Consequently, experimental and numerical crack patterns were compared with each other.

The main purpose of Bjurstrom and Lasell (2009) was to investigate the load carrying capacity considering the backfill of bridge. This research aimed to find the answer of question that is if heavier vehicles can be allowed. The results of the analysis of 2D model created in ABAQUS was compared the RING 2.0 software. It was seen that the RIN2.0 commercial software gives four times higher ultimate load capacity than ABAQUS. According to the study, the obtained load bearing capacity form RING 2.0 software was not realistic.

Pela et al. (2009) selected two particular case studies to apply pushover analysis and structural response spectrum approaches. Pushover curves were obtained for different compressive and tensile strength values. According to the selected compressive and tensile strength values, the performance points were decided for all defined spectrum in Italian Code. Besides, the research discussed the selection of control node for pushover analysis.

Bayraktar et al. (2009) performed analytical model of Komurhan Highway Bridge by using SAP2000 software. Dynamic characteristics were obtained by vibration tests, as well. Analytical and experimental dynamic characteristic were compared with each other and FE model of the bridge was updated by means of this comparison by changing some unknown parameters such as material properties and boundary conditions. This verification provided that changes parameters and boundary conditions can be effective way to reflect real behavior of masonry bridges.

Kiyono et al. (2008) studied to forecast the dynamic behavior of a masonry structure by using the DEM, and discussed the micro-modeling of individual components such as bricks and mortars. In this paper, these components were modeled with simplified micro model approach. Six different model approaches were created and analyzed by using DEM. The seismic behavior was discussed. According to the findings, the bridges with the backfill material have more resistance than the bridges without backfill material against seismic loads.

Rafiee et al. (2008) assessed the influences of the input parameters on the mechanical and dynamic behavior of the arch structure by using non smooth contact dynamic

computational method for masonry structure simulations. When they compared the effects of cohesive and non-cohesive contact on collapse mechanism of bridge, they found that arches with cohesive foundations can better resist intensive dynamic excitation.

Gencturk et al. (2007) assessed Titus Tunnel Bridge, Antalya, Turkey by using both thrust line method and virtual work method. This assessment was done by staying within preservation of historical structures laws. It was estimated the capacity of the stone arches. According to this research, virtual work method, which is one of the effortless way inside the analyses methods, gives accurate results when it applies cases with concentrated loading on the key stone.

Leon, and Espejo (2007) operated in situ test on an existing bridge and carried out ultimate strength calculation by using RING 1.5 software. According to the comparison between in situ test and numerical analysis, load-bearing capacity of the bridge was nearly as same as with the theory. Nevertheless, the failure mode was different. As stated by León and Espejo, the backfill effected the results of load bearing capacity. In addition, the damage distribution was observed under the experiment.

Diaz et al. (2007) compared the results of linear and nonlinear FE analysis with the results of limit analysis to find out load bearing capacity of the single span arch. These methods were conducted on 2D plane-stress model and contact face at joints between voussoirs was considered. Consequently, the results of nonlinear analysis with contact interface were in good agreements with the limit analysis.

Aoki et al. (2007) studied the verification of the numerical modeling approaches by comparing the results of analytical analysis with experiment, which were not only applied to understand dynamic characteristic of the Rakanji stone arch bridge but also applied to determine material properties that were used in FE analysis. They changed some parameters on bridge model, updated it, so the results correspond the results of in situ test.

Bayraktar et al. (2007) modeled 3D FE model of the bridge by SAP2000 software and conducted modal analysis on bridge model. Operational Modal Analysis determined dynamic characteristics of the bridge experimentally. FE model of the bridge was updated to minimize the differences between theoretical and experimental results. As a result, this verification showed that results nearly as same as the experiment. After

the verification, before and after models were analyzed under Erzincan earthquake. The compressive and tensile stresses, which was found by verified model with experiment, were lower than the first created model.

Ural (2005) studied on FE of Cosandere bridge, Trabzon, Turkey by SAP2000 software. It was found that the bridge could support its own weight in safe. Then, the bridge was exposed to a ground motion record to understand dynamic behavior of the bridge. The vertical stress distribution under dead load and seismic record was discussed. They suggest detailed model for the level of key stone. In addition, the research recommended that these analyses should be conducted with nonlinear material.

Boothby et al. (2005) proved that the application of 3D nonlinear FE model accurately simulates the experimental test of masonry arch bridge. In addition, while testing or modeling the bridge, the boundary conditions was very effective on the obtained results from the FEM. According to the findings, 3D nonlinear FE analysis is very useful method to assess the bridges. With the help of the nonlinear FE analysis, the ultimate load bearing capacity and crack patterns can be observed.

Toker and Unay (2004) studied mathematical modeling approaches for a prototype of arches. They observed changes on the stability of structure by defining cracks on masonry arch and discussed the importance of the modeling typology by using FEM. As claimed by Toker and Unay, nonlinear analysis approach may increase the risk of any possible mistakes in the analyses of huge structures with complex geometries. It was concluded that, the linear structural analysis should be done to understand critical regions of the bridges and the complex models should be created.

Mabon (2002) summarized a strengthening method named Archtec and analyzed a bridge by DEM before and after strengthening. The efficiency of the Archtec method was shown. Both accuracy of the assessment technique and the efficiency of the strengthening method were verified against full-scale tests.

Fanning et al. (2001) showed the importance of spandrel walls and fill to reflect the transverse effect. Because, these components of the bridge contribute to the strength and stiffness of the bridge. It was stated that neglecting 3D nature of masonry affects the ultimate load bearing capacity. Service load test and ultimate strength test were applied on bridge. In addition, according to the service load testing, the development

of cracking and nonlinearity of materials led to understand the capacity of structure. Besides, the restraint of the abutments has an important effect on the stability of structure.

Frunzio et al. (2001) showed the results of a 3D FE Method analysis by using Anysys software for a stone masonry arch bridge. The analysis was performed considering nonlinear material behavior. It was noted that the findings of the analysis could be used for restoration in future.

Fanning and Boothby (2001) modeled two historical bridges under truck load with the help of computer software Anysys and then compared with the in situ test results. It displayed that the results were compatible with the experimental test results. 3D non-linear FE analysis enabled to make a good prediction about actual behavior of the masonry arch bridge.

Karaveziroglou et al. (2001) discussed two numerical procedures for analysis of old stone arch bridges in Greece. Numerical method was ran space frame approach with FE model. The second one was based on the inequality numerical approach. They compared four bridges. According to the results, both analysis approaches can be used to understand the structural behavior of the historical stone bridges. Second approach was more time consuming than the first approach.

Alfaiate and Gallardo (2001) took the results of experiment on full scale a single span arch bridge as reference to compare the results of a FE model. The model of the masonry arch created with interface elements with zero thickness. Four different simulations were undertaken to assess the importance of the different components on the collapse load. The numerical results were compared with the data acquired from the experimental test.

Hatzigeorgiou et al. (1999) assessed the historical masonry structures by using FEM under static or dynamic loadings. The material behavior was assessed both linear elastic and inelastic. They reached a conclusion that the inelastic material modeling was essential to obtain realistic response of bridge.

NG (1999) reviewed the current assessment methods and examined their deficiencies. Then, it was developed a 2D FE model for structural analysis. A series of parametric studies were performed to examine the influence of the arch material properties,

geometric properties of the model and the load position on the ultimate load bearing capacity.

3. METHODOLOGY

3.1 History of Assessment Method of Masonry Arch Bridges

The science of arches developed slowly. Firstly, the Romans believed that semicircular arches can only carry vertical loads. However, infill materials in arches can carry the neglected horizontal forces (Harvey, 1986). Hooke was the first scientist who carried out scientific studies on arches (NG, 1999). Thrust line and the mechanism methods, which are analytical methods, have been developed after this Hooke's studies. Heyman, (1995) states that Hooke had concerned himself with "the true mathematical and mechanical form of all manner of arches for building". Then, Hooke published an anagram which gives the statement: "As hangs the flexible line, so but inverted will stand the rigid arch" in 1675 (Heyman, 1996).

Hooke used two types of model to show how arches work. Cables can support the same load in the same positions. If the cable is pulled, it will turn back to its starting point. This is named as stable. Unlike the cable, the structure of the jointed rods is unstable. Once displaced, the pinned rods will collapse. The line of the chain or cable in Hooke's models show the thrust line (Figure 3.1) (Harvey, 1986).

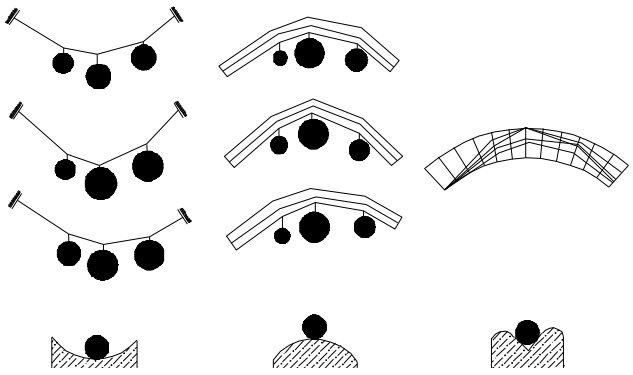

Figure 3.1 : Hooke's line of thrust models (Harvey, 1986).

After Hooke's law, in 1770, Couplet found that arches collapse by cutting in four pieces (Figure 3.2) (Heyman, 1982). It paved the way understanding of arch bridges failure mechanism. In 1733, Coulomb developed Couplet's method further (Heyman,

1982). From his study, it was concluded that, it is only necessary to find one line of thrust. This line of thrust stayed in the arch boundaries that fulfill the equilibrium conditions to be sure the stability of arch under the given loading conditions (Heyman, 1982).

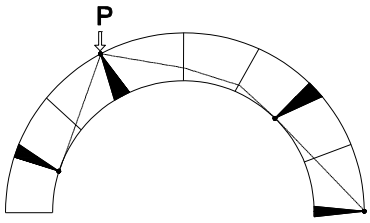

Figure 3.2 : Couplet four hinged model (Heyman, 1982).

Pippard demonstrated that the collapse of arch bridges was due to formation of hinges as the result of cracking. This assumption led to the development of no-tension criterion; however, Pippard did not take account the contribution of the infill between spandrel walls to lateral resistance of arch bridge (Yan, 1991).

Heyman (1982) reviewed many of the old theories and developed a mechanism analysis procedure using the plastic hinge method. According to the Heyman (1982) analysis, it was assumed that, if the line of thrust touches the intrados or extrados, the plactic hinge occurs. In addition, if four hinges are formed on the arch, the collapse mechanism is assumed to occur. The failure mechanism of the arches does not occur when the first crack is formed. Based on these assumptions, Heyman (1982) developed a simplified approach for the collapse of an arch. The value of the plastic moment at the hinges is obtained as follows;

$$Mp = \frac{PL}{4}\frac{(1-X)(1+X)^2}{(3-X)^2} \tag{3.1}$$

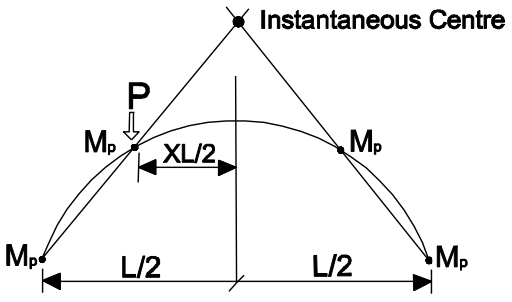

Figure 3.3 : Plastic moment in an arch (Heyman, 1982).

3.2 Finite Element Modeling for Masonry Arch Bridges

FEM is an alternative assessment method commonly used to understand structural behavior of the masonry arch bridges. This approach is very different from the others. Most recently, the FE analysis is a widely used technique to assess masonry structures nowadays and various studies have been conducted to evolve FE models as mentioned in literature review. Due to the characteristic of masonry, which contains isotropic and anisotropic materials, has unquestionably made the analysis of its structural behavior more complex. Because of this complexity of masonry structures, researchers need to pay more attention to apply FEM (Nobile and Bartolomeo, 2014). Either two dimensional or three dimensional models can be used in FE analyses.

3.2.1 Numerical modelling of masonry arch bridges with FEM

The modelling of masonry in a FE method can be done in different ways, which range from modelling on a very detailed micro level to a composite macro level. The components of masonry are given in figure 3.4.

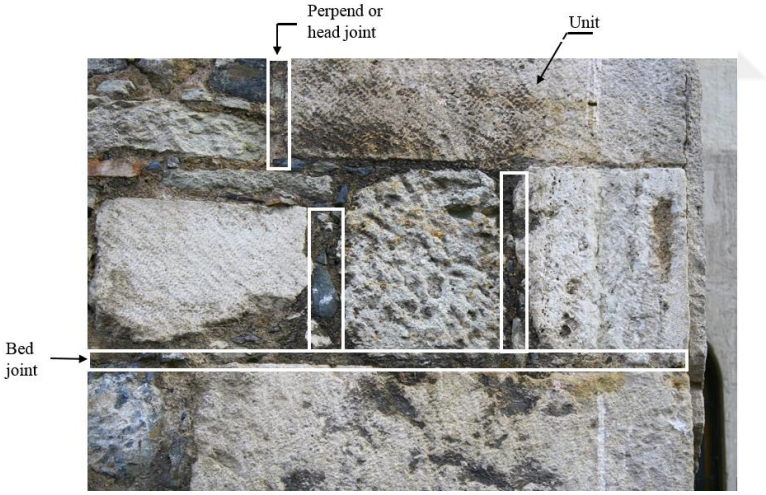

Figure 3.4 : Components of the masonry.

There are three main ways, which are detailed micro-model (Figure 3.5), simplified micro-model (Figure 3.6) and composite macro-model (Figure 3.7) (Lourenco, 1994) to model the masonry. For the first approach, detailed micro model, units and mortars in the joints are modeled with continuum elements separately and the unit/mortar interface between these two components is created by discontinuous elements. This enables to study deeply the combined behavior of unit, mortar and interface (Lourenco, 1994).

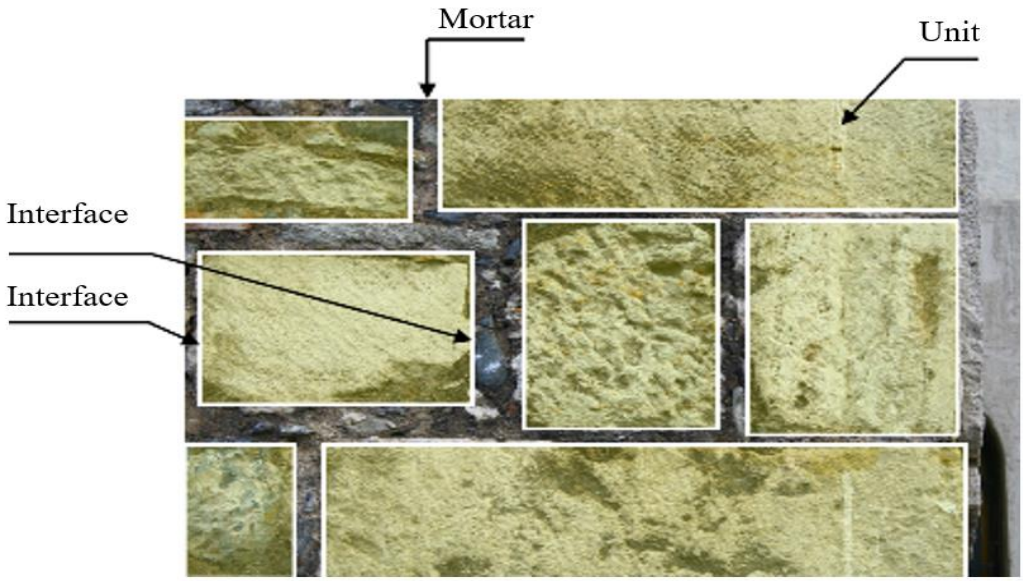

Figure 3.5 : Micro modelling approach (adapted from Lourenco, 1994).

The behavior of the mortar joints and unit-mortar interface are created by discontinuous elements with zero thickness and expended units are represented by continuum elements in simplified micro model (Lourenco, 1994).

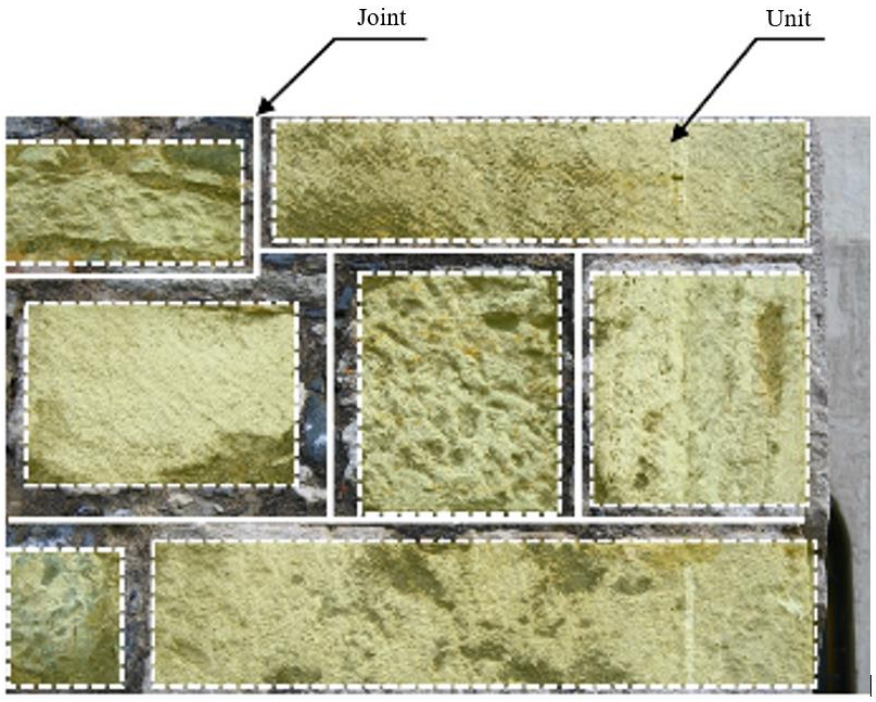

Figure 3.6 : Simplified micro modelling approach (adapted from Lourenco, 1994).

The third approach does not make any distinctions between units and joints. Macro modeling is more practical than the other two approaches (Lourenco, 1994).

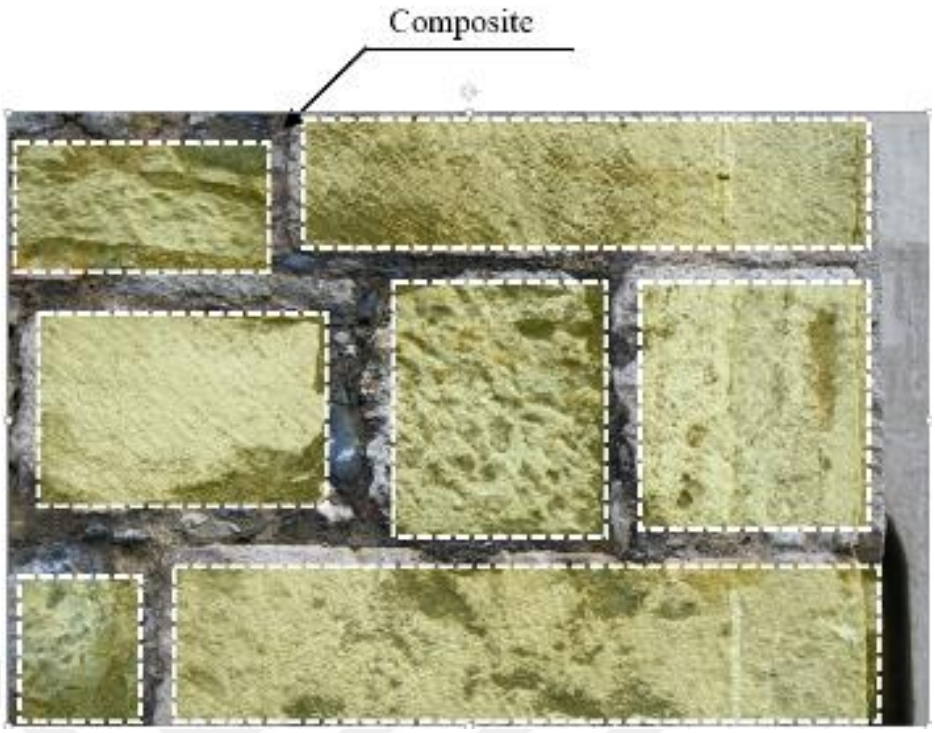

Figure 3.7 : Macro modelling approach (adapted from Lourenco, 1994).

For accurate micro or macro-modeling of masonry structures material properties should be identified with experimental work (Lourenco, 1994). Micro-modeling studies are necessary to give a better understanding about the local behavior of masonry structures.

3.3 FX+ DIANA- Finite Element Method

The FE Method provides good representations of complex structures. FE Method enables to mesh the structures into small sub domains and obtain deformation and stress values of the whole sub structures (TNO DIANA, 2014). FX+ for DIANA is a FE Method software, which uses displacement method. FX+ for DIANA does not only led to define FE model under perfect mesh quality by controlling all mesh set, but also controls the mesh sets to not cause any error at Mesh Editor tool. FX+ for DIANA has wide range material library and used widely by researchers. It allows for a variety analysis such as both linear and non-linear static and dynamic analyses (TNO DIANA, 2014)

The FE Method software FX+ for DIANA software and Mesh Editor tool have been used in this research work. The workflow of the programme is given in figure 3.8 with basic steps.

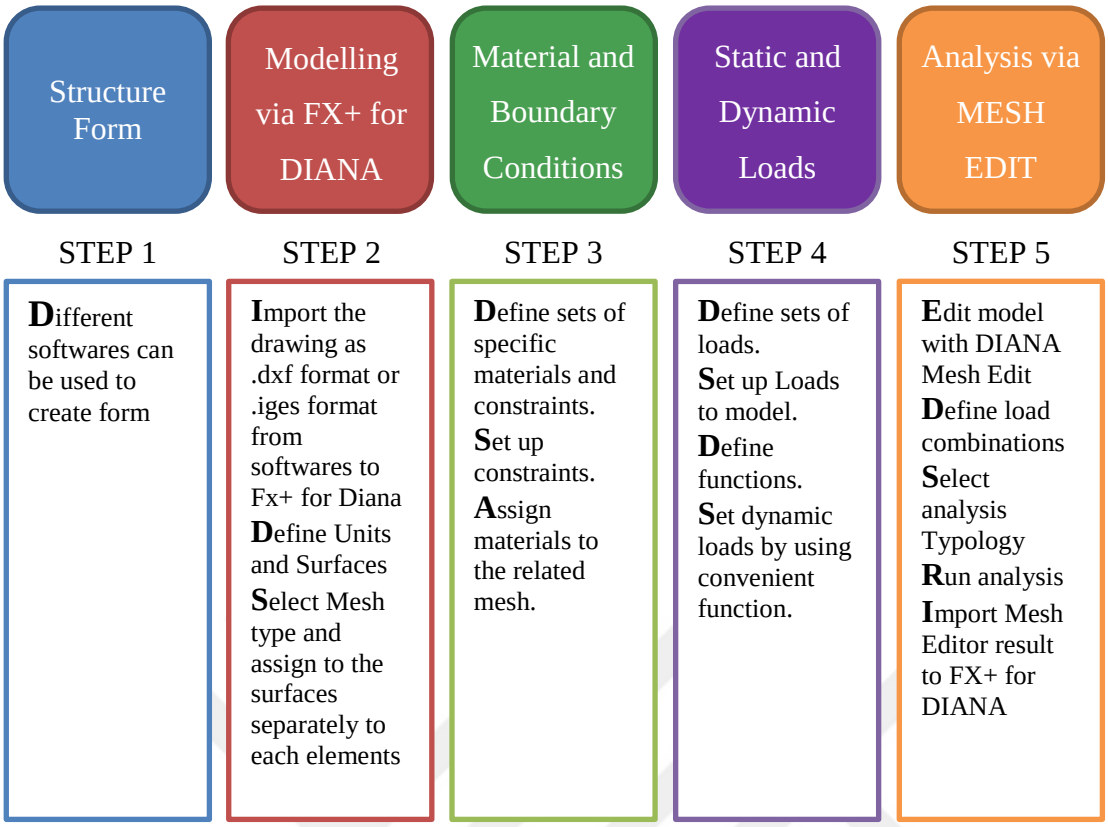

Figure 3.8 : Software usage steps.

In the modelling process, the solid model was divided into sub domains by using create mesh tool. There are two types of solid elements used in this research: first one is the TP18L element (Figure 3.9) that has a six-node isoparametric solid wedge element. Second one is the HX24L element (Figure 3.9) which has an eight-node isoparametric solid brick element used widely in 3D modelling (TNO DIANA, 2014).

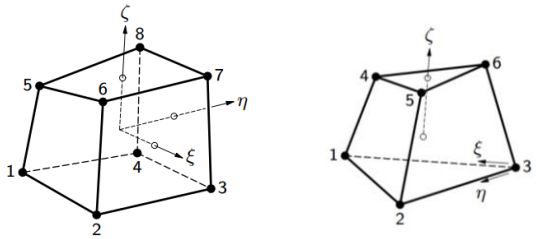

Figure 3.9 : HX24L and TP18L (TNO DIANA, 2014).

For solid elements, DIANA do not need special user input data to set up the element axes. By default, the element X, Y and Z axes are set up parallel to the global X, Y and Z axes, respectively (Figure 3.10) (TNO DIANA, 2014). DIANA software gives tension stress as positive, and compression stress is negative. Default directions of normal and shear stresses as well as displacements are shown in figure 3.11 (TNO

DIANA, 2014). The highest and lowest values for results are represented by blue and red colors respectively.

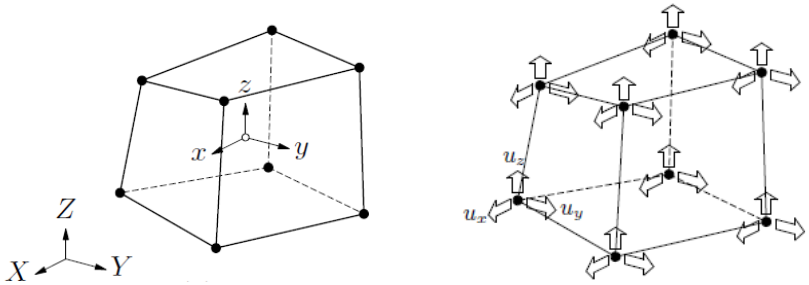

Figure 3.10 : Default element axes and displacements (TNO DIANA, 2014).

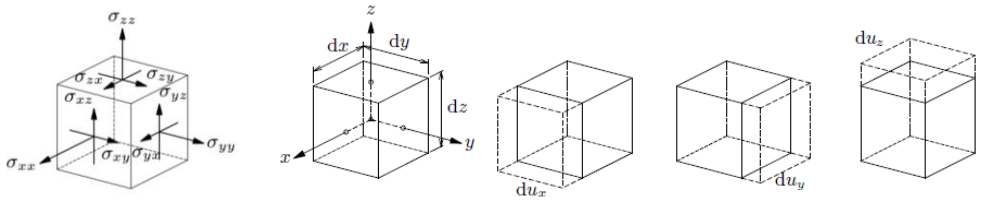

Figure 3.11 : Cauchy stresses and deformations (TNO DIANA, 2014).

4. STRUCTURAL INVESTIGATION OF SELECTED BRIDGES

4.1 General Information

3D modeling and analyses of historical Dicle, Malabadi, Papaz and Sinanlı-Alpullu Bridges were performed by using FX+ for DIANA software (TNO DIANA, 2014). The selected bridges have important value with their history which dates back to different selected periods. The bridges have same construction material which is mainly limestone (KGM, 2015). Geometric features and some details about bridges are given comparatively in table 4.1. Selected bridges have different geometric properties. Dicle and Malabadi bridges belong to same period. The bridges have different geometry. Papaz and Sinanlı-Alpullu bridges belong to same period also, and they have nearly same geometry.

Malabadi Bridge has the maximum span with 38.6m. Papaz Bridge has the minimum span with 6.7m, and it is the shortest bridge within selected bridges. Dicle Bridge is the longest bridge. Arch typologies of bridge are mostly pointed arch. Within selected bridges, Papaz Bridge has been damaged. Malabadi and Dicle Bridges have been rehabilitated recently.

4.2 Geometric Definition and 3D Modeling of the Bridges

4.2.1 Dicle (On Gozlu) Bridge

Dicle Bridge, located in Diyarbakır metropolitan, was built over the Dicle River in between years of 1065–1067 during Artuqids ruling period in Anatolia. The architect of the bridge is Sancaroglu Ubeydoglu Yusuf. The bridge which has 10 span and total length is 172m in plan as shown in figure 4.1 and figure 4.2, mainly consists of pointed arches, rectangular piers, spandrel walls and parapets (Figure 4.3). The width is ~11m from east side to 5^{th} span and then it decreases hereafter. The width varies in between 4m to 7m from 5^{th} span up to the west side as seen in figure 4.3 (KGM, 2015). The 3^{rd}, 4^{th} and 5^{th} arches exceed longer bay span where 3^{rd} one has the maximum span of 13.91m. The spans of 4^{th} and 5^{th} arches are 11.96m and 13.82m respectively.

Table 4.1 : Geometric properties of the selected bridges (KGM, 2015).

Bridge	Location	Construction Year	Total Length (Plan)	Number of Span	Arch Typology	Maximum Span	Thickness of Arch	Rise of largest span	Width	Restoration Background
Dicle	Diyarbakır	11th	172m	10	Pointed Arch	14m	0.40-0.70m	6.9m	11m -6m	2009
Malabadi	Diyarbakır	12th	150m	5	Pointed and Semi Circular Arch	38.6m	1.40-1.80m	22m	6.8m	2014
Papaz	İstanbul	16th	40m	3	Semi Circular	6.7m	0.45-0.55m	4.8m	4.4m	Unknown
Sinanlı-Alpullu	Kırklareli	16th	120m	9	Pointed Arch	20m	0.60m	7m	6.8m	1987

Spans of remaining arches vary in between 8.00m to 8.74m. The thickness of main load bearing arches range from 0.4m to 0.7m (Figure 4.1). Total height of the bridge is 10m. Flood splitters having pyramidal coned and triangular prism forms exist as attached to the bridge piers (Figures 4.3). Parapet walls exist through the sides of bridge deck level having height of 0.55m~0.85 m (Figure 4.4) (KGM, 2015). The plan dimensions of piers are 5m to 6m along with X direction and 11m along with Y direction (KGM, 2015)**.**

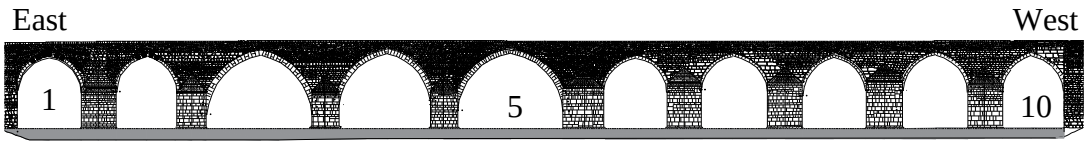

Figure 4.1 : Upstream view of Dicle (On Gozlu) Bridge (Scale: 1/1000) (KGM, 2015).

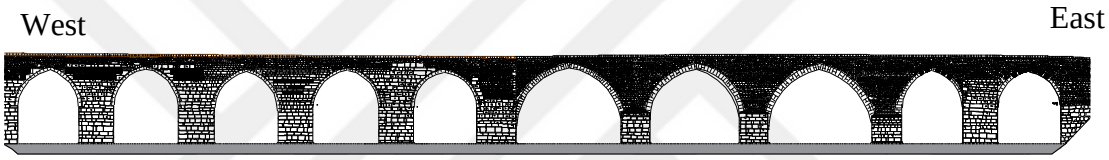

Figure 4.2 : Downstream view of Dicle (On Gozlu) Bridge (Scale: 1/1000) (KGM, 2015).

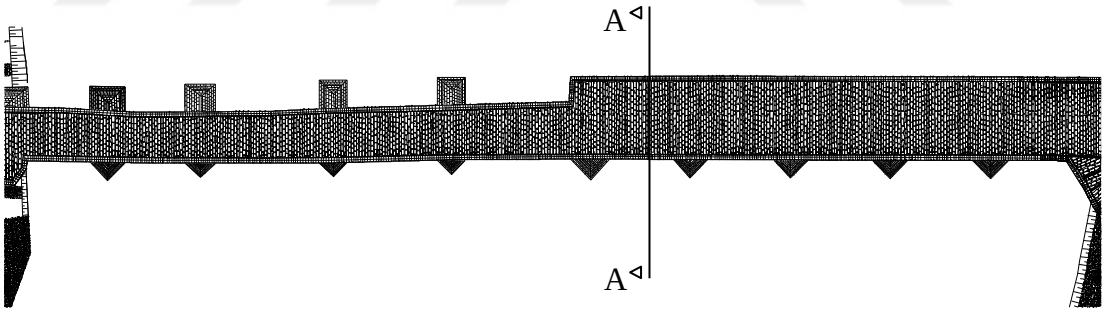

Figure 4.3 : Layout plan of Dicle (On Gozlu) Bridge (Scale: 1/1000) (KGM,2015).

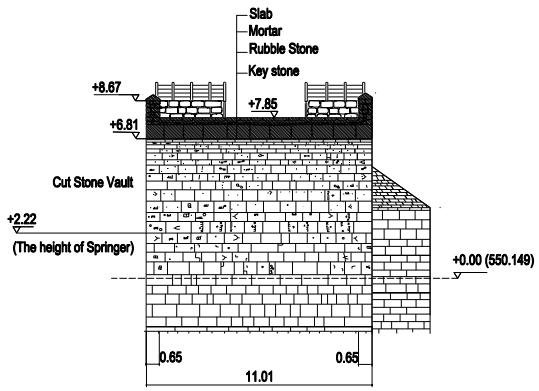

Figure 4.4 : Cross section (A-A) of the Dicle (On Gozlu) Bridge (KGM,2015).

In 2009, a restoration work was fulfilled by General Directorate of Highways and required interventions were applied to the bridge. With this restoration, the slab, which was paved with asphalt because of bringing into the road open to traffic, was altered to original stone of pavement, and the bridge was closed to traffic (KGM, 2015).

Figure 4.5 : Upstream and downstream views of the Dicle (On Gozlu) Bridge (URL 1, 2016).

Dicle Bridge has seven different structural elements which are arch, spandrel wall, infill, parapet, slab, flood splitter and pier. FE models of the bridge was modelled considering the whole structural elements. Each length of the element that used in the modelling process varies between 0,15m~0,5m for fine meshes. The dimensions of the elements are in between 0,6m~2m for the coarse meshes. The dimensions of fine mesh were approximately four times of the dimensions of coarse mesh. Details of both mesh sets are given in table 4.2. The 3D model view from upstream and downstream, section and the mesh quality of the model with fine and coarse meshes are given in figure 4.6 to figure 4.12.

Table 4.2 : Details of mesh sets used in 3D model of Dicle (On Gozlu) Bridge.

Type of Mesh	Total number of Solid element	Total Number of Element Face	Total Number of Node	Total Weight of Bridge (kN)	Total Volume (m^3)
Fine Mesh	338,017	246,657	377,286	248,596	13,018.1
Coarse Mesh	11,318	18,613	14,810	233,155	12,184.5

Figure 4.6 : 3D modeling of Dicle (On Gozlu) Bridge with fine mesh-upstream.

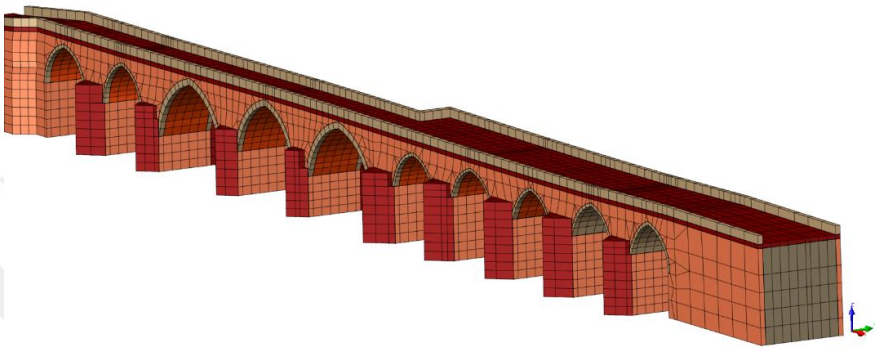

Figure 4.7 : 3D modeling of Dicle (On Gozlu) Bridge with coarse mesh-upstream.

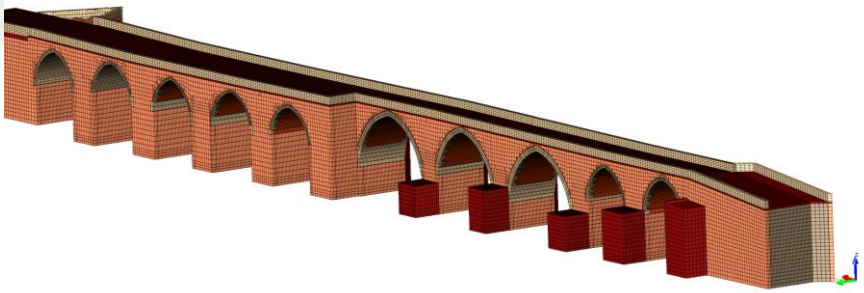

Figure 4.8 : 3D modeling of Dicle (On Gozlu) Bridge with fine mesh-downstream.

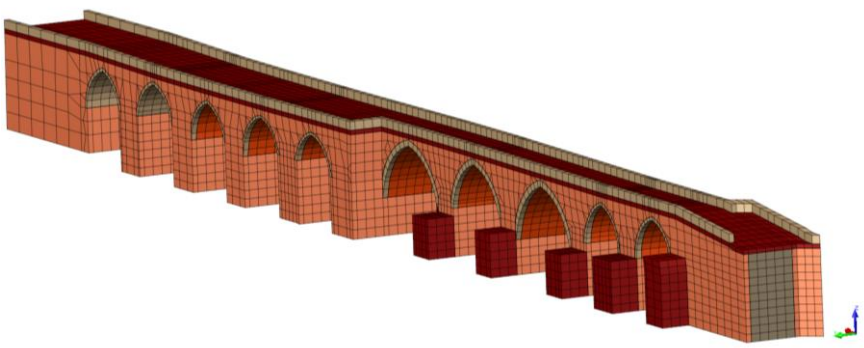

Figure 4.9 : 3D modeling of Dicle (On Gozlu) Bridge with coarse mesh-downstream.

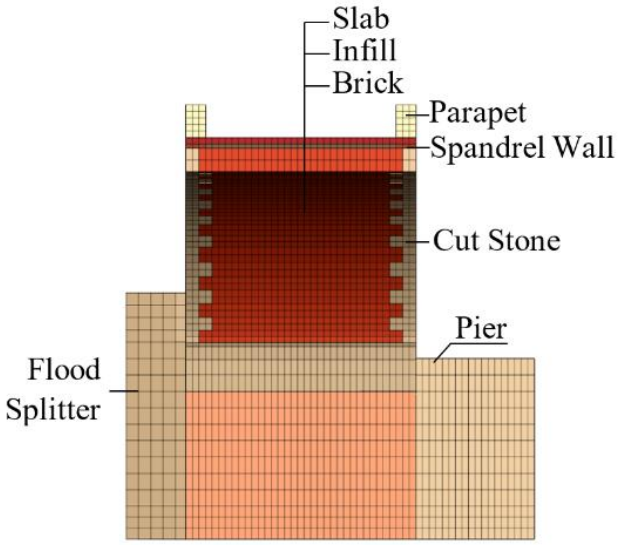

Figure 4.10 : Cross section of the Dicle (On Gozlu) Bridge 3D model.

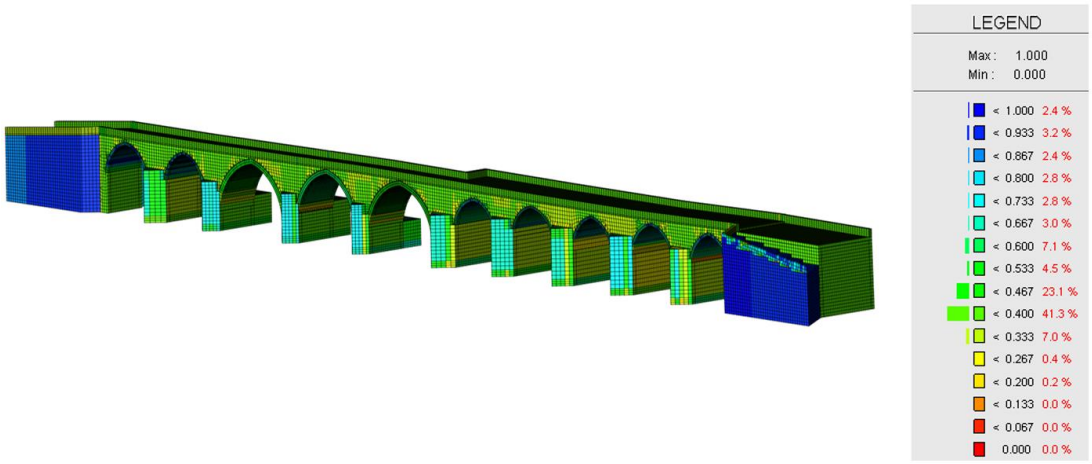

Figure 4.11 : Mesh quality of 3D model of Dicle (On Gozlu) Bridge with fine meshing.

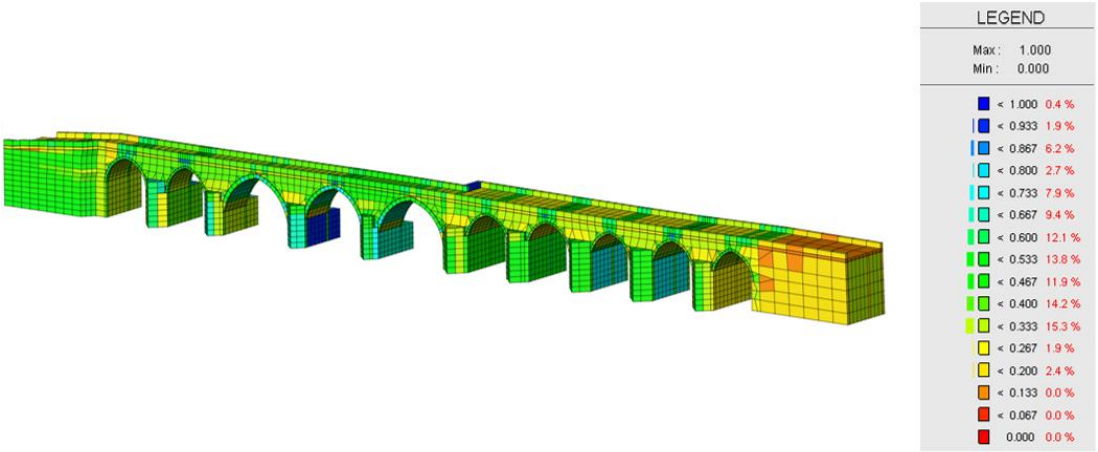

Figure 4.12 : Mesh quality of 3D model of Dicle (On Gozlu) Bridge with coarse meshing.

4.2.2 Malabadi Bridge

Malabadi Bridge that extends over the Batman Creek is located in Silvan, Diyarbakır. The masonry bridge was built in 12th century (in between 1147 and 1148). The architect of the bridge is Timurtas Bin Ilgazi Bin Artuk. The bridge has two different parts and these parts are in a nonlinear row. The middle mass part is supported by a rocky ground and the largest span is located at this part as seen in figure 4.13. The span of this arch is 38.6m and rise of the arch is approximately 24m (Figure 4.14). At the second part of the bridge, there are two pointed arch spans those have 5.8m width and approximately 9~10m height. The smallest span is close to the left side, its width is about 2.5m and height is 1.2m. The thickness of the largest arch is about 2m (KGM, 2015). The bridge has five spans, the length of the bridge is 150m and the width is approximately 7m as seen in figure 4.15 and figure 4.16. The structural system consists of semi-circle and pointed vaults those are carried by variable-height rectangular piers. The radius of the arches is variable. Cut stone blocks were used in the construction (KGM, 2015).

There are two shelters at the both inner sides of the Malabadi Bridge. Passengers and bridge guards used these shelters especially during the winter conditions in old times. To control the traffic on the bridge, there is a 5m masonry door. Two stairs at the left sides of the doors go down to the small rooms. These rooms were constructed by using brick and they have large windows. Under the largest arch and two sides of one of the small arches there are two flood splitters. One of them has triangle form, the other one is hexagonal. During the restoration work that was completed in 2014 considered necessary interventions were applied to improve the structural behavior and original characteristics of the bridge (KGM, 2015).

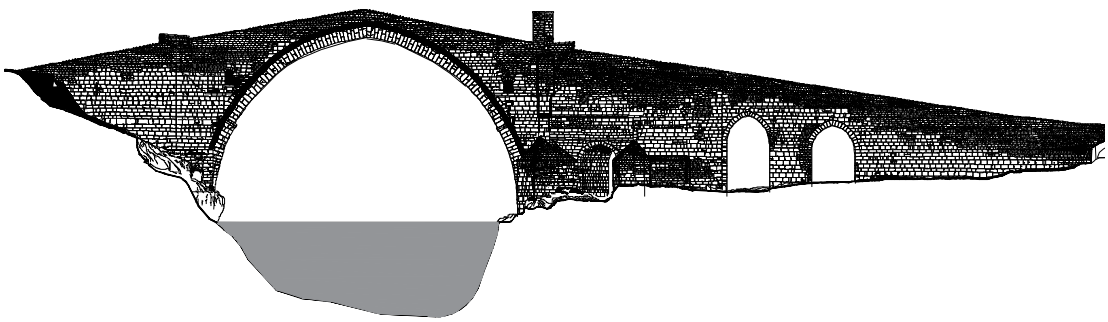

Figure 4.13 : Upstream view of Malabadi Bridge (Scale: 1/1000) (KGM, 2015).

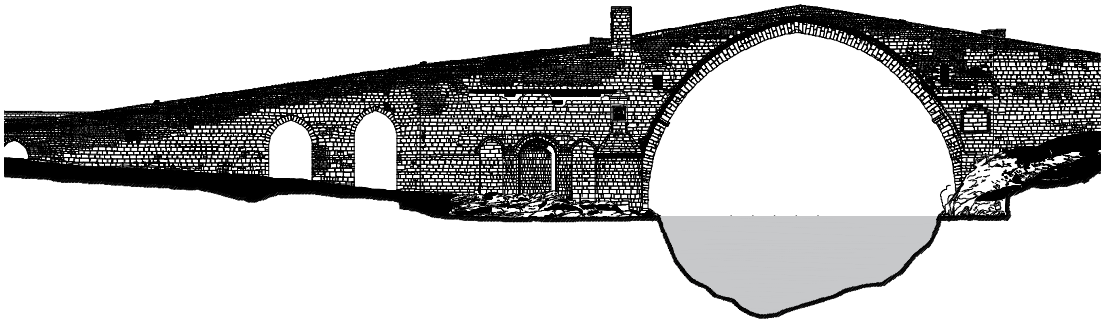

Figure 4.14 : Downstream view of Malabadi Bridge (Scale: 1/1000) (KGM, 2015).

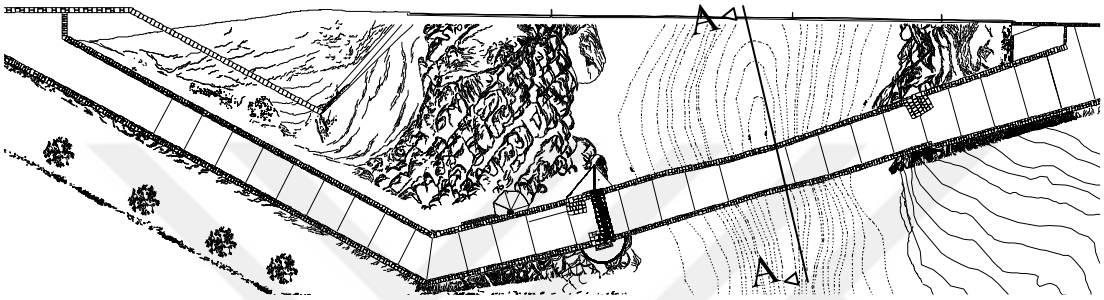

Figure 4.15 : Layout plan of Malabadi Bridge (Scale: 1/1000) (KGM, 2015).

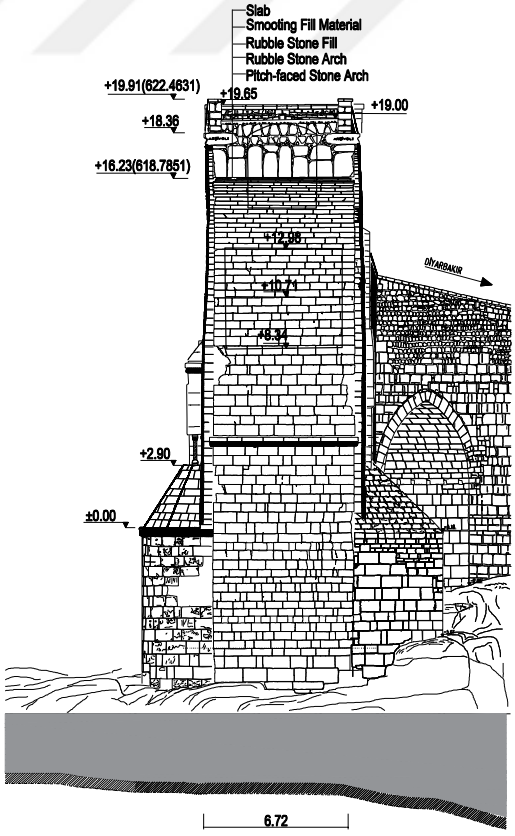

Figure 4.16 : Cross section (A-A) of Malabadi Bridge (KGM, 2015).

Figure 4.17 : Upstream and downstream views of Malabadi Bridge (URL 2, 2016).

In the modelling process of the Malabadi Bridge, six different types of structural elements which are arch, spandrel wall, infill, parapet, slab, flood splitter were modelled. Each length of the elements differs between 0.3m-0.5m and 0.4m-2m for fine and coarse meshes, respectively. Detail features of the mesh sets are given in the table 4.3. The 3D model details of the Malabadi Bridge and the mesh quality of the model can be seen in figure 4.18 to figure 4.24.

Table 4.3 : Details of mesh sets used in 3D model of Malabadi Bridge.

Type of Mesh	Total number of Solid element	Total Number of Element Face	Total Number of Node	Total Weight of Bridge (kN)	Total Volume (m^3)
Fine Mesh	231,321	138,912	256,883	244,879	13,075.6
Coarse Mesh	13,524	17,431	16,370	252,698	13,510.3

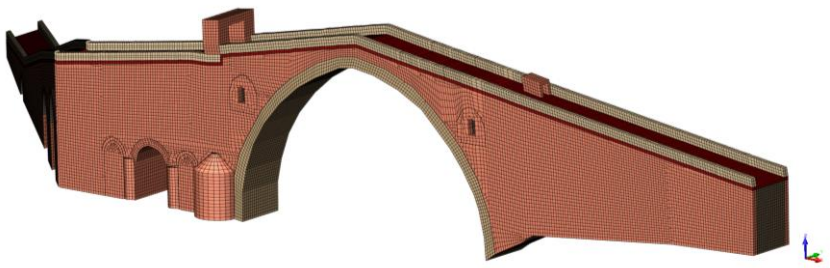

Figure 4.18 : 3D modeling of Malabadi Bridge with fine mesh-downstream.

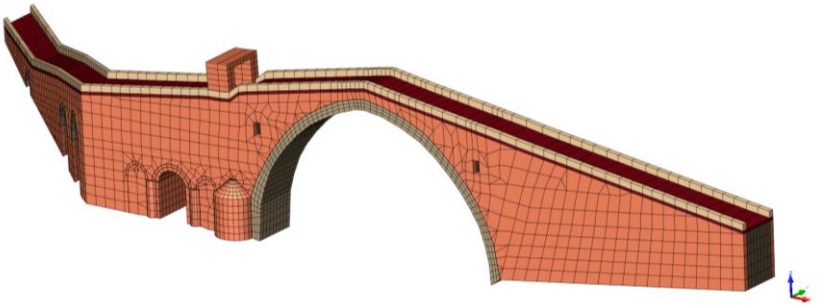

Figure 4.19 : 3D modeling of Malabadi Bridge with coarse mesh-downstream.

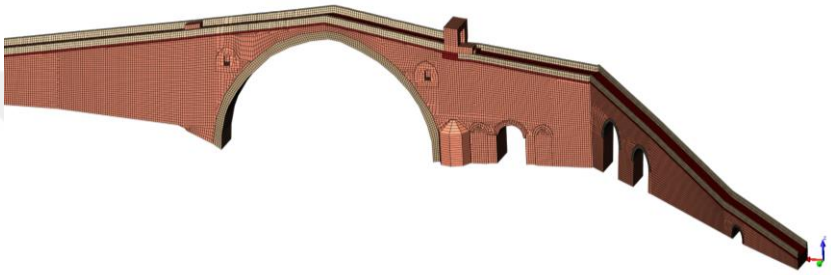

Figure 4.20 : 3D modeling of Malabadi Bridge with fine mesh-upstream.

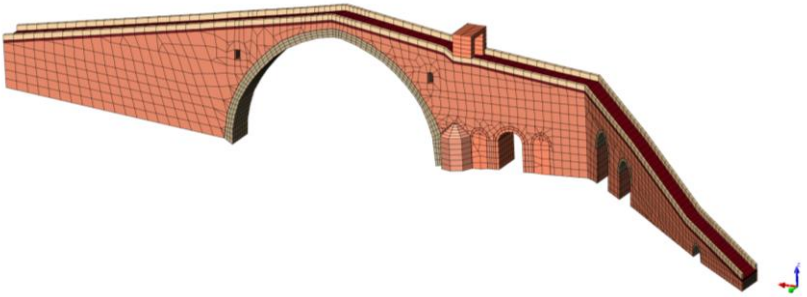

Figure 4.21 : 3D modeling of Malabadi Bridge with coarse mesh-upstream.

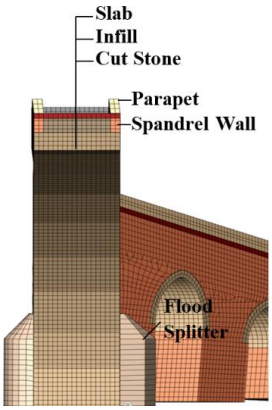

Figure 4.22 : Cross section of the Malabadi Bridge.

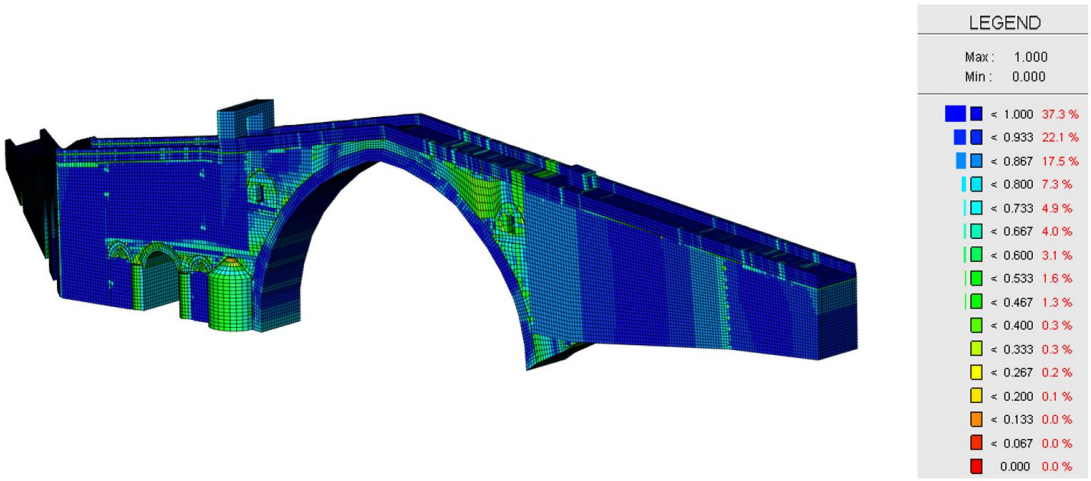

Figure 4.23 : Mesh quality of 3D model of Malabadi Bridge with fine meshing.

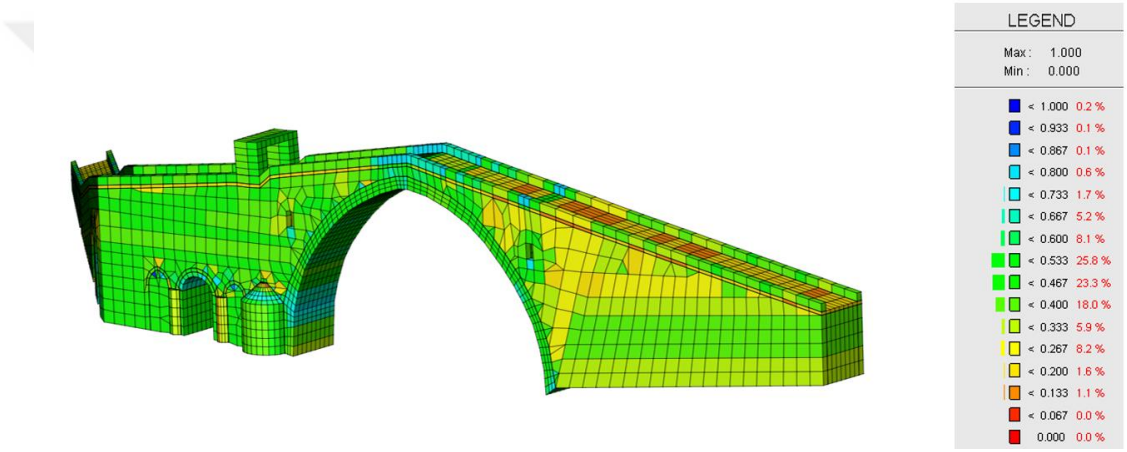

Figure 4.24 : Mesh quality of 3D model of Malabadi Bridge with coarse meshing.

4.2.3 Papaz Bridge

Historical Papaz Bridge was built in 16th century over the Ayamama Creek. The bridge that has three spans and the plan length of the bridge on upstream side is approximately 34m (Figure 4.25). Downside plan length is approximately 38.5m (Figure 4.26) and the width of the bridge is 4.5m (Figure 4.28). The largest span that is in the middle of the bridge has pointed arch shape and has 25 cut stone blocks. It geometrically consists of 3.67m and 4.32m radius two arc segments. The radius values of the other short span arches are different at the upstream and downstream side and those are approximately 1.90m~2.15m. The thicknesses of main support arches are varying between 0.45m~0.55m (Figure 4.28). These arches both have 14 cut stone blocks. The maximum height of the bridge is about 5.5m (KGM, 2015). Load bearing system of

the bridge that consists of three pointed vaults are carried by the different size rectangular piers.

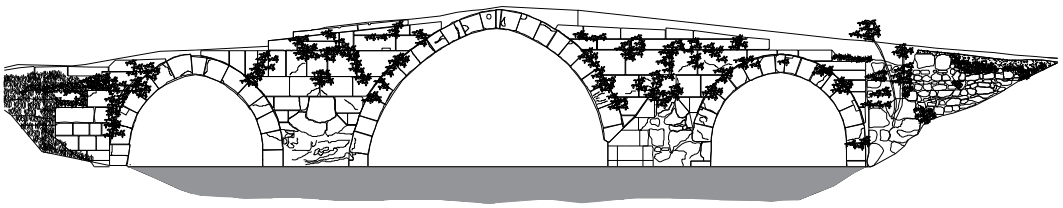

Figure 4.25 : Upstream view of Papaz Bridge (Scale: 1/200) (KGM, 2015).

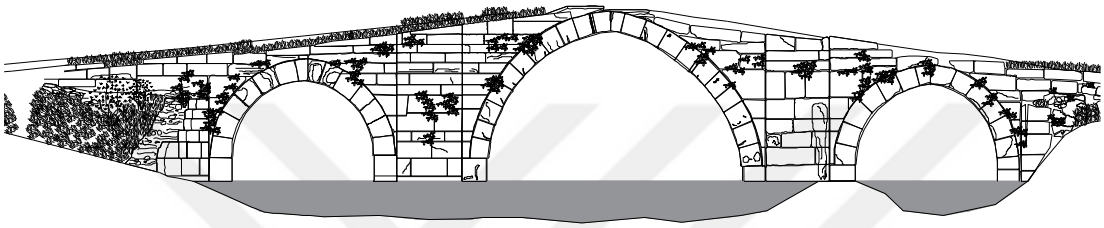

Figure 4.26 : Downstream view of Papaz Bridge (Scale: 1/200) (KGM, 2015).

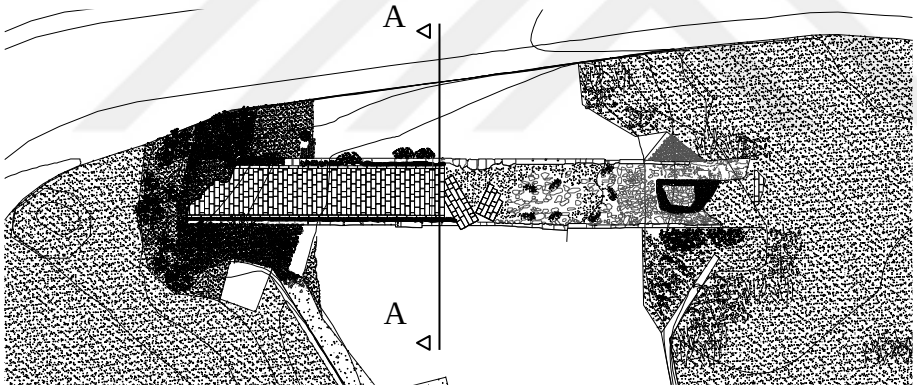

Figure 4.27 : Layout plan of Papaz Bridge (Scale: 1/500) (KGM, 2015).

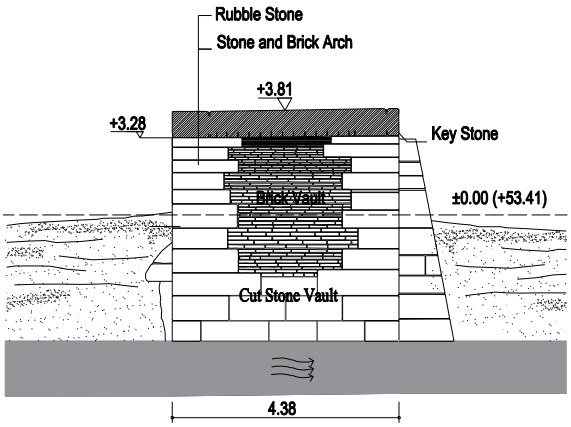

Figure 4.28 : Cross section (A-A) of Papaz Bridge (KGM, 2015).

Vaults consist cut stone blocks and brick units together. Stone block units used in the masonry construction has different dimensions. Rubble stone was used as a infill material between the spandrel walls. The bridge has several damages such as deformation and deflection on the wall bonds, deterioration on the floor coating, and loss of material in the joints. Interior backfill materials between the spandrel walls appear on the ground floor level of the bridge due to the extinction of slab. Currently, parapets and flood splitters of the bridge are considerably vanished (Figure 4.29).

Figure 4.29 : Upstream and downstream views of the Papaz Bridge.

In the modelling process, the bridge was modelled with four different types of structural elements which are vault, spandrel, infill, buttress. The slab and parapet were vanished. Flood splitter were demolished, as well. Papaz Bridge was modelled by using TP18L and HX24L elements with coarse and fine mesh. Each length of the elements differs between 0.1m~0.2m for fine mesh, and also the voussoirs were modelled according to the current dimensions. The dimensions of the elements are between 0.2m~0.7m for 3D model created with coarse mesh. The characteristics of the mesh sets are given in table 4.4. The 3D models of the Papaz Bridge with the damages are shown in between figure 4.30 and figure 4.34 from upstream to downstream. The mesh quality of the models with fine and coarse meshes can be seen in figure 4.35 and figure 4.36.

Table 4.4 : Details of mesh sets used in 3D model of Papaz Bridge.

Type of Mesh	Total number of Solid element	Total Number of Element Face	Total Number of Node	Total Weight of Bridge (kN)	Total Volume (m^3)
Fine Mesh	107,014	67,029	118,469	9,028.3	490.1
Coarse Mesh	8,496	9,742	10,590	9,011.9	488.6

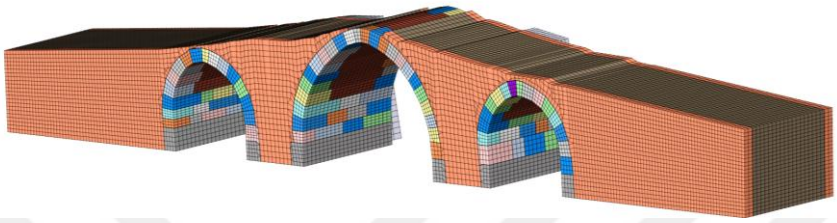

Figure 4.30 : 3D modeling of Papaz Bridge with fine mesh-upstream.

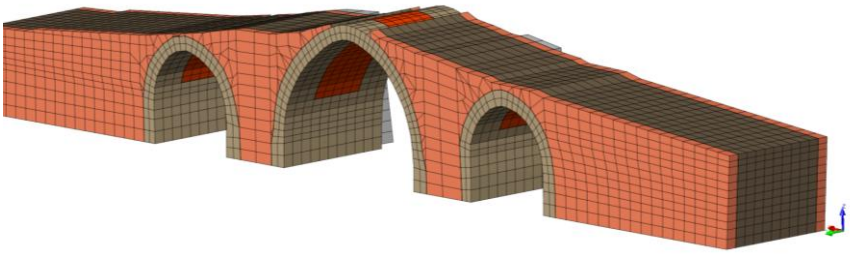

Figure 4.31 : 3D modeling of Papaz Bridge with coarse mesh-upstream.

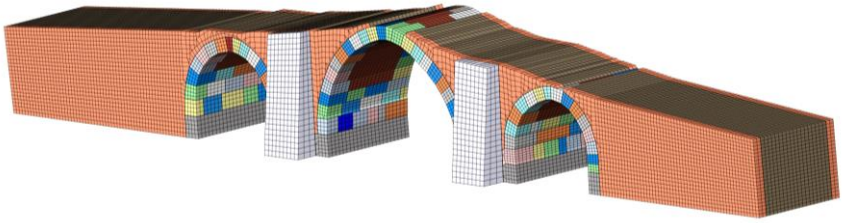

Figure 4.32 : 3D modeling of Papaz Bridge with fine mesh-downstream.

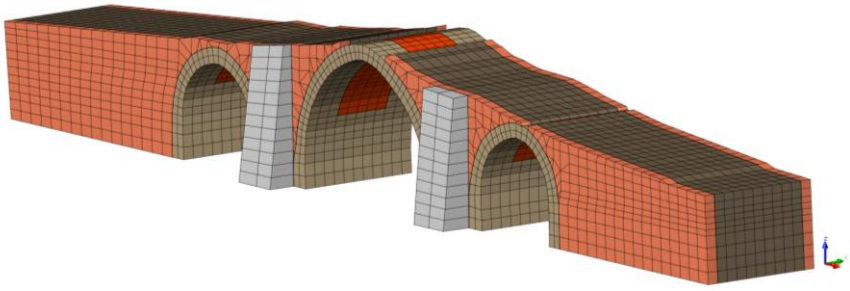

Figure 4.33 : 3D modeling of Papaz Bridge with coarse mesh-downstream.

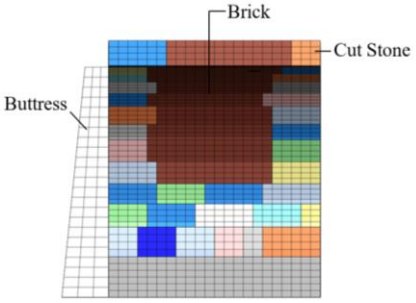

Figure 4.34 : Cross section of the Papaz Bridge.

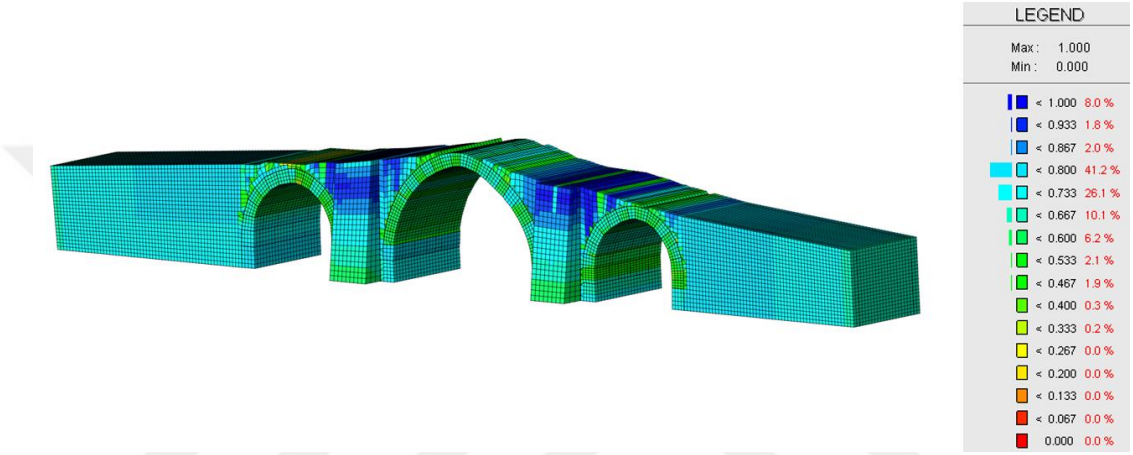

Figure 4.35 : Mesh quality of 3D model of Papaz Bridge with fine meshing.

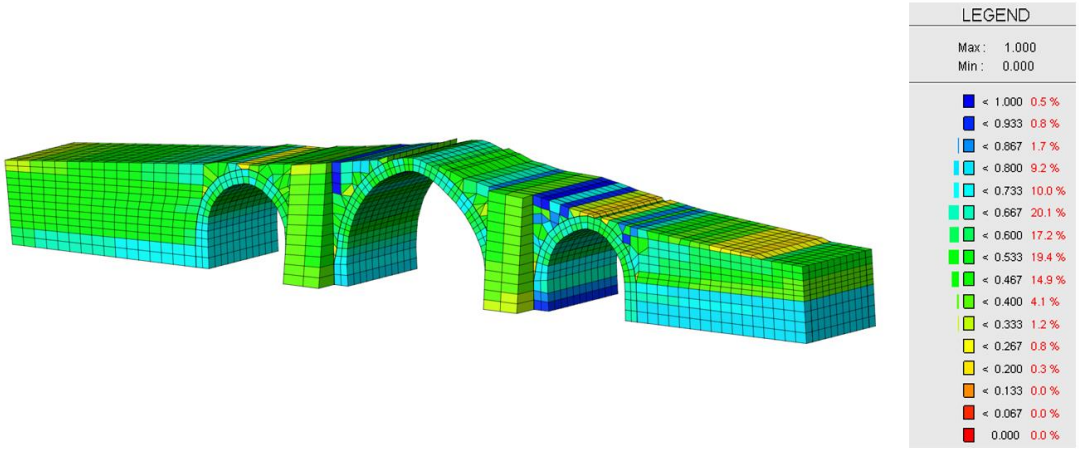

Figure 4.36 : Mesh quality of 3D model of Papaz Bridge with coarse meshing.

4.2.4 Sinanlı-Alpullu Bridge

Sinanlı-Alpullu Bridge was built in 16th century (in between 1488 and 1587) and the architect of the bridge is Architect Sinan. The bridge extends over the Ergene River and it has totally nine spans with discharging cells as seen in figure 4.37 and figure

4.38. The plan length of the bridge is approximately 120m (Figure 4.39) and the width is 6m (Figure 4.40 and Figure 4.38). The largest span locates at the middle of the bridge, the span of arch is 20m and rise is 5.9m. The dimensions of spans decrease from the middle to the both left and right direction symmetrically. The smallest span is located at the right side of the bridge from downstream with nearly 5m span (KGM, 2015).

There are four discharging cells of the bridge. Two of them are located at both of two side of the middle arch and they have circular form. The other two discharging cells have pointed arch form. Main arch form is pointed arch type. The thickness of cut stone blocks used for main arch varies in between 1.4m-1.8m. The bridge that has high-sloped floor was constructed by considering of features of the river.

Figure 4.37 : Upstream view of Sinanlı-Alpullu Bridge (Scale: 1/1000) (KGM, 2015).

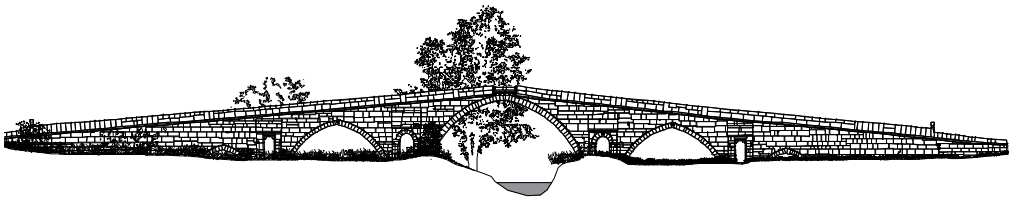

Figure 4.38 : Downstream view of Sinanlı-Alpullu Bridge (Scale: 1/1000) (KGM, 2015).

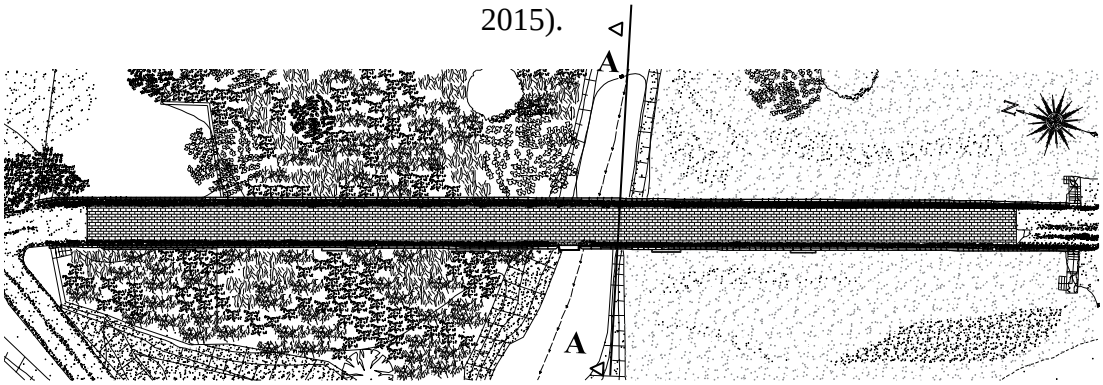

Figure 4.39 : Layout plan of Sinanlı-Alpullu Bridge, (Scale: 1/1000) (KGM, 2015).

From top of the largest arch span toward the two sides, coping stone continues. The maximum height of the parapet wall is 1.1m. Spandrel walls of the bridge were constructed by using thin free stones and the joints between the stones are quite slim. Cut stone blocks were used for the parapets and spandrel walls as well. The slab was constructed with natural stone as seen in figure 4.40 (KGM, 2015).

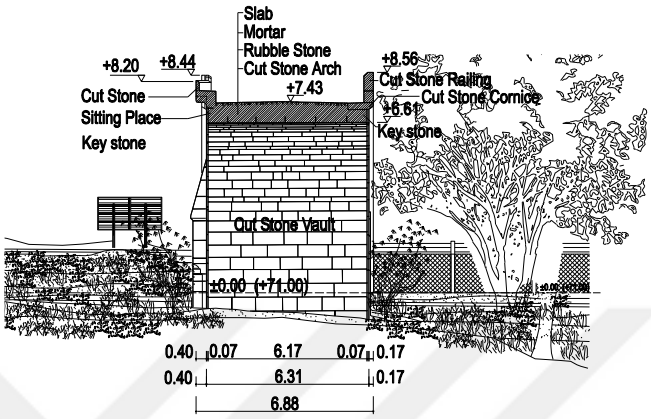

Figure 4.40 : Cross section (A-A) of the Sinanlı-Alpullu Bridge (KGM, 2015).

As a result of observations and site investigation (Figure 4.41 and Figure 4.42); it was observed that there are some material problems, damages and environmental issues (KGM, 2015).

Figure 4.41 : Current view of the Sinanlı-Alpullu Bridge

Figure 4.42 : Detail views of the Sinanlı-Alpullu Bridge.

Sinanlı-Alpullu Bridge was modelled through fine mesh and course mesh which comprise of TP18L and HX24L elements. Each length of the elements for fine mesh is approximately 0.25m. In the second model with coarse mesh, mesh dimension of the arch is 0.4m, but the spandrel wall's mesh dimensions vary in 0.3m to 2m.

The 3D model and section of the Sinanlı-Alpullu Bridge are given in figure 4.43 and in figure 4.45, and the mesh quality of the structure is shared in figure 4.46 and figure 4.47. Details of the 3D models created by using both fine and coarse meshes are given in table 4.5.

Table 4.5 : Details of mesh sets used in 3D model of Sinanlı-Alpullu Bridge.

Type of Mesh	Total Number of Solid element	Total Number of Element Face	Total Number of Node	Total Weight of Bridge (kN)	Total Volume (m^3)
Fine Mesh	363,660	198,550	400,394	63,738.6	3,441.93
Coarse Mesh	11,272	16,500	14,062	56,626	3,187.96

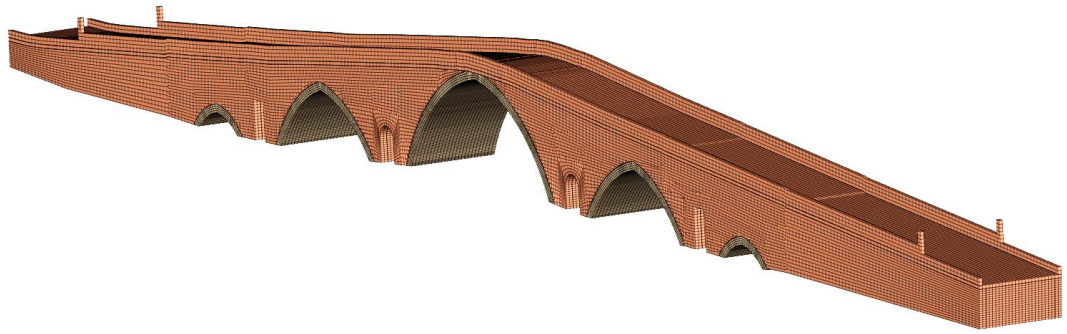

Figure 4.43 : 3D modeling of Sinanlı-Alpullu Bridge with fine mesh.

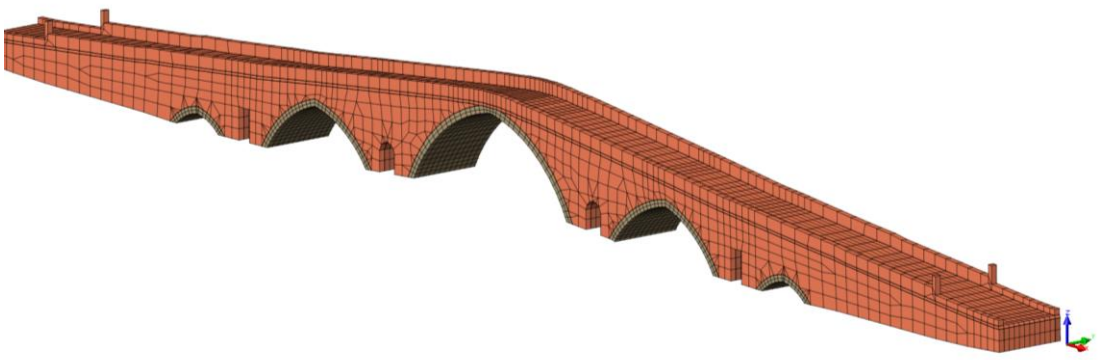

Figure 4.44 : 3D modeling of Sinanlı-Alpullu Bridge with coarse mesh.

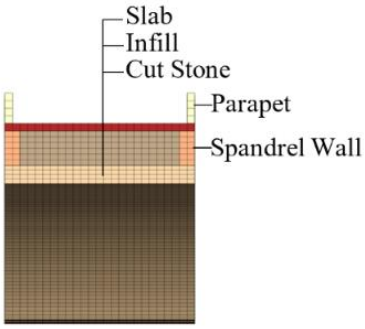

Figure 4.45 : Cross section of the Sinanlı-Alpullu Bridge 3D Model.

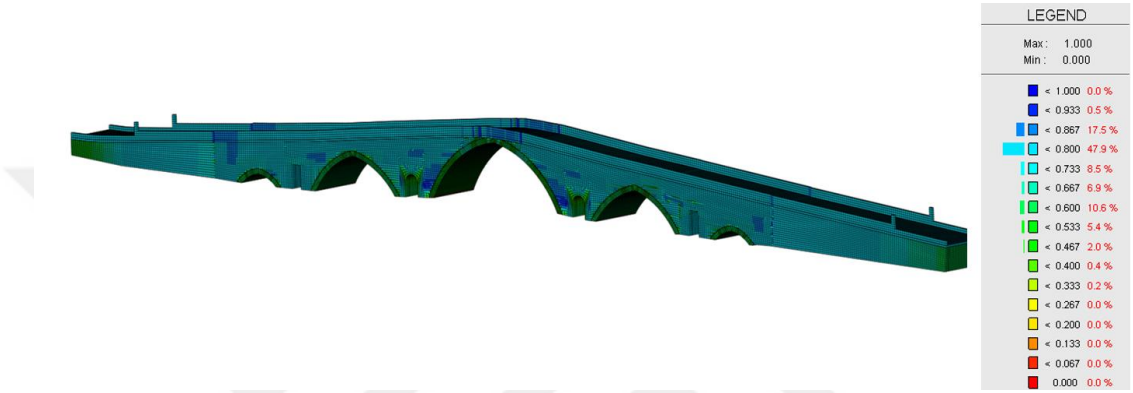

Figure 4.46 : Fine mesh quality of 3D modeling of Sinanlı-Alpullu Bridge.

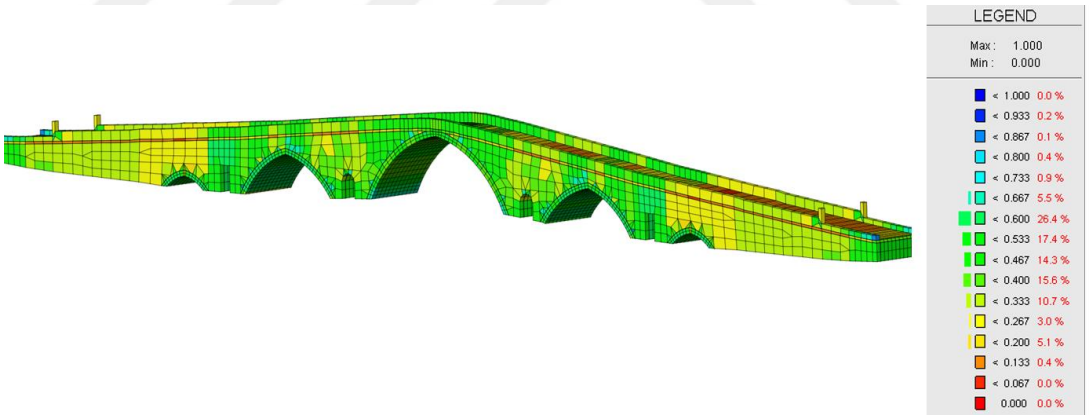

Figure 4.47 : Coarse mesh quality of 3D modeling of Sinanlı-Alpullu Bridge.

4.3 Analyses of the Bridges

In the first step of the analyses, to determine appropriate mesh type for nonlinear analysis, structural linear analysis was applied on both model created by using course and fine meshes. Then, in terms of the results obtained, nonlinear static and dynamic analyses were conducted on coarse mesh. The point was to decrease the duration of the analyses and the size of output files, which run out of space of computers, and need of the high computational performance.

4.3.1 Structural linear static and structural response spectrum analyses

Currently vehicle traffic is not allowed by the authority for the selected bridges. Selected bridges were exposed to the load of traffic prior to this restriction. Thus, the vertical load was assumed just 0,0049N/mm^2 per live load (Q) and the dead load (G) was taken account. In structural linear static analysis process, the selected bridges were analyzed with the combination self-weight and 0.0049N/mm^2 live load. In structural response spectrum analysis, first 20 mode shapes of the bridges were assessed to reach mass participating ratio defined as 90% in Turkish Seismic Code, 2007. However, in masonry structures this ratio can be obtained with more than 20 mode shapes. It increases the time of the analysis.

In the response spectrum analysis process, the seismic load was defined as a lateral force in X and Y directions according to the Turkish Seismic Code, 2007 (Ex and Ey). Two types of load cases were defined as G+Q+Ex and G+Q+Ey which are the combinations of dead load, live load and seismic load in both X and Y directions. Elastic Seismic load definition was applied according to the spectral acceleration coefficient, which shows differences from one to another construction due to the effective ground acceleration coefficient and building importance factor shown in equation 4.1.

$$A(T)=A_0\, I\, S(T) \tag{4.1}$$

Table 4.6 : Effective ground acceleration coefficient (Turkish Seismic Code, 2007).

Seismic Zone	**1**	**2**	**3**	**4**
A_0	0.4	0.3	0.2	0.1

Elastic spectral acceleration Sae (T) is derived by multiplying Spectral Acceleration Coefficient with accelaration of gravity (Equation 4.2).

$$Sae\ (T)=A(T)\ g \tag{4.2}$$

The Spectrum Coefficient, appearing in equations 4.3, 4.4 and 4.5 are determined depending on the local site conditions and the building natural period.

$$S(T) = 1 + 1.5 * \frac{T}{T_A} \qquad (0 \leq T \leq T_A) \qquad (4.3)$$

$$S(T) = 2.5 \qquad (T_A < T \leq T_B) \qquad (4.4)$$

$$S(T) = 2.5 * \left(\frac{T_B}{T}\right)^{0.8} \qquad (T_B < T) \qquad (4.5)$$

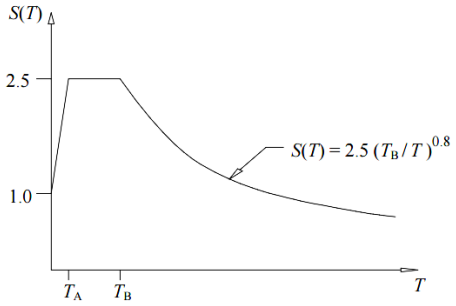

Figure 4.48 : The design spectra (Turkish Seismic Code, 2007).

Spectrum Characteristic Periods, T_A and T_B, appearing in equation 4.4 are specified, depending on local site classes are defined in table 4.7. Table 4.8 gives the all-seismic parameters for all bridges separately. The analyses were carried out by using these parameters.

Table 4.7 : Spectrum characteristic periods (Turkish Seismic Code).

Local Site Class	T_A(second)	T_B(second)
Z1	0.10	0.30
Z2	0.15	0.40
Z3	0.15	0.60
Z4	0.20	0.90

Table 4.8 : Seismic assessment parameters for selected bridges.

Bridge	Location	Seismic	Soil	A_0	I
Dicle	Diyarbakır	2	Z1	0.3	1.2
Malabadi	Diyarbakır	1	Z1	0.4	1.2
Papaz	İstanbul	1	Z1	0.4	1.2
Sinanlı-Alpullu	Kırklareli	4	Z1	0.1	1.2

Due to the historical value of bridges, the material properties cannot be obtained easily. In this thesis, the KGM provided some information about the property of the materials. Additional information about material properties was obtained from literature review (Pela et al, 2009). The material properties were shown in the table 4.9. The most appropriate properties were applied to analyze the structure.

Table 4.9 : Material properties used in analyses (adopted from Pela et al., 2009).

Material	Modulus of Elasticity (MPa)	Poisson Ratio	Mass Density (ρ) ($N/mm^3/g$)	Tensile Strength (f_t) (MPa)	Compression Strength (f_c) (MPa)
Stone	5000	0.2	$2.16*10^{-9}$	0.3	3
Brick	4000	0.2	$1.76*10^{-9}$	0.2	2
Infill	500	0.2	$1.76*10^{-9}$	0.1	1

4.3.2 Nonlinear static analysis (NLSA)

In nonlinear analysis process for both static and dynamic analyses, Total Stain Crack Rotating constitutive model was used. This model was determined according to the study of Scheibmeir (2012) which discussed four different constitutive materials which is found in DIANA library. This method is based on total strain where the stress is described as a function of the strain (Scheibmeir, 2012). The total strain based crack models follow a smeared crack approach. Selected compression and tension softening for Total Strain crack model was given in figure 4.49 for selected bridges.

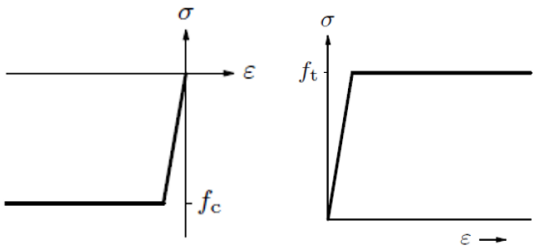

Figure 4.49 : Predefined ideal compression and tension softening for Total Strain crack model (TNO DIANA, 2014).

The analysis processes were conducted in Mesh Edit program (TNO DIANA, 2014). Two different load steps were applied in the analysis. First step was eigenvalue analysis to determine mode shapes which are effective while running nonlinear static

analysis named push over analysis. Then the second step was nonlinear analysis. The structural model was subjected to gravitational load and then lateral forces according to the mass distribution obtain from eigenvalue analysis in nonlinear analysis.

The assumptions in DIANA during analysis for the nonlinear static analysis are:

- Steps for self-weight was 0.2(5).
- Steps for push over load was 1(250).
- Arc length control was used in the second load step (push over).
- Physical nonlinearity of the model was taken into account.
- Maximum number of iterations was 100.
- Convergence tolerance for displacement and force were selected 0.0001.
- The iterative method used was Secant (Quasi-Newton).

4.3.3 Nonlinear dynamic analysis (NLDA)

Nonlinear Dynamic Analysis is the most powerful tool as for seismic assessment. But, the definition of the parameters used in analysis is not easy and need complicated knowledge. It is also named as time history analysis. Selected set of ground motion records were applied to the bridges. For local soil class A which is defined as massive volcanic rocks, unweathered sound metamorphic rocks, stiff cemented sedimentary rocks, very dense sand, gravel and hard clay and silty clay according to the Turkish Seismic Code, 2007, ten ground motion records obtained from Pasific Earthquake Engineering Research (PEER) database were chosen to apply for time history analyses (URL-3). Selected ground motions are given in table 4.10. The nonlinear material properties used at the model were given in table 4.9, previously.

As for the nonlinear dynamic analysis, the assumptions in DIANA during analysis that are:

- Damping ratio was given in eigenvalue analyses prior to structural nonlinear analysis to introduce into the model.
- Load step for self-weight was entered before time steps.
- Physically nonlinear and transient effects were added as a nonlinear effect.

- Maximum number of iterations was 10.
- Convergence tolerance for displacement and force were selected 0.01.
- The iterative method was Newton-Raphson method.

Table 4.10 : Ground motion records for soil A.

No	Earthquake Name	Date	Magnitude (M_w)	Record	Vs (cm/s)	Peak Ground Motion (g)	Rjb (km)	Mechanism
1	Morgan Hill	24/04/1984	6.2	G01320	2.9	0.098	16.2	Strike Slip
2	Coyote Lake	06/08/1979	5.7	G01320	8.3	0.132	9.3	Strike Slip
3	Landers	28/06/1992	7.3	ABY090	20	0.146	69.2	Strike Slip
4	Loma Prieta	18/10/1989	6.9	MCH000	3.5	0.073	44.8	Reverse Oblique
5	Lytle Creek	12/09/1970	5.9	CSM095	1.8	0.071	88.6	Reverse Oblique
6	N. Palm Springs	08/07/1986	6.0	AZF225	5.8	0.099	20.6	Reverse Oblique
7	Whittier Narrows	01/10/1987	5.3	MTW000	40	0.123	20.4	Reverse Oblique
8	Kocaeli	17/08/1999	7.5	IZT180	8.1	0.19	3.62	Strike Slip
9	Kocaeli	17/08/1999	7.5	GBZ270	7.9	0.19	7.57	Strike Slip
10	Duzce	12/10/1999	7.14	RSN8165	7.6	0.29	4.21	Strike Slip

5. ANALYSES RESULTS

In this research, four bridges which have different geometric properties were selected to assess these bridges in 3 different approaches which are:

- The selected bridges were modelled with two different mesh sizes. The structural linear and structural response spectrum analyses were performed for the selected bridges. Obtained results from modal analysis and structural response spectrum analysis was compared for the model with fine and coarse meshesing. The differences between the vertical stress, shear stress and maximum displacements, which were obtained both model types, were discussed in section 5.1.
- To carry out nonlinear analyses, which approximate give more realistic results than structural response spectrum, but they are complex and time consuming., the 3D models of selected bridges with coarse meshing were chosen. Nonlinear static analyses (pushover) were performed for selected bridges by using same material properties. In this step, the geometric properties of the selected bridges such as span, rise and thickness of the arches were compared in section 5.2 according to the obtained pushover curves for each selected bridges.
- Nonlinear dynamic analyses were performed for each bridge with ten ground motion records for A soil class in section 5.3.

In the graphs, tension stress is positive given in red color, and compression stress is negative given in blue color. The stress units are N/mm^2 (MPa).

5.1 Structural Linear Static and Structural Response Spectrum Analyses

5.1.1 Dicle (On gozlu) Bridge

To obtain modal characteristics of the bridge, free vibration analysis was carried out. Frequencies of the bridge for the first eight modes are given in table 5.1. The mode shapes for the first three modes of the bridge with fine and coarse meshes are shown

in figure 5.1. Although the modal frequencies are the same for the model both with fine and coarse meshes, mode shapes are different (Figure 5.1). The model with fine mesh gives a complex vertical and longitudinal response in the first mode and mostly transverse response of the bridge was observed for the second mode. However, the model with coarse mesh gives transverse response only in the first mode. The third and some higher mode shapes represent a complex torsional response of the structure for both models. The natural period, in the first mode of the models with fine and coarse meshes, are 7.1Hz and 6.9Hz, respectively.

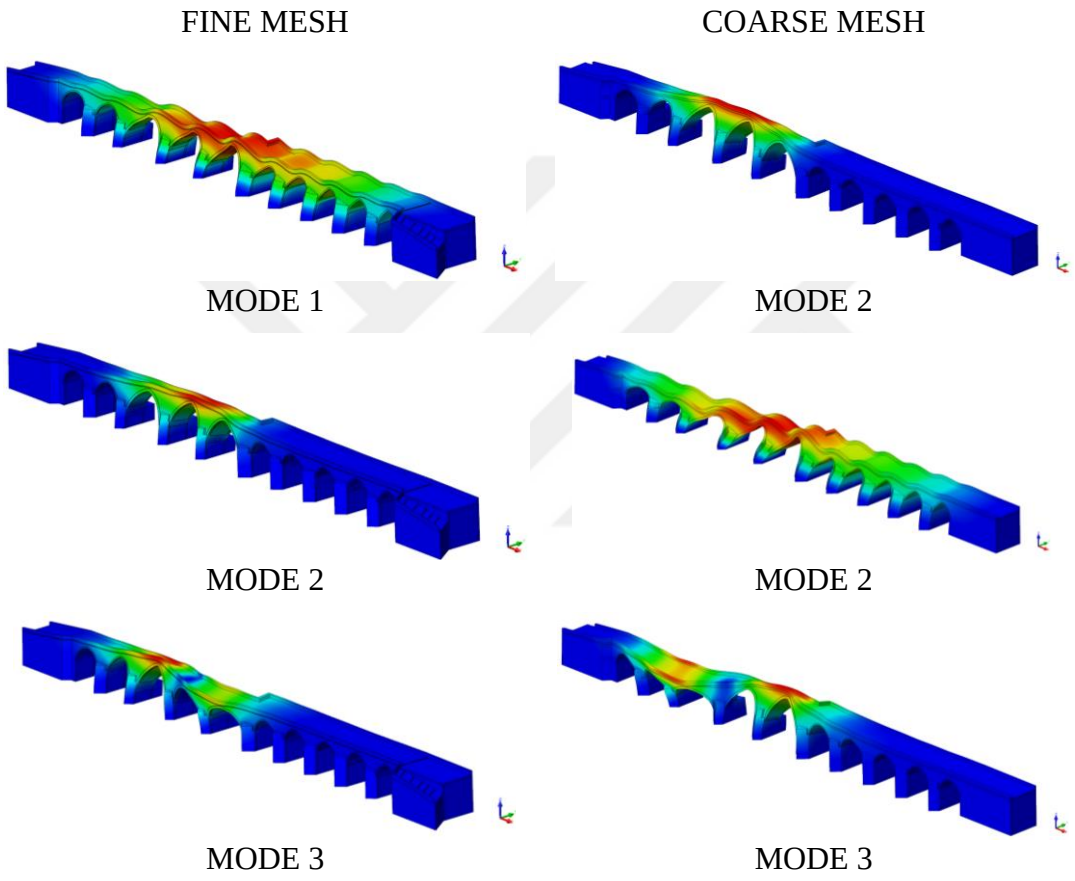

Figure 5.1 : Modal deformed shapes of Dicle (On gozlu) Bridge, the models with fine and coarse meshes, respectively.

Table 5.1 : Modal frequencies of Dicle (On Gozlu) Bridge.

Mode shape	**1**	**2**	**3**	**4**	**5**	**6**	**7**	**8**
Fine Mesh-f (Hz)	7.1	7.2	8	8.4	8.5	8.7	9.3	9.7
Coarse Mesh-f (Hz)	6.9	7.7	7.8	8.4	8.8	8.9	9.2	9.6
Differences	-2%	5%	-2%	1%	3%	3%	-1%	-2%

Analysis with G+Q combination gave the maximum vertical displacement (DtZ) value of -1.5mm and the maximum compression stresses (SZZ) reached up to 0.8MPa for both models created by using fine and coarse meshes. The vertical stress distribution of the models with fine mesh and coarse mesh are given in figure 5.2 and figure 5.3, respectively. Compression stresses (SZZ) were mainly localized around the piers and flood splitters as well as springing levels of the arches.

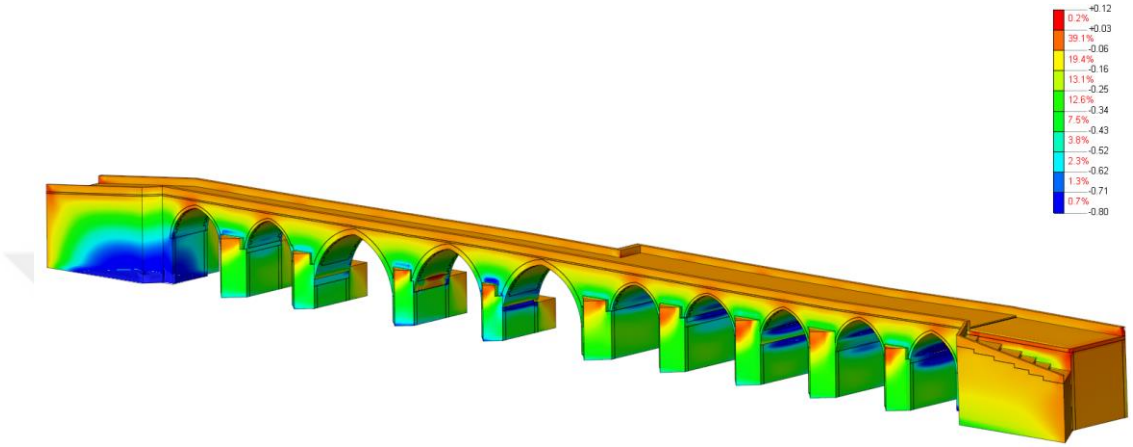

Figure 5.2 : Vertical stress distribution (SZZ) under G+Q load case (Scale: 0.12MPa /-0.8MPa), model with fine mesh.

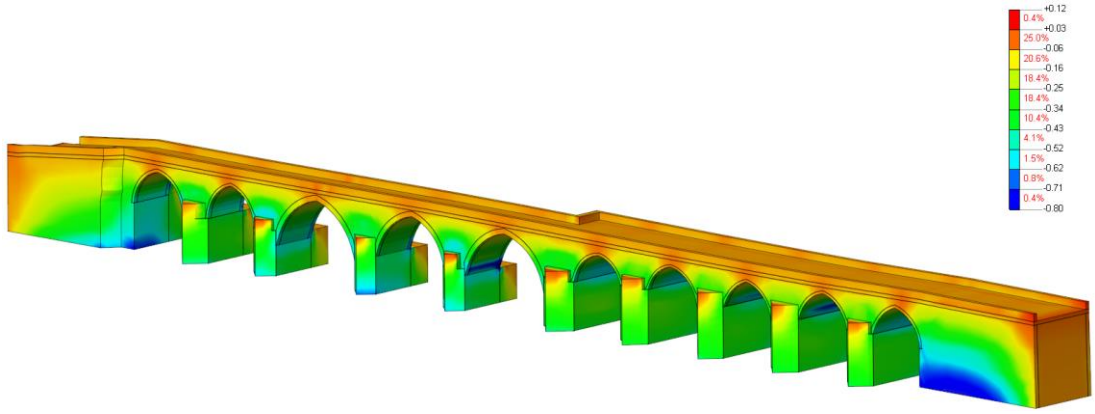

Figure 5.3 : Vertical stress distribution (SZZ) under G+Q load case (Scale: 0.12MPa /-0.8MPa), model with coarse mesh.

Under G+Q+Ex load case along with longitudinal direction, 7.5mm and 6.8mm maximum displacement were obtained at the region with sudden section change along with X direction for both models (Figure 5.4 and Figure 5.5). The tension and compression stresses (SZZ) were at around 1.5MPa and 0.5MPa for both models. In figure 5.6 and figure 5.7, the range of the results of the models are matching up with each other. In G+Q+Ex case, the shear stress SZX varies in between 0.7MPa to -0.1MPa mostly on the spandrels (Figure 5.8 and Figure 5.9).

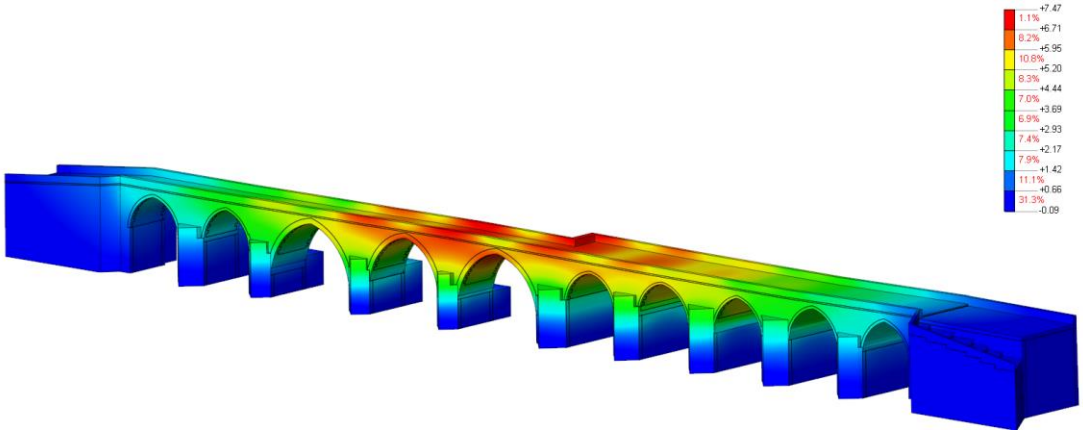

Figure 5.4 : The transversal displacement (DtX) (mm) with G+Q+Ex load case, model with fine mesh.

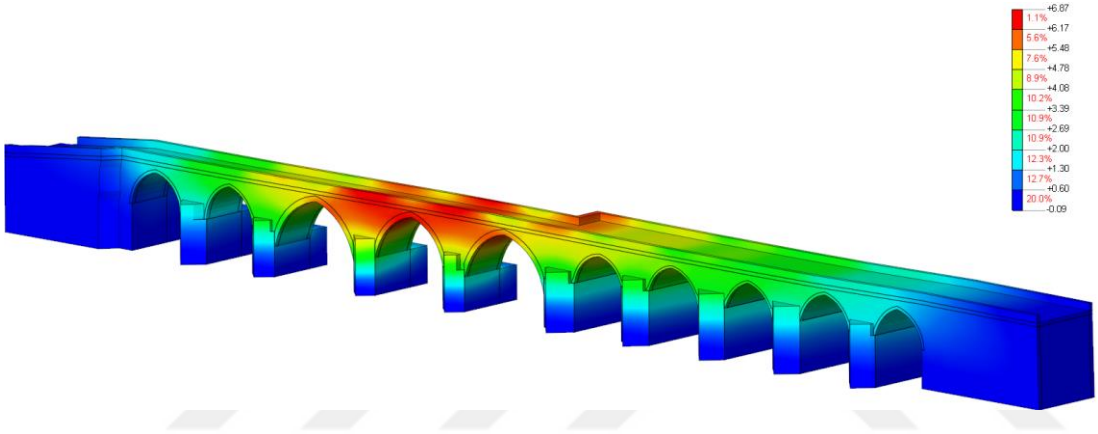

Figure 5.5 : The transversal displacement (DtX) (mm) under G+Q+Ex load case, model with coarse mesh.

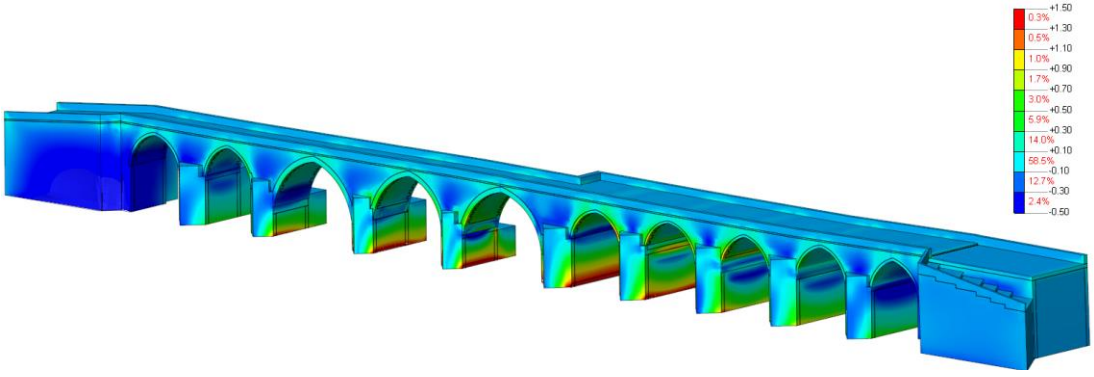

Figure 5.6 : Vertical stress distribution (SZZ) under G+Q+Ex load case (Scale 1.5MPa /-0.5MPa), model with fine mesh.

Furthermore, the 6th span of the bridge from the west side shows the maximum values for SZX shear stress. However, the shear stress of other spans varies from 0MPa to 0.4MPa.

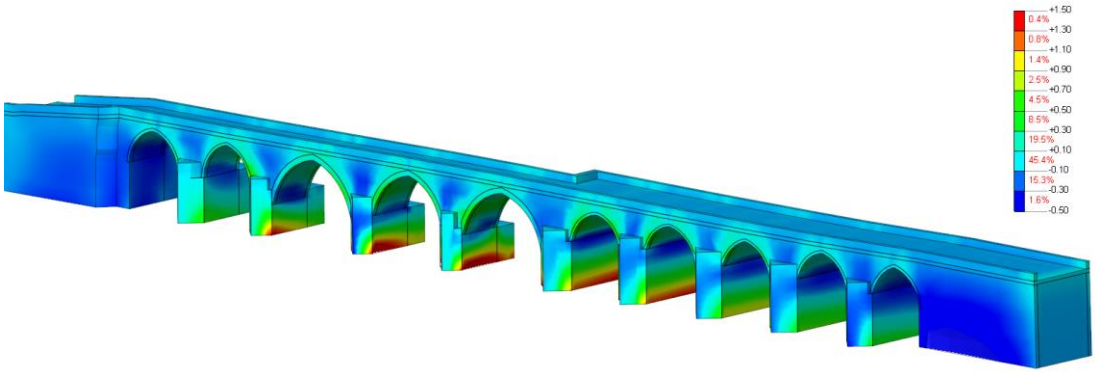

Figure 5.7 : Vertical stress distribution (SZZ) under G+Q+Ex load case (Scale: 1.5MPa /-0.5MPa), model with coarse mesh.

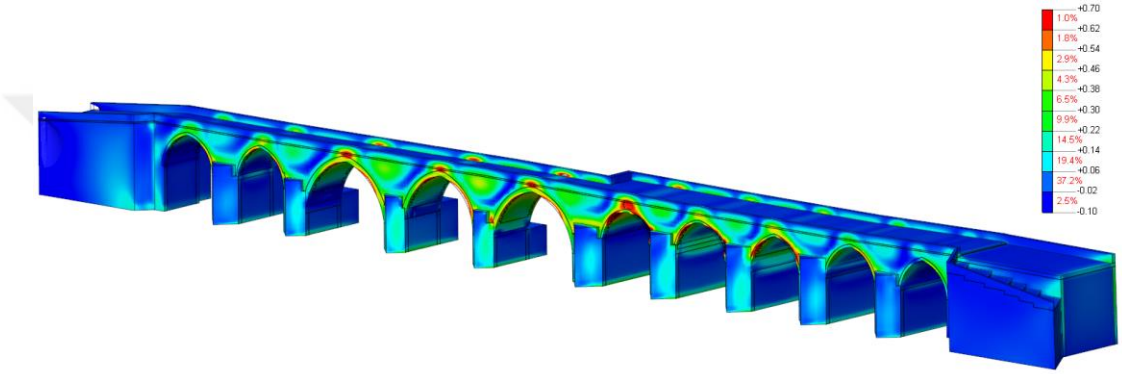

Figure 5.8 : SZX Shear stress distribution under G+Q+Ex load case, (Scale: 0.7MPa/ -0.1MPa), model with fine mesh.

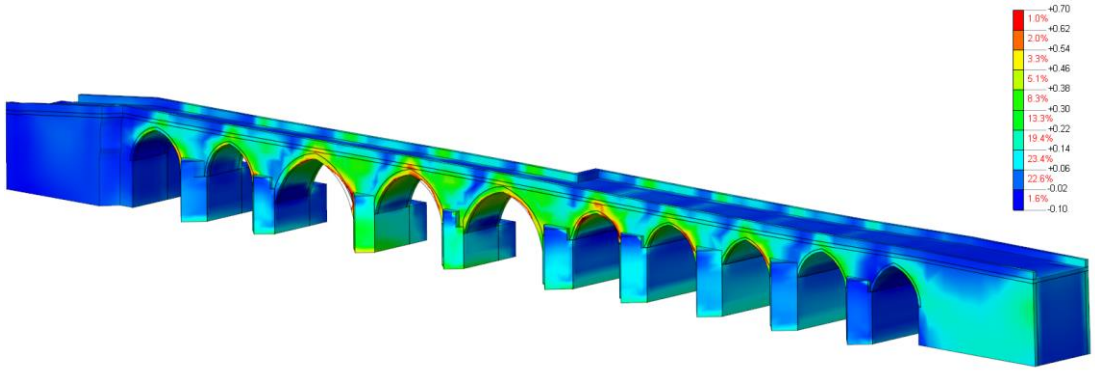

Figure 5.9 : SZX Shear distribution under G+Q+Ex load case, (Scale: 0.7MPa/ -0.1MPa), model with coarse mesh.

Under G+Q+Ey load combination including seismic loading along transverse direction, in terms of vertical normal stresses (SZZ), the tension stress of 1MPa and compression stress of -0.5MPa were obtained. The maximum values were generally observed around flood splitters attached piers between spans of 2-3 and 3-4 (Figure 5.10 and Figure 5.11).

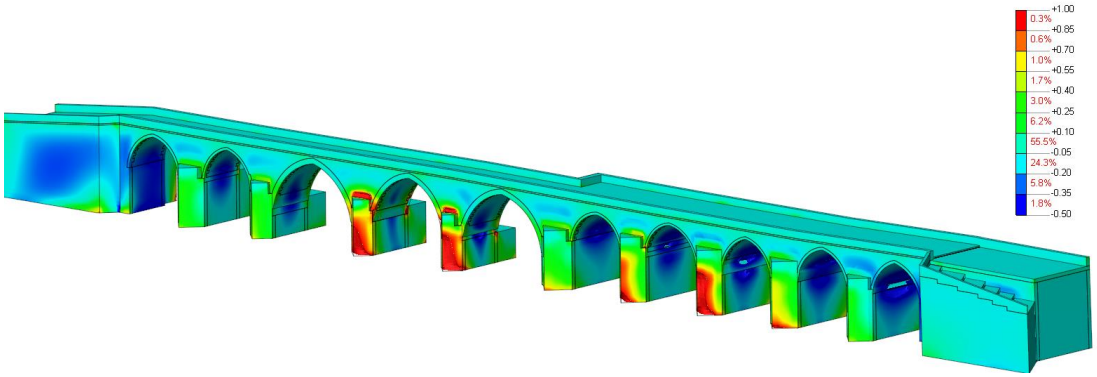

Figure 5.10 : Vertical stress distribution (SZZ) under G+Q+Ey load case (Scale: 1.0MPa /-0.5MPa), model with fine mesh.

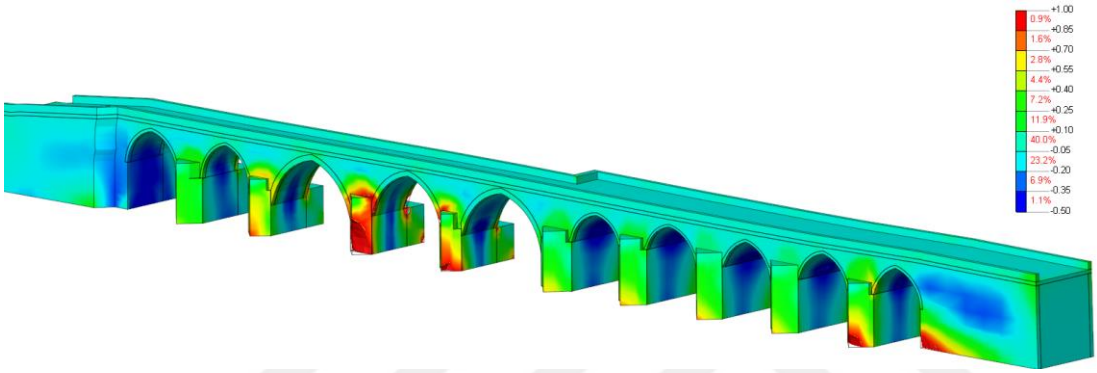

Figure 5.11 : Vertical stress distribution (SZZ) under G+Q+Ey load case (Scale: 1.0MPa /-0.5MPa), model with coarse mesh.

Maximum tension stresses occurred at near downstream side of piers. 8.5mm and 9.2mm maximum displacements were investigated at the top of the parapet on the maximum span in Y direction for both models as seen in figure 5.12 and figure 5.13 under G+Q+Ey load combination. Shear stresses are also evaluated. The shear stress obtained for SYZ (σ_{yz}), reached up 0.8MPa (Figure 5.14 and Figure 5.15). Shear stress of SYZ also mostly localized at inner surfaces of the arches.

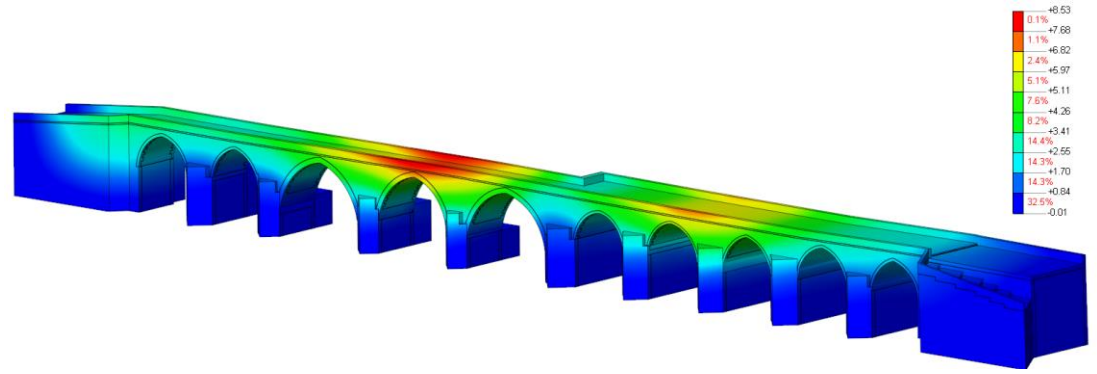

Figure 5.12 : The transversal displacement (DtY) (mm) under G+Q+Ey load case, models with fine mesh.

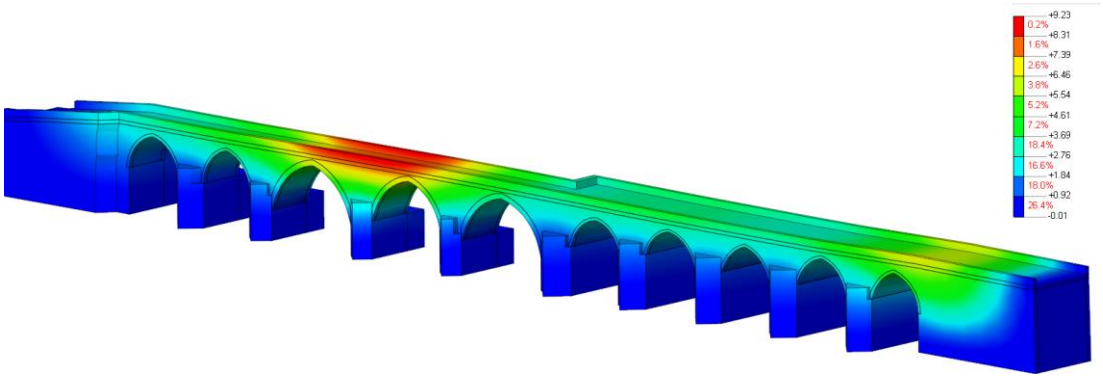

Figure 5.13 : The transversal displacement (DtY) (mm) under G+Q+Ey load case, models with coarse mesh.

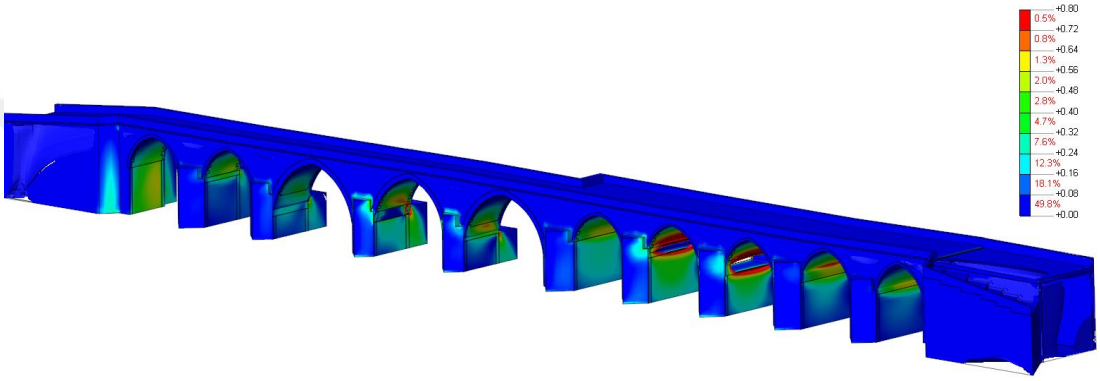

Figure 5.14 : SYZ Shear stress distribution under G+Q+Ey load case, (Scale: 0.8MPa/ 0MPa), model with fine mesh.

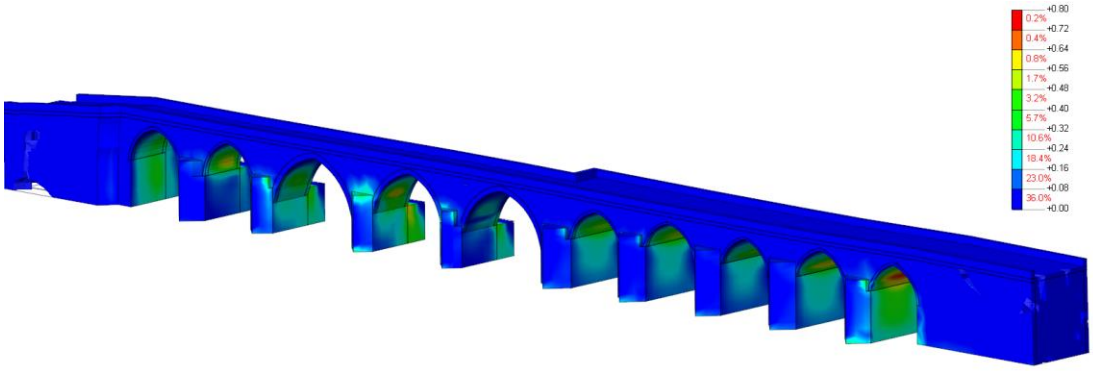

Figure 5.15 : SYZ Shear stress distribution under G+Q+Ey load case, (Scale: 0.8MPa/ 0MPa), model with fine mesh.

The global stress and shear distributions are given in table 5.2. Maximum displacements in X and Y directions are given and compared for fine and coarse meshes in table 5.3. The extreme and localized values for normal stress and shear stress values obtained under two different load combinations were eliminated from results in table 5.2.

Table 5.2 : The differences between stress results of the models with fine and coarse meshes for Dicle Bridge.

Normal and Shear Stresses (MPa)	**Global maximum stresses under 2 different load cases**		**Global minimum stresses under 2 different load cases**		**Percentage of stress distribution under g+q+ex load case for 2 different model approaches**			**Percentage of stress distribution under g+q+ey load case for 2 different model approaches**		
	Under G+Q+Ex Load Case	Under G+Q+Ey Load Case	Under G+Q+Ex Load Case	Under G+Q+Ey Load Case	Fine Mesh	Coarse Mesh	Difference of stress distribution	Fine Mesh	Coarse Mesh	Difference of stress distribution
SXX	0.80MPa	0.60MPa	-0.10MPa	-0.20MPa	94.7	94.2	-1%	99.1	98.7	0%
SYY	0.20MPa	0.70MPa	-0.10MPa	-0.20MPa	89.3	90.2	1%	99.7	99.6	0%
SZZ	1.50MPa	1.00MPa	-0.50MPa	-0.70MPa	99.2	98.9	0%	98.5	96.7	-2%
SXY	0.10MPa	0.70MPa	0MPa	0MPa	88.6	86.9	-2%	98.1	96.5	-2%
SYZ	0.20MPa	1.00MPa	0MPa	0MPa	83	84.3	2%	93.1	94.5	1%
SZX	0.40MPa	1.00MPa	0MPa	0MPa	83.1	83.2	0%	99.4	99.3	0%

Table 5.3 : The differences between displacement results of the models with fine and coarse meshes for Dicle (On gozlu) Bridge.

Displacements	Fine Mesh	Coarse Mesh	Difference of Displacements	Load Case
DtX	7.47mm	6.87mm	-9%	G+Q+EX Load Case
DtY	8.53mm	9.23mm	8%	G+Q+EY Load Case

5.1.2 Malabadi Bridge

Malabadi has the biggest span within the case study, and it has the second biggest span in Turkey inside historical stone arch bridges. The increase of the span and height result in the increase of the fragility. The natural frequency of the Malabadi Bridge starts from 2.14Hz and 2.12Hz for the models with fine and coarse meshes. The modal frequencies are given in table 5.4. The models with fine mesh show transverse response in the first mode and mostly vertical and longitudinal response of the bridge was observed for the second mode.

Table 5.4 : Modal frequencies of Malabadi Bridge.

Mode shape	1	2	3	4	5	6	7	8
Fine Mesh-f (Hz)	2.14	3.55	4.6	5.06	5.6	5.99	6.53	6.86
Coarse Mesh-f (Hz)	2.12	3.47	4.47	5.06	5.6	5.88	6.5	6.73
Difference	-1%	-2%	-3%	0%	0%	-2%	0%	-2%

The deformed shapes obtained from free vibration analysis also can be seen in figure 5.16. The higher values were recorded at west side of the bridge. Because there are angular breaks which divide bridge into the two pieces, east and west; west side has the biggest span from upstream. Deformation can be seen at the west side of the bridge. Models with fine and coarse meshes show the same deformed shaped for first three modes, and the frequencies are approximately the same.

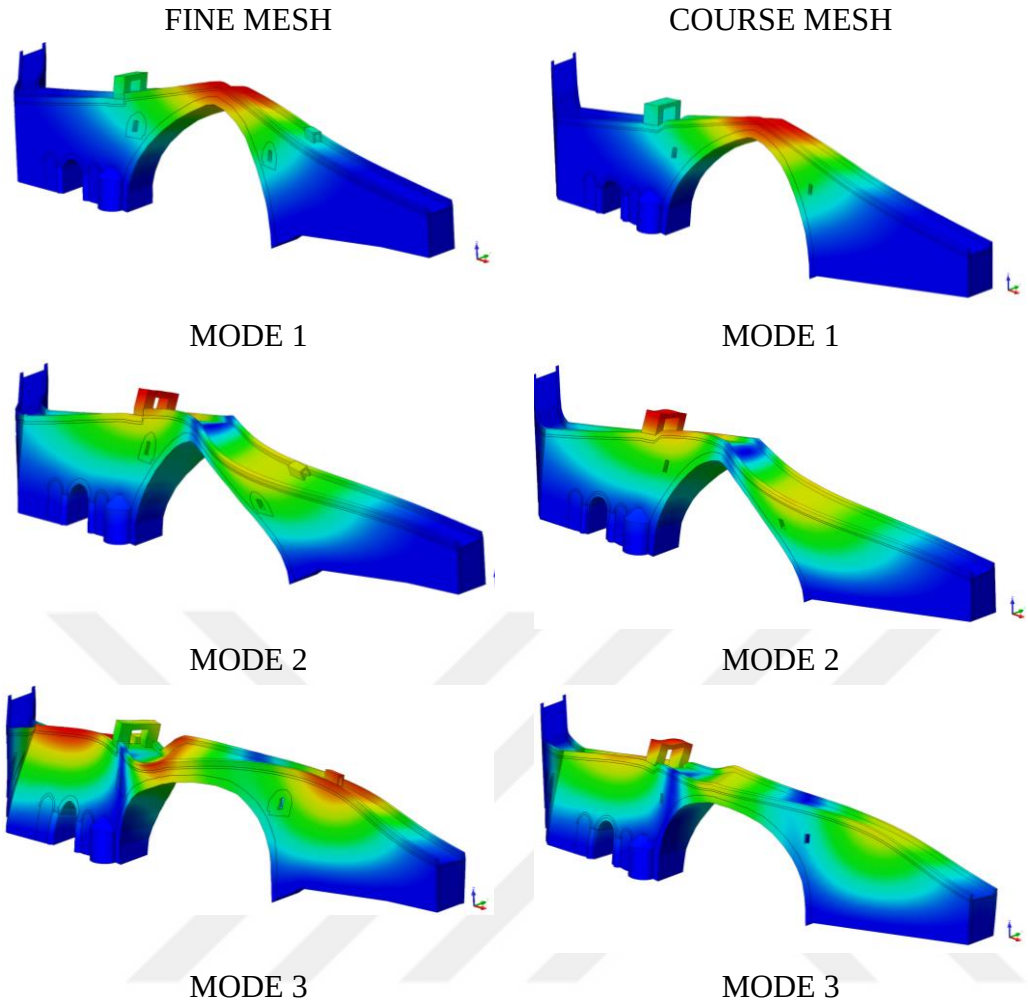

Figure 5.16 : Modal deformed shapes of Malabadi Bridge, the models with fine and coarse meshes, respectively.

With G+Q+Ex load case, due to the shape of bridge, it showed important deflections both in X and Y directions. The highest displacement in X direction, which can be seen at the top of the gate of the bridge, was approximately 15mm for both models (Figure 5.17 and Figure 5.18).

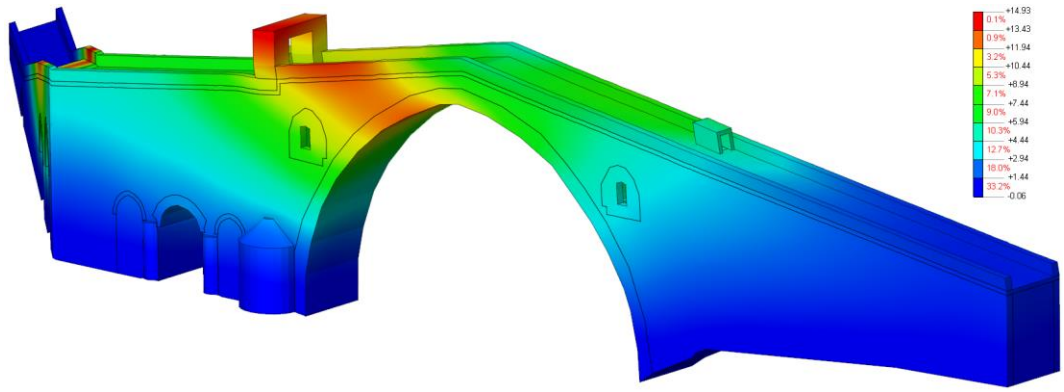

Figure 5.17 : The transversal displacement (DtX) (mm) under G+Q+Ex load case, model with fine mesh.

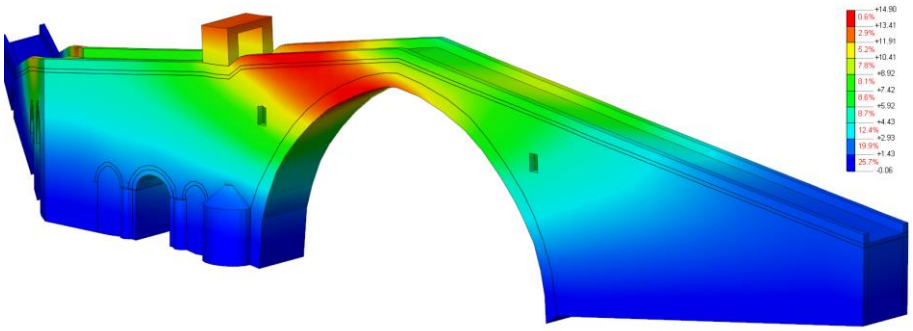

Figure 5.18 : The transversal displacement (DtX) (mm) under G+Q+Ex load case, model with coarse mesh.

In addition, meaningfully displacements around 14mm occurred at the east part of the bridge which has two small span in Y direction (Figure 5.19 and Figure 5.20). As shown in obtained results under G+Q+Ex load case, the results obtained from both models have good agreement with each other.

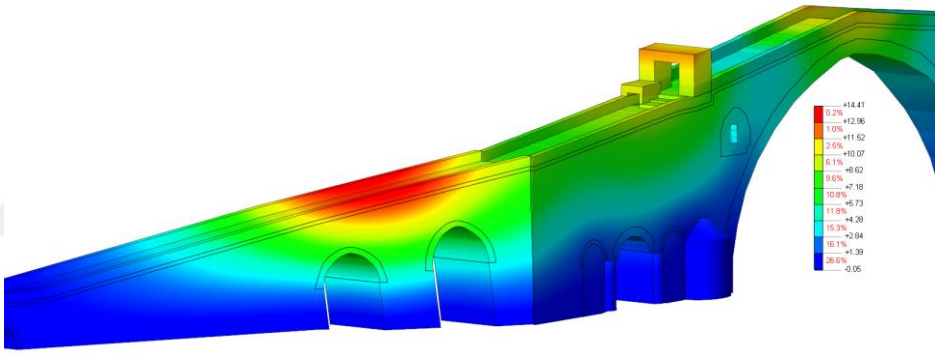

Figure 5.19 : The longitudinal displacement (DtY) (mm) under G+Q+Ex load case, model with fine mesh.

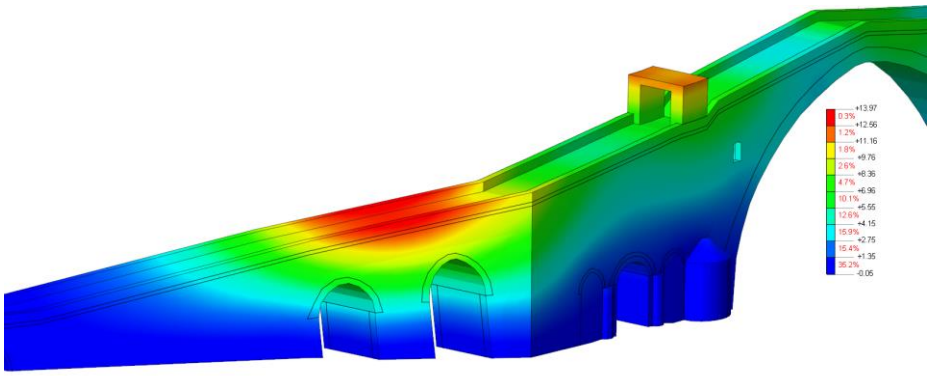

Figure 5.20 : The longitudinal displacement (DtY) (mm) under G+Q+Ex load case, model with coarse mesh.

The tension and compression stresses (SZZ) were around 2MPa and 0.7MPa for both models. The range of the tension and compression stresses were same for both models

to determine differences between them. The highest tension stress occurred at the pier which is located between two arches of east side of bridge as seen in figure 5.21 to figure 5.23. In G+Q+Ex case, the shear stress (SZX) fluctuated between 1MPa to -0.1MPa mostly on the spandrels (Figure 5.24 and Figure 5.25). Furthermore, the maximum span of the bridge from the west side gives the maximum values for SZX shear stress. However, the shear stress of other spans varied from zero to 0.4MPa.

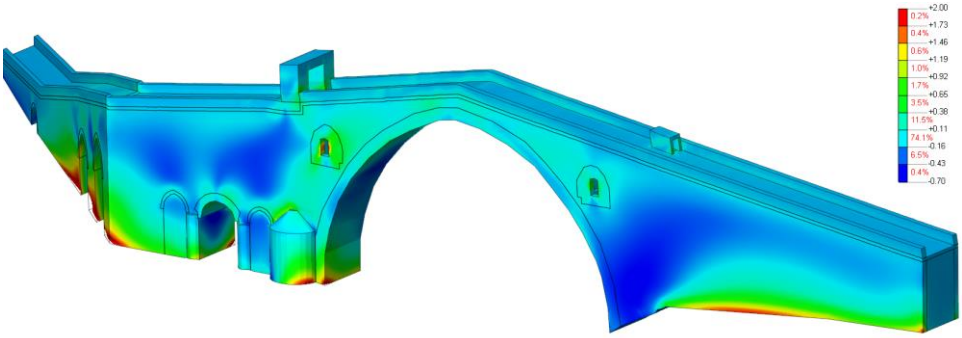

Figure 5.21 : Vertical stress distribution (SZZ) under G+Q+Ex load case (Scale 2MPa /-0.7MPa), model with fine mesh, downstream.

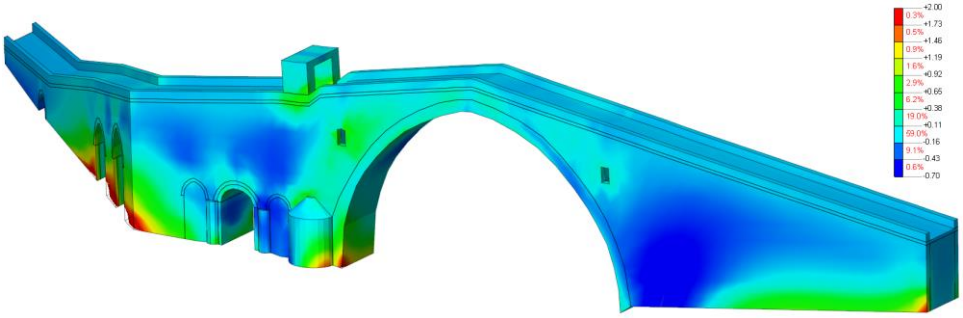

Figure 5.22 : Vertical stress distribution (SZZ) under G+Q+Ex load case (Scale 2MPa /-0.7MPa), model with coarse mesh, downstream.

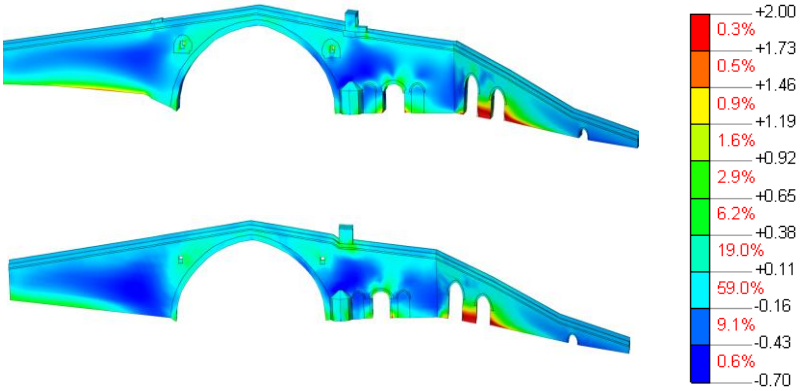

Figure 5.23 : Vertical stress distribution (SZZ) under G+Q+Ex load case(Scale 2MPa /-0.7MPa), the models with fine and coarse meshes, upstream.

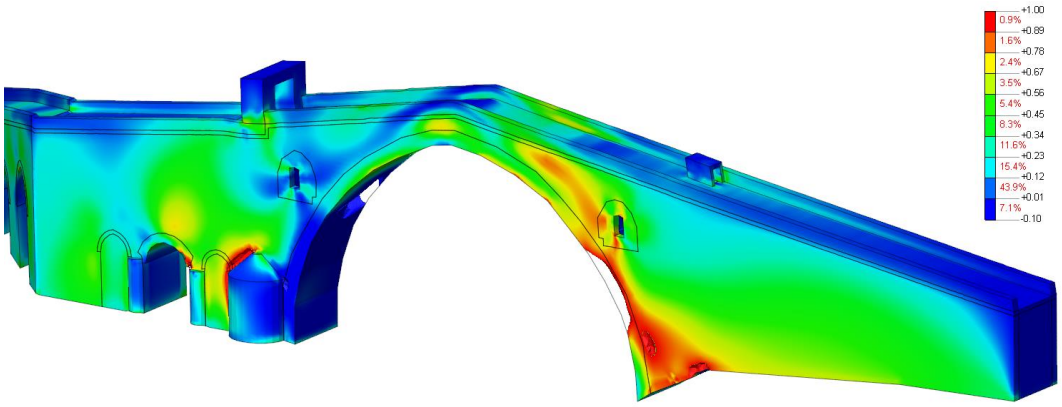

Figure 5.24 : SZX Shear stress distribution under G+Q+Ex load case, (Scale: 1MPa/ 0.1MPa), model with fine mesh.

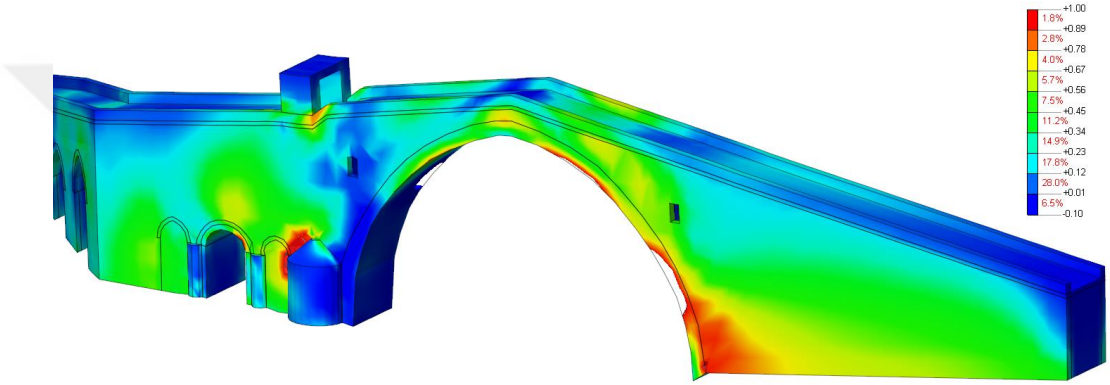

Figure 5.25 : SZX Shear stress distribution under G+Q+Ex load case, (Scale: 1MPa/ 0.1Mpa), model with coarse mesh.

Under G+Q+Ey load case, the maximum longitudinal displacement (DtY), which was around 96mm and 98mm for both models with fine and coarse meshes, respectively, was at the top of the parapet upper maximum span. Both models have close displacements in Y direction under G+Q+Ey load case as seen in figure 5.26 and figure 5.27.

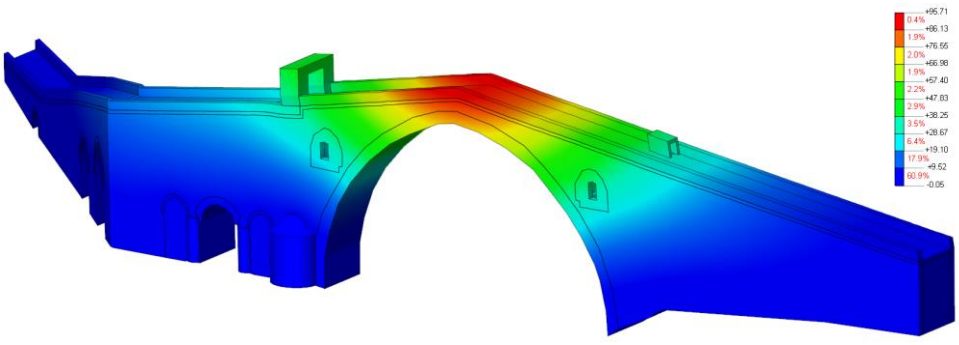

Figure 5.26 : The longitidunal displacement (DtY) (mm) under G+Q+Ey load case, model with fine mesh.

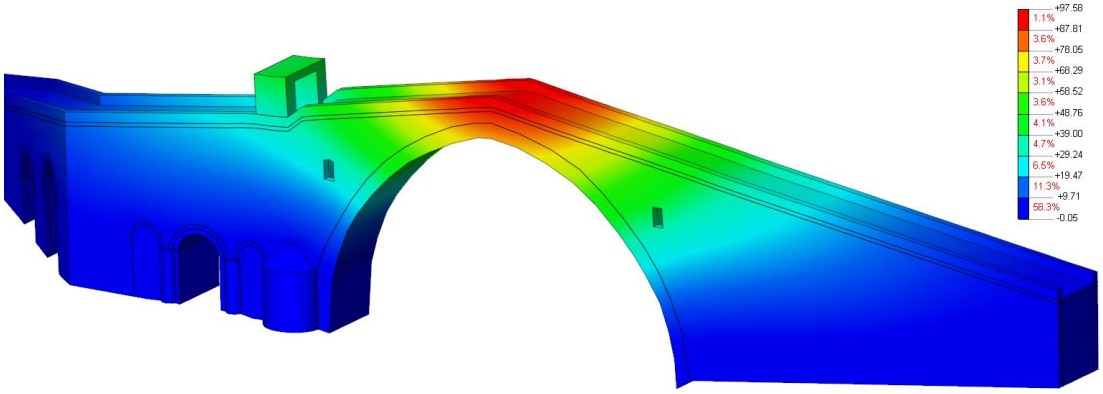

Figure 5.27 : The longitidunal displacement (DtY) (mm) under G+Q+Ey load case, model with coarse mesh.

The maximum tensile stress under G+Q+Ey load case was 3.0MPa. However, according to the results, the majority part of the spandrel walls were exposed tensile stresses which were higher than 0.3MPa as seen between in figure 5.28 to figure 5.31.

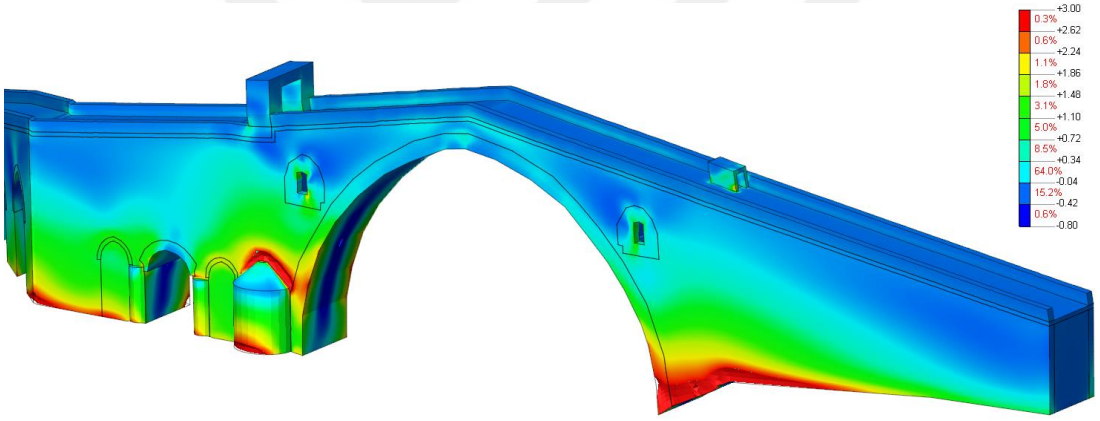

Figure 5.28 : Vertical stress distribution (SZZ) under G+Q+Ey load case (Scale 3MPa /-0.8MPa), model with fine mesh, downstream.

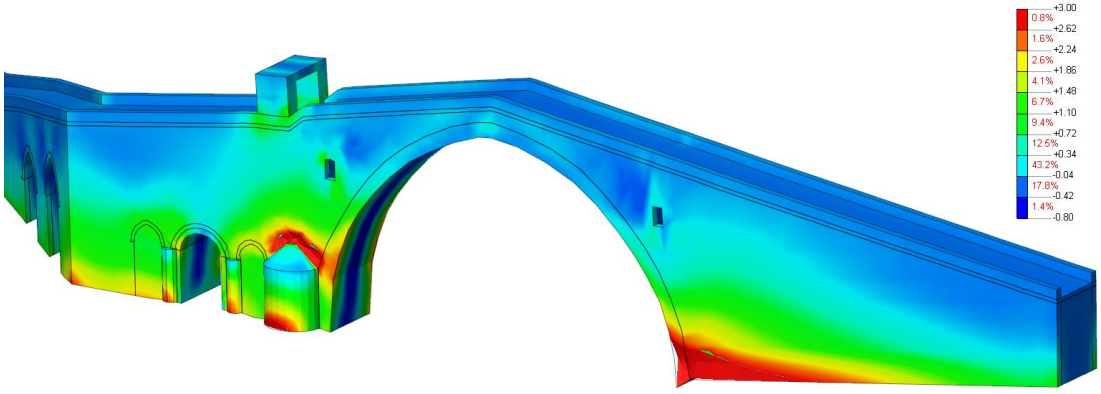

Figure 5.29 : Vertical stress distribution (SZZ) under G+Q+Ey load case (Scale 3MPa /-0.8MPa), model with coarse mesh, downstream.

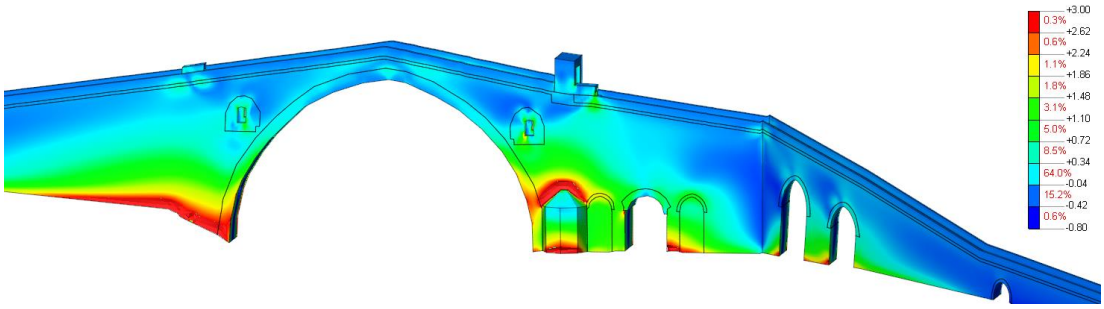

Figure 5.30 : Vertical stress distribution (SZZ) under G+Q+Ey load case (Scale 3MPa /-0.8MPa), model with fine mesh, upstream.

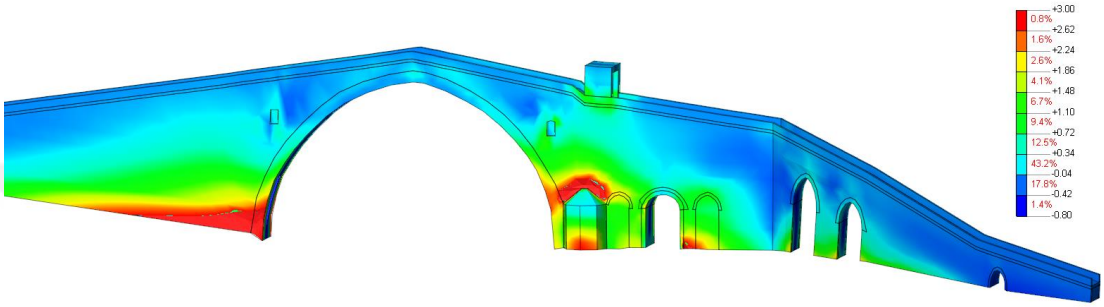

Figure 5.31 : Vertical stress distribution (SZZ) under G+Q+Ey load case (Scale 3MPa /-0.8MPa), model with coarse mesh, upstream.

The maximum tensile stress (SZZ) were located at the piers. The stresses accumulated at that pier. The flood splitter also had the maximum tension stresses at the connection point. The main arch had the peak compression stress as 0.8MPa on the both sides of the arches bottom (Figure 5.32). SZX shear stress shown in figure 5.33 and figure 5.34 comes up to 2MPa level at the west side of the main arch.

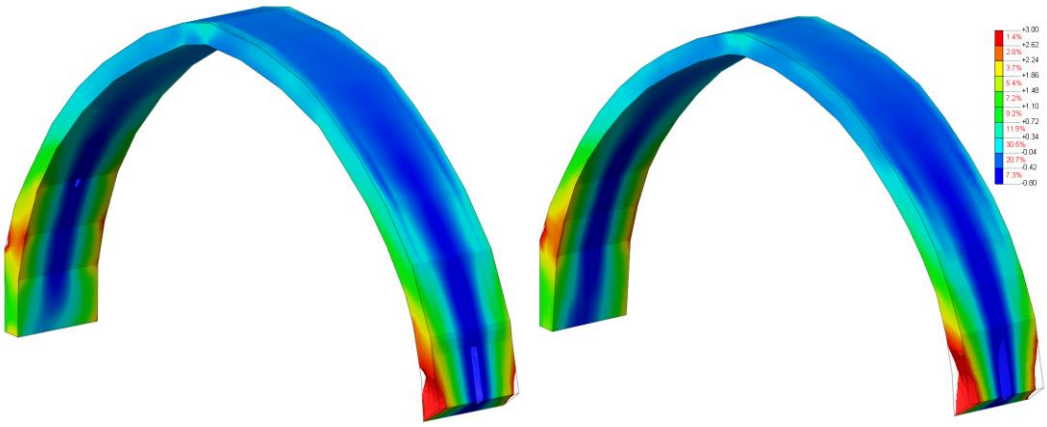

Figure 5.32 : Vertical stress distribution (SZZ) under G+Q+Ey load case (Scale 3MPa /-0.8MPa), model with fine and coarse meshes, maximum span of bridge.

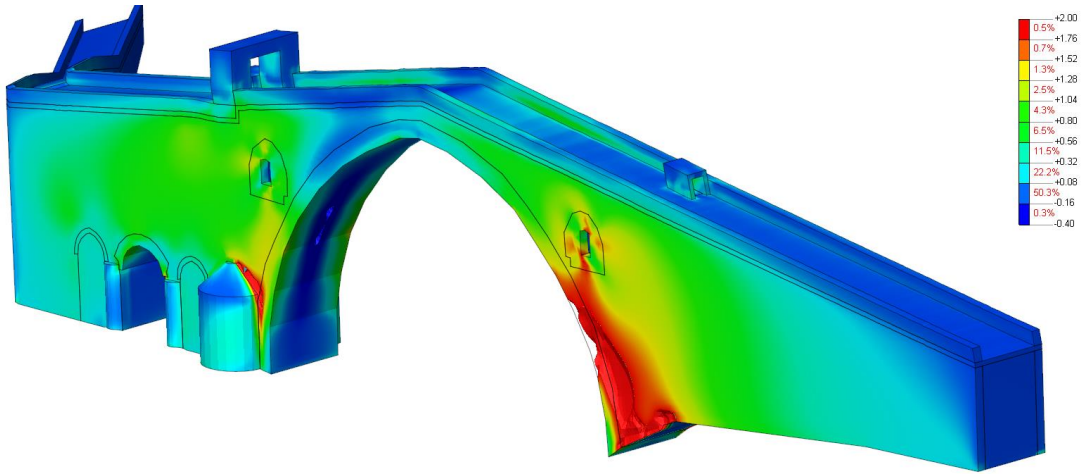

Figure 5.33 : SZX Shear stress distribution under G+Q+Ey load case, (Scale: 2MPa/ -0.4MPa), model with fine mesh.

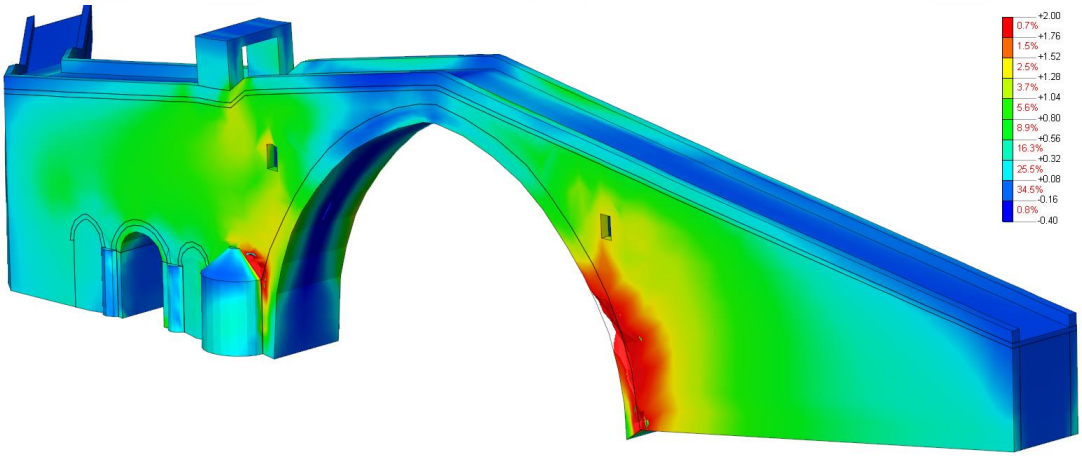

Figure 5.34 : SZX Shear stress distribution under G+Q+Ey load case, (Scale: 2MPa/ -0.4MPa), model with coarse mesh.

The results obtained from two different models with different mesh sizes were compared with each other. The distribution of the normal and shear stresses were discussed for the same scale. The differences of the results within the same scale are shown in table 5.5 and table 5.6.

Table 5.5 : The differences between displacement results of the models with fine and coarse meshes for Malabadi Bridge.

Displacements	Fine Mesh	Coarse Mesh	Difference of Displacements	Load Case
DtX	14.93mm	14.9mm	0%	G+Q+EX Load Case
DtY	95.71mm	97.58mm	2%	G+Q+EY Load Case

Table 5.6 : The differences between stress results of the models with fine and coarse meshes for Malabadi Bridge.

Normal and Shear Stresses	Global maximum stresses under 2 different load cases		Global minimum stresses under 2 different load cases		Percentage of stress distribution under g+q+ex load case for 2 different model approaches			Percentage of stress distribution under g+q+ey load case for 2 different model approaches		
	Under G+Q+Ex Load Case	Under G+Q+Ey Load Case	Under G+Q+Ex Load Case	Under G+Q+Ey Load Case	Fine Mesh	Coarse Mesh	Distribution of fine and coarse meshes	Fine Mesh	Coarse Mesh	Distribution of fine and coarse meshes
SXX	2.00MPa	4.00MPa	-0.10MPa	-0.10MPa	98.7	96.1	-3%	98.5	94	-5%
SYY	0.50MPa	0.50MPa	-0.10MPa	-0.10MPa	98.3	96	-2%	97.8	93.1	-5%
SZZ	2.00MPa	2.50MPa	-0.20MPa	-0.10MPa	94.4	90.6	-4%	99.4	97.1	-2%
SXY	0.50MPa	1.50MPa	0MPa	0MPa	97.1	94.2	-3%	98.3	96.2	-2%
SYZ	0.70MPa	1.00MPa	0MPa	0MPa	94.7	93.2	-2%	97.2	95.7	-2%
SZX	1.00MPa	1.00MPa	0MPa	-0.20MPa	93.9	88.9	-6%	95.1	91.5	-4%

5.1.3 Papaz Bridge

Papaz Bridge is the shortest one within the case studies. Hence, the obtained results for natural frequency are logical when compare with the other bridge due to resemblance of the material properties used in analysis process. The first frequencies of the Papaz Bridge are 20.55Hz for the model with fine mesh and 20.84 Hz for the model with coarse mesh. The modal frequencies belong to first eight modes are shown in Table 5.7. The deformed shapes obtained from free vibration analysis can be seen in figure 5.35.

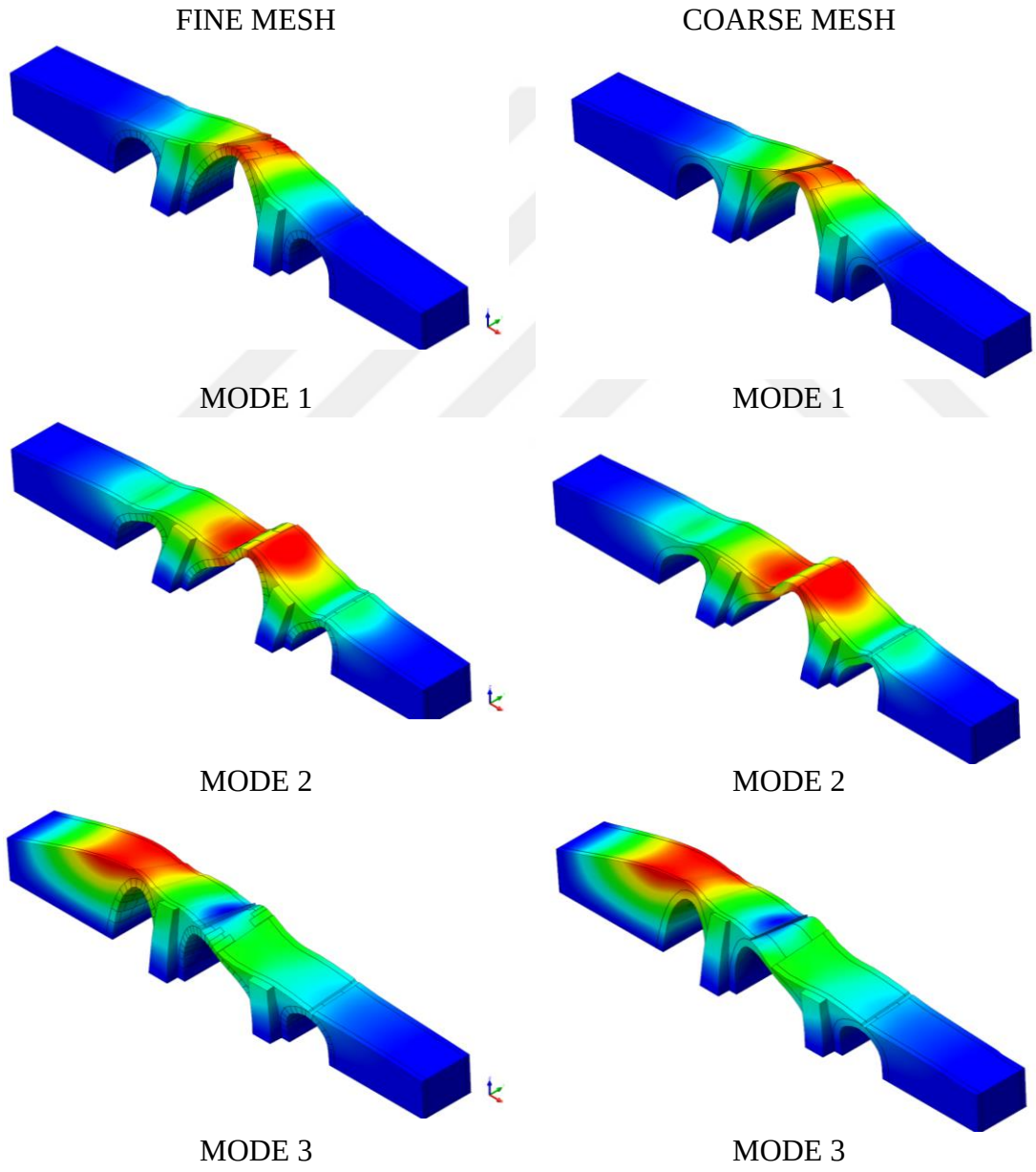

Figure 5.35 : Modal deformed shapes of Papaz Bridge, the models with fine and coarse meshes, respectively.

Table 5.7 : Modal frequencies of Papaz Bridge.

Mode shape	1	2	3	4	5	6	7	8
Fine Mesh-f (Hz)	20.55	21.02	24.34	26.58	27.3	28.9	32.1	36.9
Coarse Mesh-f (Hz)	20.84	21.21	24.54	26.8	27.58	29.14	32.47	37.29
Differences	-1%	-1%	-1%	-1%	-1%	-1%	-1%	-1%

The displacement was 0.8mm in X direction at the top of the central arch under G+Q+Ex load case for both models (Figure 5.36 and Figure 5.37). These results were associated with the rigid structure in spite of the high deformation level on bridge. The maximum tensile and compression stresses (SZZ) were around 0.2MPa.

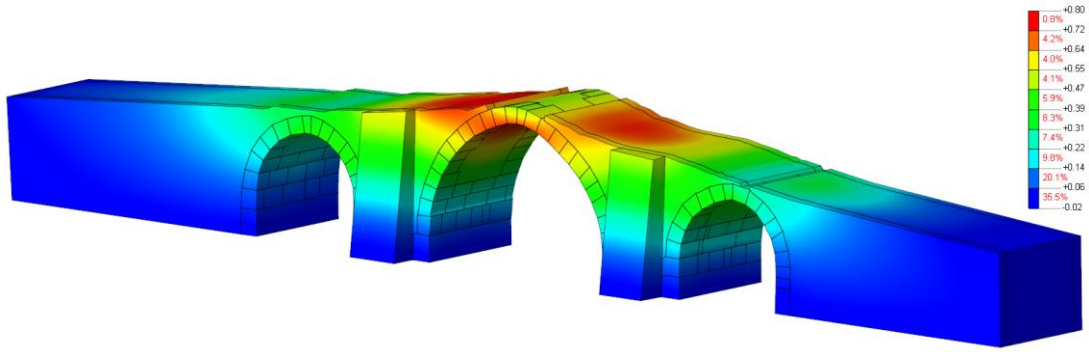

Figure 5.36 : The transversal displacement (DtX) (mm) under G+Q+Ex load case, the models with fine mesh.

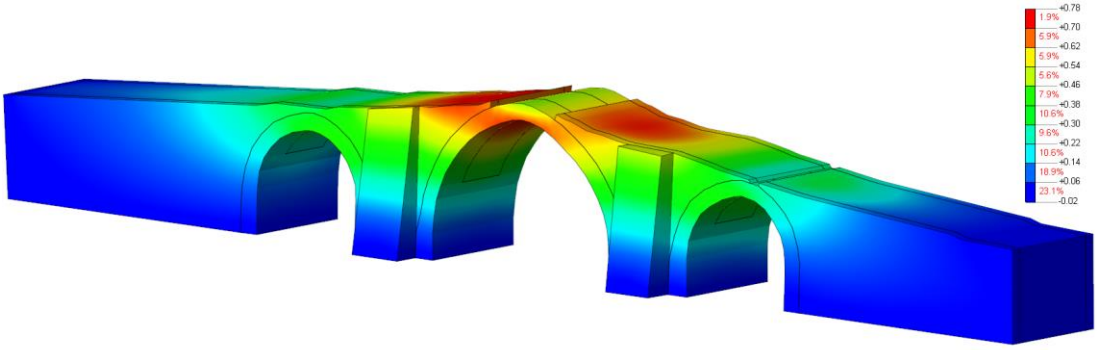

Figure 5.37 : The transversal displacement (DtX) (mm) under G+Q+Ex load case, the models coarse mesh.

The maximum tensile stress was mostly found at the level of springer stones and the bottom of buttresses (Figure 5.38 and Figure 5.39).

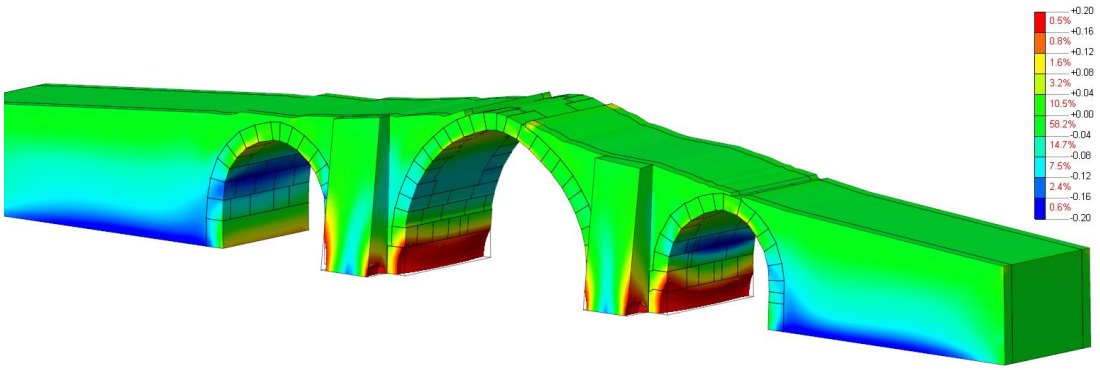

Figure 5.38 : Vertical stress distribution (SZZ) under G+Q+Ex load case (Scale 0.2MPa /-0.2MPa), model with fine mesh.

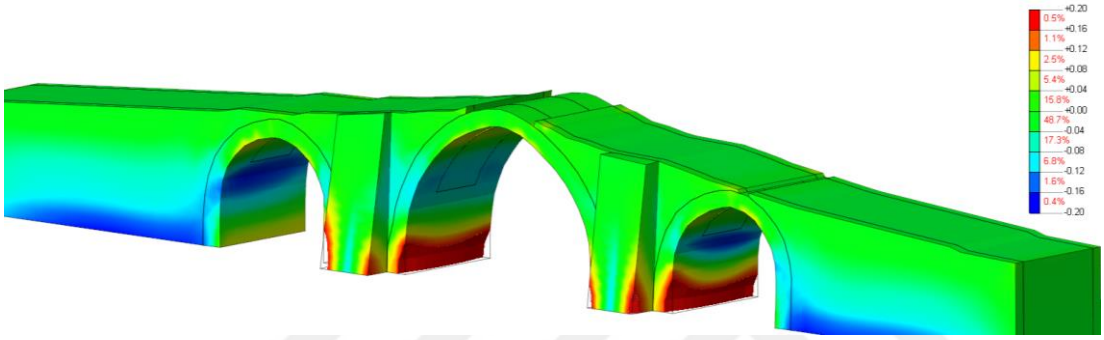

Figure 5.39 : Vertical stress distribution (SZZ) under G+Q+Ex load case (Scale 0.2MPa /-0.2MPa), model with coarse mesh.

Under G+Q+Ey load case, maximum longitudinal displacement (DtY) was 1mm at the top of the key stone for both models (Figure 5.40 and Figure 5.41). The maximum tensile stress (SZZ) located on the buttresses. Besides, the maximum compression stress (SZZ) occurred at the bottom level of the vaults as seen in figure 5.42 and figure 5.43.

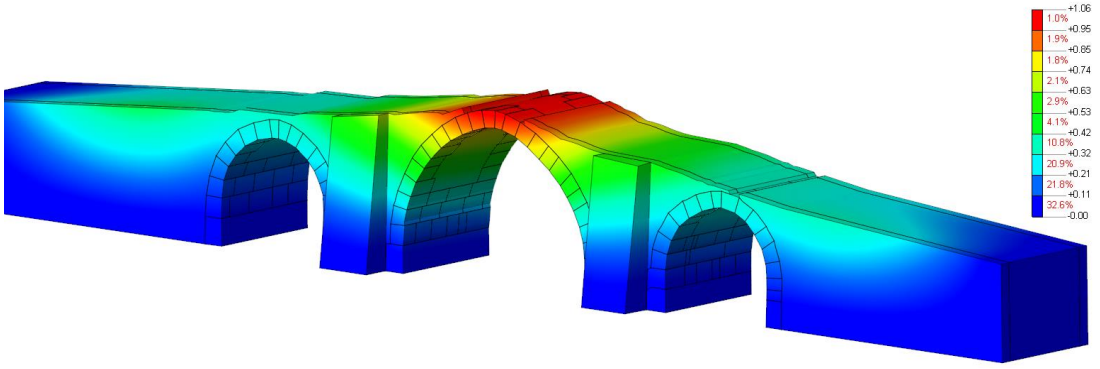

Figure 5.40 : The longitudinal displacement (DtY) (mm) under G+Q+Ey load case, the models with fine mesh.

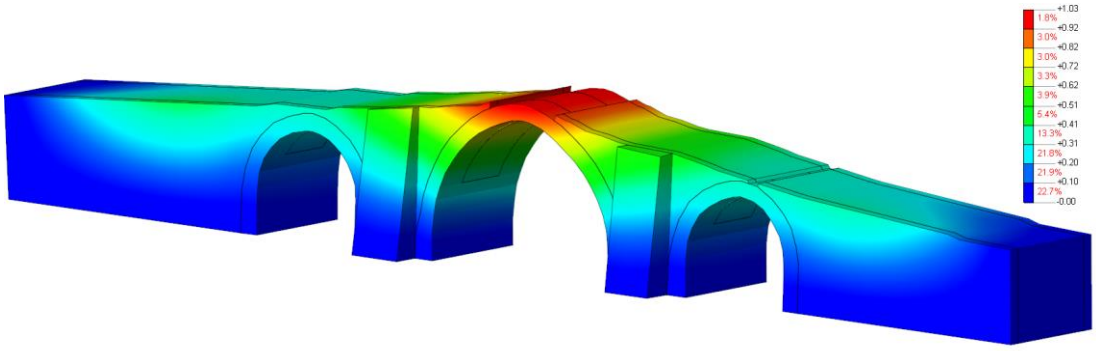

Figure 5.41 : The longitudinal displacement (DtY) (mm) under G+Q+Ey load case, the models with coarse mesh.

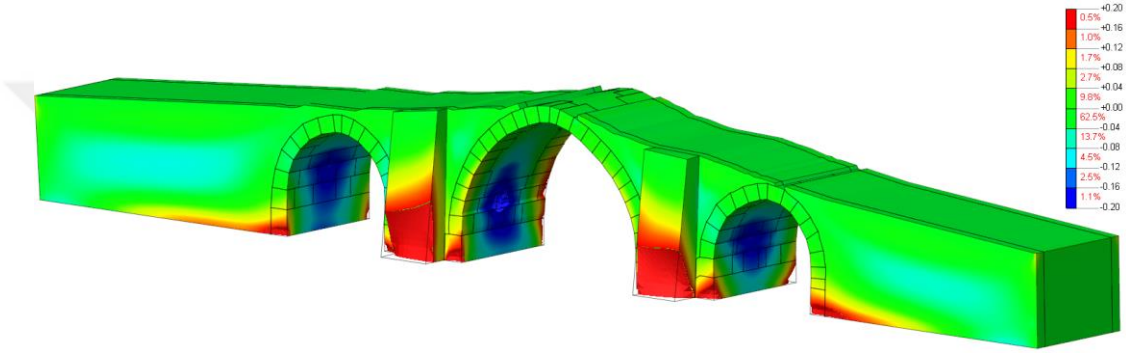

Figure 5.42 : Vertical stress distribution (SZZ) under G+Q+Ey load case(Scale 0.2MPa /-0.2MPa), model with fine mesh.

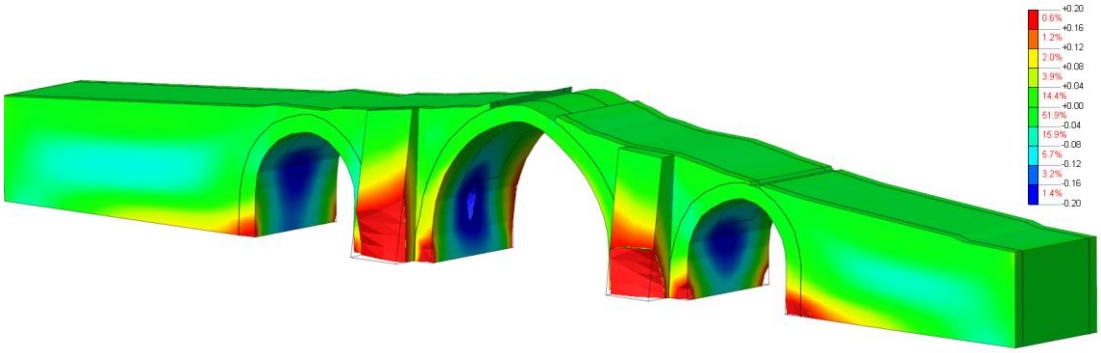

Figure 5.43 : Vertical stress distribution (SZZ) under G+Q+Ey load case (Scale 0.2MPa /-0.2MPa), model with coarse mesh.

The shear stress reached up maximum 0.24MPa level. This peak level occurred at the connection between buttress and spandrel wall. Especially, peak level can be seen at the level of vanished flood splitter. The invisible part of the results given in figure 5.44 and figure 5.45 demonstrate the extracted part of shear stress which is bigger than 0.2MPa and smaller than 0MPa. The differences of the results within the same scale are shown in table 5.8 and table 5.9.

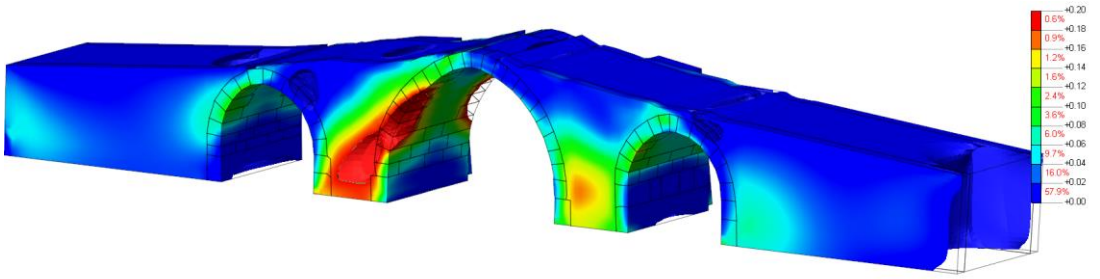

Figure 5.44 : SZX Shear stress distribution under G+Q+Ey load case, (Scale: 0.2MPa/ 0.0MPa), model with fine mesh.

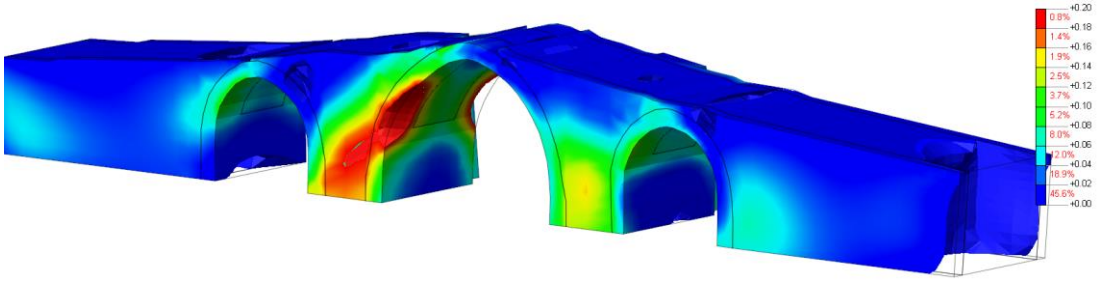

Figure 5.45 : SZX Shear stress distribution under G+Q+Ey load case, (Scale: 0.2MPa/ 0MPa), model with coarse mesh.

Table 5.8 : The differences between displacement results of the models with fine and coarse meshes for Papaz Bridge.

Displacements	Fine Mesh	Coarse Mesh	Difference of Displacements	Load Case
DtX	0.8mm	0.78mm	-9%	G+Q+EX Load Case
DtY	1.06mm	1.03mm	8%	G+Q+EY Load Case

5.1.4 Sinanlı-Alpullu Bridge

The natural frequencies of the Sinanlı-Alpullu bridge models with fine and coarse meshes are 7.8Hz and 8Hz. The deformed shapes obtained from free vibration analysis can be seen in figure 5.46 for both models. The frequencies of first eight modes are given in table 5.10. The difference of the modal frequencies of two models with fine and coarse meshes does not exceed 10%. In addition, the deformed shapes of the models are close to each other for first three modes.

Table 5.9 : The differences between stress results of the models with fine and coarse meshes for Papaz Bridge.

Normal and Shear Stresses (MPa)	**Global maximum stresses under 2 different load cases**		**Global minimum stresses under 2 different load cases**		**Percentage of stress distribution under g+q+ex load case for 2 different model approaches**			**Percentage of stress distribution under g+q+ey load case for 2 different model approaches**		
	Under G+Q+Ex Load Case	Under G+Q+Ey Load Case	Under G+Q+Ex Load Case	Under G+Q+Ey Load Case	Fine Mesh	Coarse Mesh	Difference between stress distribution of fine and coarse meshes	Fine Mesh	Coarse Mesh	Difference between stress distribution of fine and coarse meshes
SXX	0.40	0.10	-0.02	-0.05	96.3	92.9	-4%	98.8	97.8	-1%
SYY	0.10	0.50	-0.02	-0.02	97.9	95	-3%	99.1	98.6	-1%
SZZ	0.25	0.20	-0.10	-0.10	93.1	92.8	0%	95.2	93	-2%
SXY	0.04	0.50	-0.01	0	98.1	97.2	-1%	98.9	98.9	0%
SYZ	0.06	0.25	-0.01	0	96.3	98.1	2%	93.4	93.9	1%
SZX	0.20	0.25	-0.02	-0.03	96.5	95.4	-1%	97.8	96.6	-1%

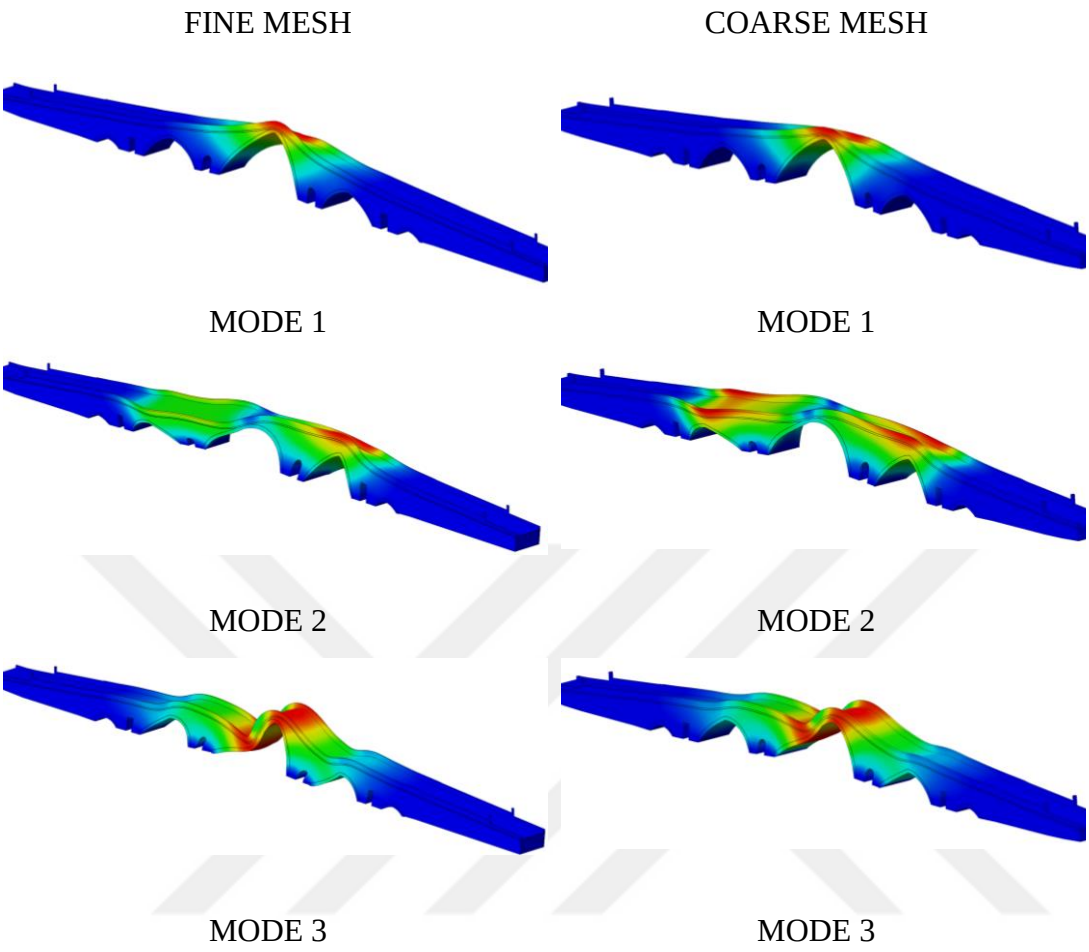

Figure 5.46 : Modal deformed shapes of Sinanlı-Alpullu Bridge, respectively.

Table 5.10 : Modal frequencies of Sinanlı-Alpullu Bridge.

Mode shape	**1**	**2**	**3**	**4**	**5**	**6**	**7**	**8**
Fine Mesh f (Hz)	7.8	9.9	10.2	10.8	13.3	13.9	14.8	15.5
Coarse Mesh f (Hz)	8.0	10.7	11.0	11.4	13.9	14.9	15.3	16.9
Differences	-3%	-8%	-8%	-6%	-5%	-7%	-4%	-9%

The displacement of the bridge under the G+Q+Ex load case was obtained 1.36mm and 1.12mm for the models created fine and coarse meshes (Figure 5.47 and Figure 5.48). After removed localized stress values, the most intense stress distribution (SZZ) varies between 0MPa/ -0.5MPa under G+Q+Ex load case (Figure 5.49 and Figure 5.50). According to this distribution, tensile stress had ignorable percentage within the

vertical stress (SZZ). The bridge had compression stress which located mainly around the bottom side of the spans.

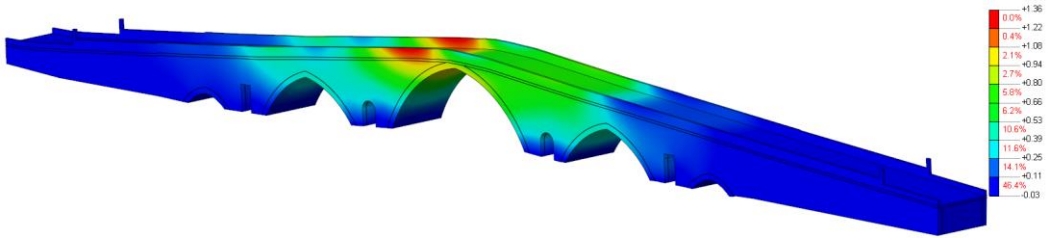

Figure 5.47 : The transversal displacement (DtX) (mm) under G+Q+Ex load case, the models with fine mesh.

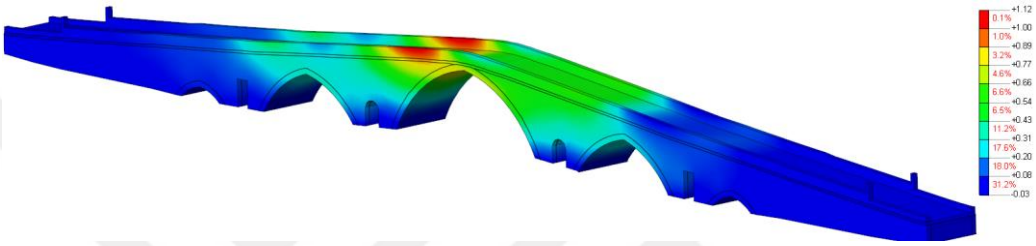

Figure 5.48 : The transversal displacement (DtX) (mm) under G+Q+Ex load case, the models with coarse mesh.

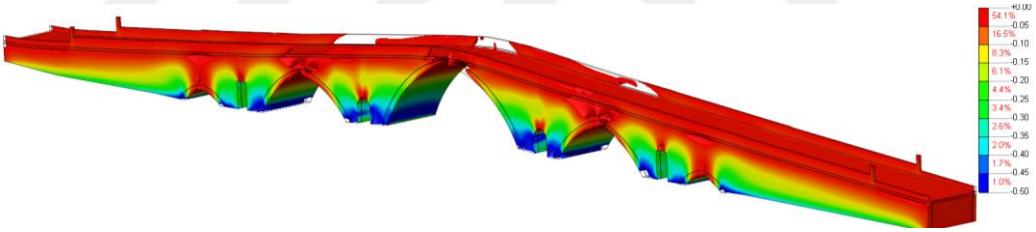

Figure 5.49 : Vertical stress distribution (SZZ) under G+Q+Ex load case (Scale 0MPa /-0.5MPa), model with fine mesh.

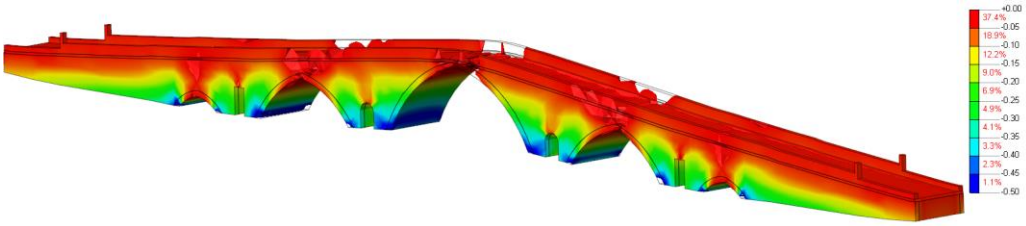

Figure 5.50 : Vertical stress distribution (SZZ) under G+Q+Ex load case (Scale 0MPa /-0.5MPa), model with coarse mesh.

Under G+Q+Ey load case, obtained results were as expected. Maximum longitudinal displacements (DtY) were 2.85mm and 2.55mm at the top of the maximum span for both models (Figure 5.51 and 5.52). The vertical stress (SZZ) reached up maximum 0.5MPa compression stress as seen in figure 5.53 and figure 5.54.

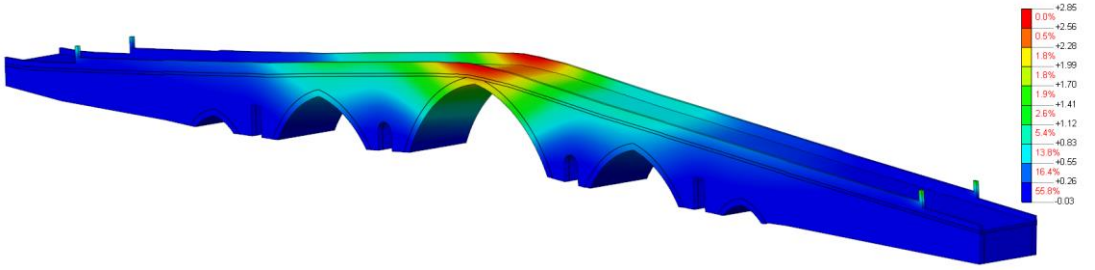

Figure 5.51 : The longitudinal displacement (DtY) (mm) under G+Q+Ey load case, the models with fine mesh.

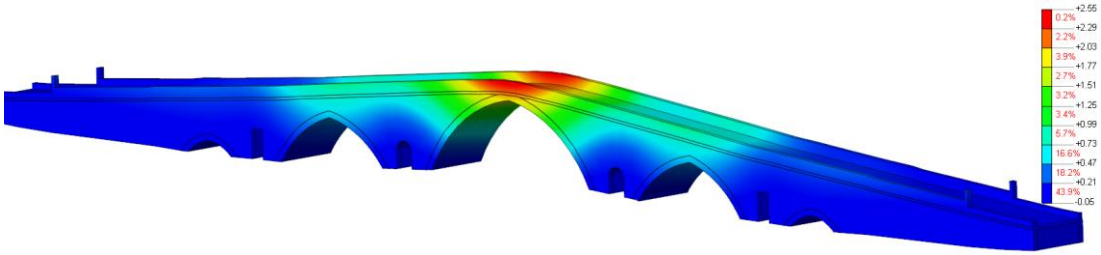

Figure 5.52 : The longitudinal displacement (DtY) (mm) under G+Q+Ey load case, the models with coarse mesh.

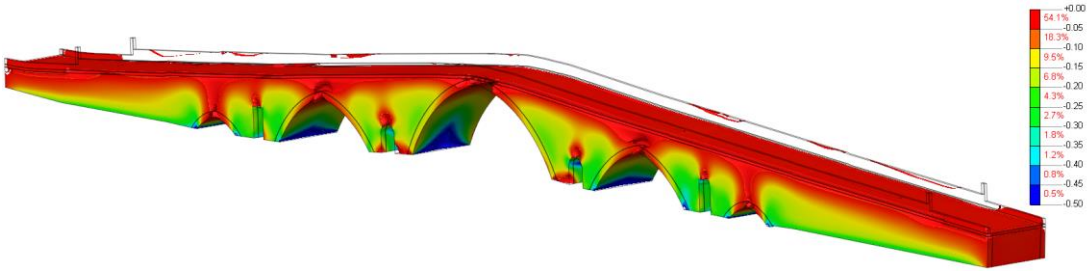

Figure 5.53 : Vertical stress distribution (SZZ) under G+Q+Ey load case (Scale 0MPa /-0.5MPa), model with fine mesh.

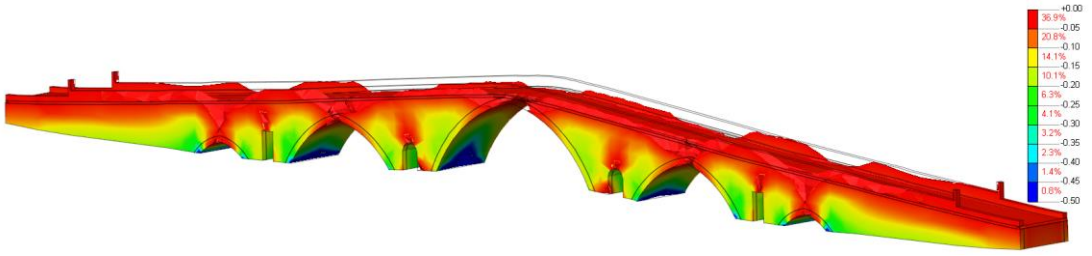

Figure 5.54 : Vertical stress distribution (SZZ) under G+Q+Ey load case (Scale 0MPa /-0.5MPa), model with coarse mesh.

The shear stress (SZX) reached the maximum 0.5MPa at the main arch (Figure 5.48 and Figure 5.49). The stress distribution of the west side and east side of the bridge was the same due to its symmetric geometry. The differences of the results within the same scale are shown in table 5.11 and table 5.12.

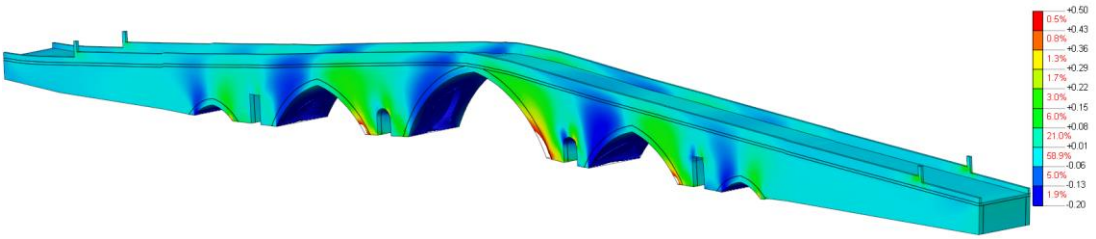

Figure 5.55 : SZX Shear stress distribution under G+Q+Ey load case, (Scale: 0.2MPa/ 0MPa), model with coarse mesh.

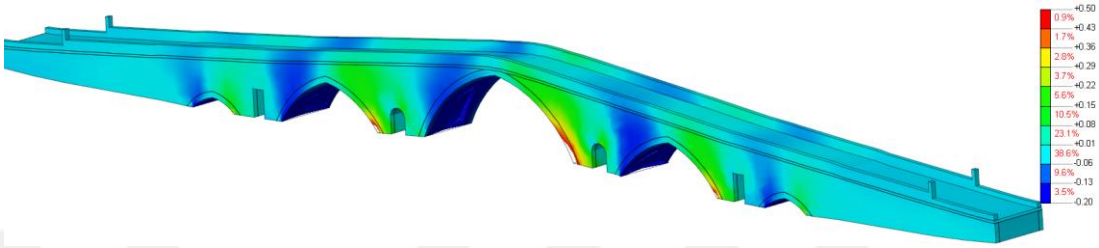

Figure 5.56 : SZX Shear stress distribution under G+Q+Ey load case, (Scale: 0.2MPa/ 0MPa), model with coarse mesh.

Table 5.11 : The differences between displacement results of the models with fine and coarse meshes for Sinanlı-Alpullu Bridge.

Displacements	Fine Mesh	Coarse Mesh	Difference of Displacements	Load Case
DtX	1.36mm	1.12mm	-21%	G+Q+EX Load Case
DtY	2.85mm	2.55mm	-12%	G+Q+EY Load Case

5.2 Nonlinear Static Analysis

Nonlinear static analysis named as push over analysis was performed to estimate structural behavior by applying a constant gravity load that was increased step by step. According to the Turkish Seismic Code, 2007 before application of incremental load pattern, a nonlinear static analysis should be conducted. The results of nonlinear static analysis can be considered as the initial conditions of the push over analysis (Turkish Seismic Code, 2007). Applied load should be proportional to the vibration mode type of the primary (dominant in the seismic direction) (Turkish Seismic Code, 2007).

Table 5.12 : The differences between stress results of the models with fine and coarse meshes for Sinanlı-Alpullu Bridge.

Normal and Shear Stresses	Global maximum stresses under 2 different load cases		Global minimum stresses under 2 different load cases		Percentage of stress distribution under g+q+ex load case for 2 different model approaches			Percentage of stress distribution under g+q+ey load case for 2 different model approaches		
	Under G+Q+Ex Load Case	Under G+Q+Ey Load Case	Under G+Q+Ex Load Case	Under G+Q+Ey Load Case	Fine Mesh	Coarse Mesh	Difference between stress distribution of fine and coarse meshes	Fine Mesh	Coarse Mesh	Difference between stress distribution of fine and coarse meshes
SXX	0.20MPa	0.10MPa	-0.20MPa	-0.30MPa	96.3	91.9	-5%	97.1	94.2	-3%
SYY	0.10MPa	0.50MPa	-0.10MPa	-0.20MPa	97	93.1	-4%	99.9	99.7	0%
SZZ	0MPa	0.10MPa	-0.80MPa	-0.60MPa	94.3	83.7	-13%	99.7	99.3	0%
SXY	0.03MPa	0MPa	-0.03MPa	-0.10MPa	96.5	92.4	-4%	90.4	88.2	-2%
SYZ	0.02MPa	0.10MPa	-0.02MPa	-0.02MPa	94.5	89.5	-6%	96	94.8	-1%
SZX	0.20MPa	0.10MPa	-0.20MPa	-0.30MPa	94.4	88.3	-7%	99.8	99.4	0%

Within the scope of this study, pushover analyses were performed with the DIANA nonlinear static algorithm on the selected bridges. Same material properties were selected to determine the influence of the geometric properties on the results. The influence of the geometric properties was determined according to the pushover curves which was created for randomly selected control node which is located at the facade on the top of the maximum span of the bridges. The pushover curves of selected bridges obtained with the Total Strain Based Cracked material model for control nodes of selected bridges as seen in Figure 5.57. The pushover curves were formed according to the ratio of base shear to weight (V/W) versus the ratio of displacement to height (d/h) of the selected nodes.

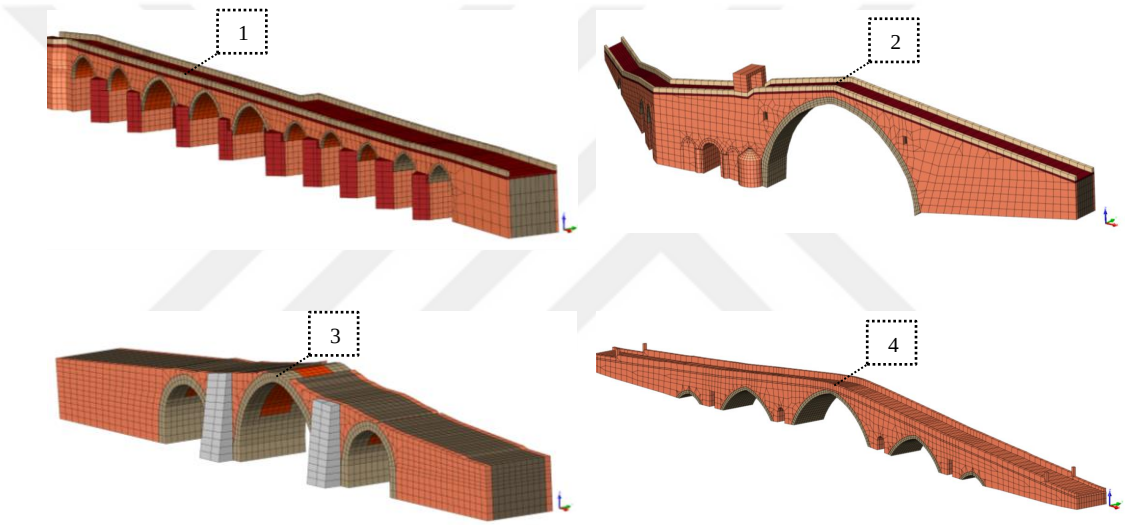

Figure 5.57 : Control nodes of nonlinear static analysis.

Dicle Bridge gave maximum drift ratio (d/h) as 0.003 under maximum base shear force that is 13% of the weight of the bridge. Malabadi Bridge also gave the maximum drift ratio as 0.012 with maximum base shear that is 9% of the weight of the Malabadi Bridge. Papaz Bridge gave the maximum drift capacity as 0.0025 under base shear that is the 62% of its weight.

The maximum drift ratio of Sinanlı-Alpullu is 0.006 under maximum base shear, which is 23% of its own weight. The pushover curves for all selected bridges discussed as sketched in Figure 5.58. According to the sketched pushover curves, Papaz Bridge is more rigid comparing to the others. It gives smallest drift ratio against highest V/W Ratio. At the drift ratio of 0.002 for each bridge, the V/W ratio of Papaz, Sinanlı-Alpullu, Dicle (On Gozlu) and Malabadi Bridge are 0.60, 0.19, 0.13 and 0.07,

respectively. This means that to occur same drift ratio, Papaz Bridge needs more force than the other bridges (Figure 5.58).

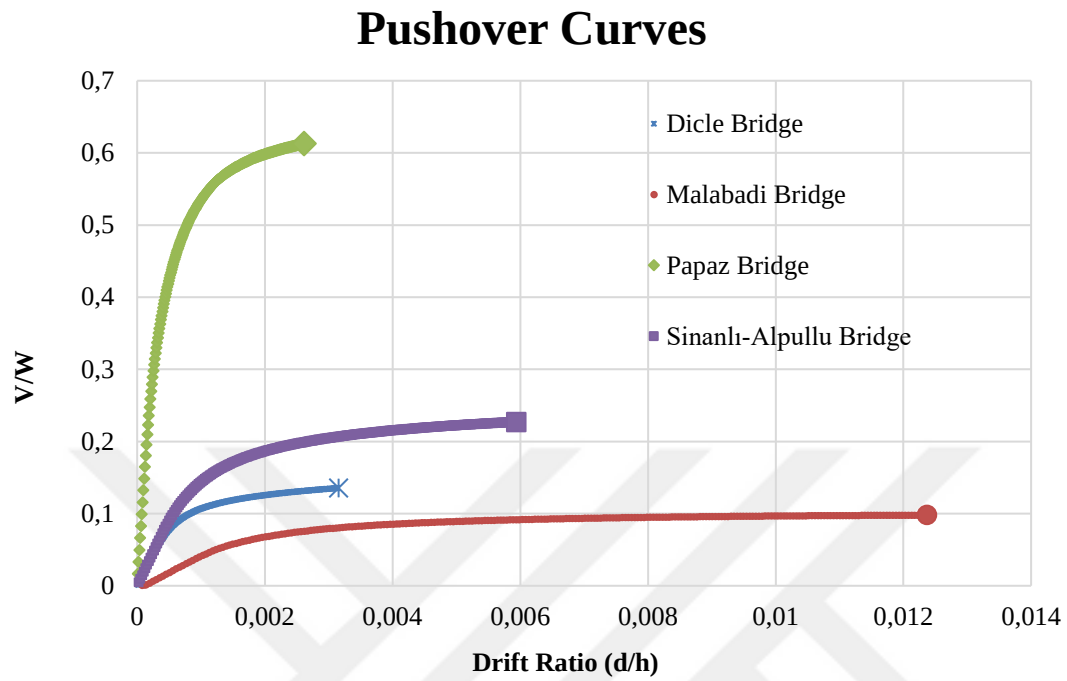

Figure 5.58 : Pushover curves with Total Strain Cracked Model.

Cracked elements were considered according to the principle tensile stress distribution. The crack percentage of the bridges and vaults were discussed with the increase of base shear force in figure 5.59 and figure 5.60.

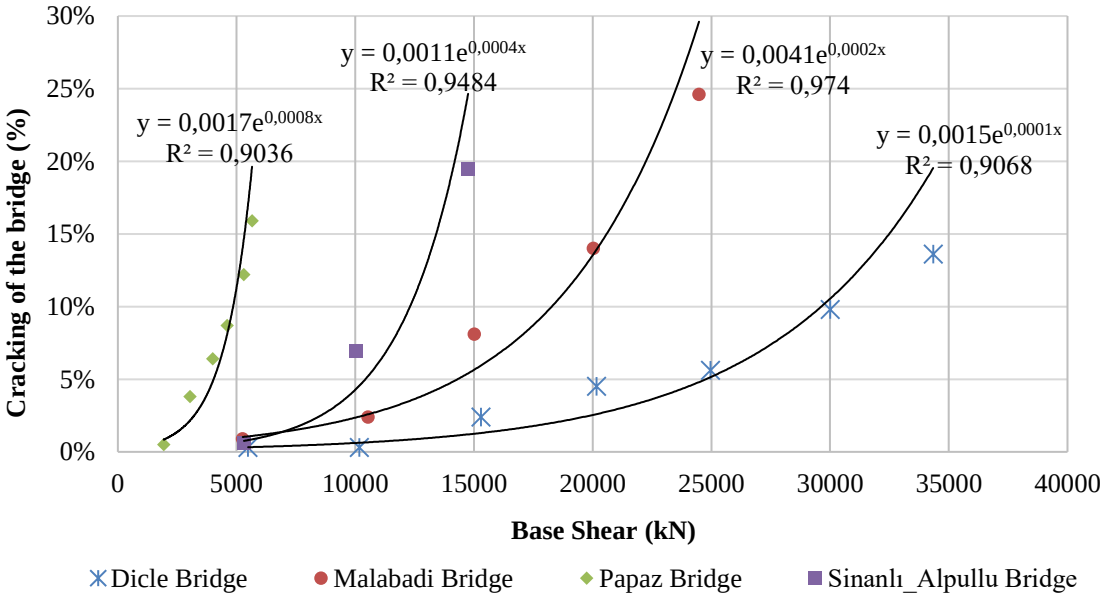

Figure 5.59 : % of cracked elements of the bridges in Y direction vs base shear.

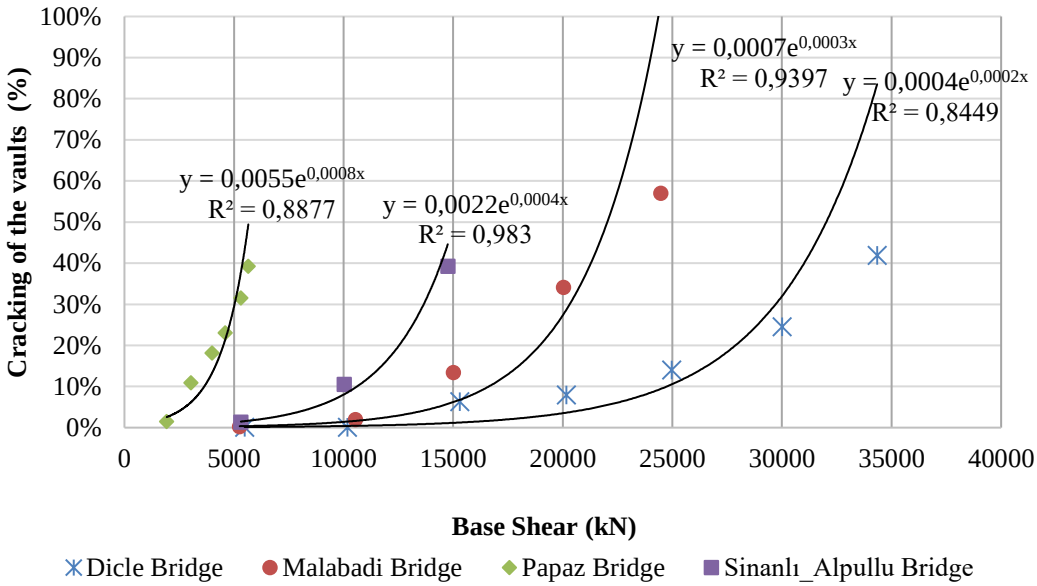

Figure 5.60 : % of cracked elements of the vaults in Y direction vs base shear.

The last convergence step which used to decide crack percentage finish the analysis when the bridge pass the threshold of the bearing capacity of the bridge. According to the obtained results, for approximately 5000kN base shear force, Dicle (On Gozlu), Malabadi, and Sinanlı-Alpullu bridges showed near-zero crack. However, Papaz Bridge's last convergence step was concluded under 5652kN. It showed maximum cracking of 16% at this last step. The reason of that Papaz Bridge has the shortest length and weight when compared the other three bridges. It gave the maximum cracking with the force, which is 60% of its weight. The cracking percentage increased exponentially by increasing of base shear.

To compare cracking of vaults, three spans of Papaz and Sinanlı Alpullu Bridges were investigated. However, Malabadi Bridge has the vaults with maximum span and its first mode shape is mainly located at this span. Thus, the pushover analysis was performed on transversal direction of bridge. This approach was also applied to Dicle (On Gozlu) Bridge as well. Three spans of the Dicle Bridge were taken account to understand cracking ratio of spans. As expected, Malabadi Bridge which has the maximum span within selected bridges, it gave the maximum cracking percentage at last convergence step of nonlinear static analysis. Although, the Dicle, Papaz and Sinanlı-Alpullu Bridges has different spans, they gave nearly same cracking at the last step of pushover analysis. However, base shear force are very different from each other to led to this cracking percentage which is shown in figure 5.60. By comparing

cracking results versus V/W ratio, the effects of the geometry were taken into account. The only assessment based on base shear force may lend to misevaluation. Malabadi, Dicle, Sinanlı-Alpullu and Papaz Bridges need the V/W ratio which are 0.09, 0.13, 0.20, and 0.58, respectively, to result in 15% cracking of bridge (Figure 5.61). The rigidity of the bridges can be lined up bigger than the smaller as Papaz, Sinanlı-Alpullu, Dicle and Malabadi Bridges. Under same V/W ratio, the bridges vaults show approximately 40% cracking on the vaults (Figure 5.62).

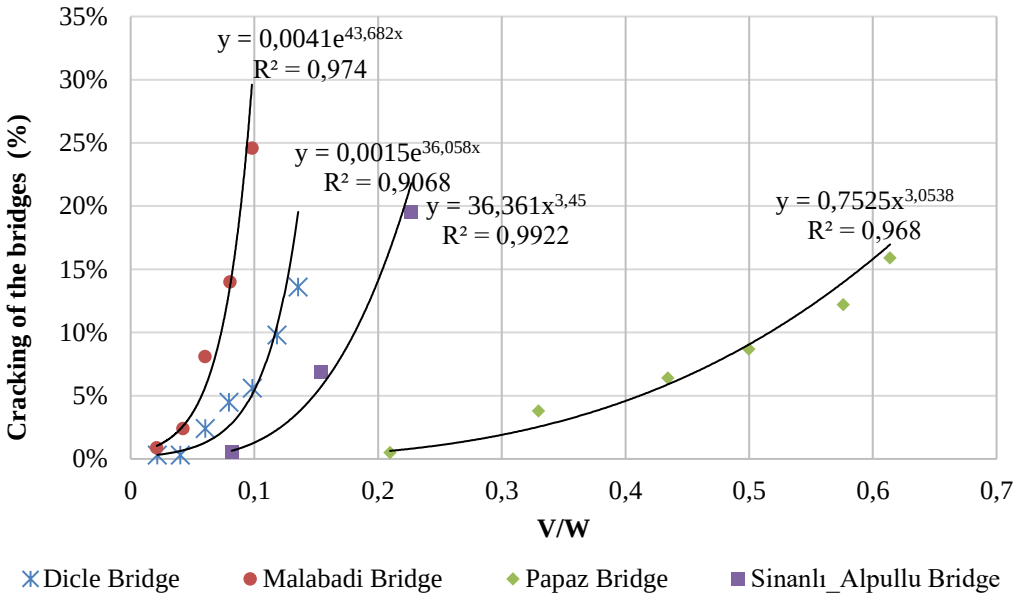

Figure 5.61 : % of cracked elements of the bridges in Y direction vs V/W ratio.

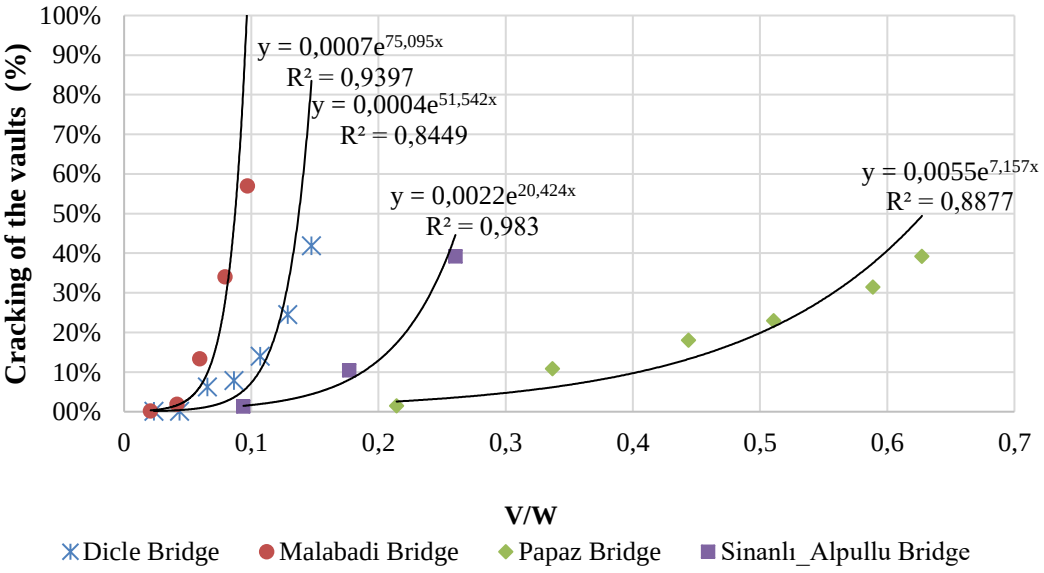

Figure 5.62 : % of cracked elements of the vaults in Y direction vs V/W ratio.

Crack patterns were obtained by assessing the tensile strength. According to the last convergence step, 13.6% of the Dicle (On Gozlu) Bridge was exceed the tensile strength of 0.3MPa (Figure 5.63). The pushover force was effective on the weak part of the bridge which has 6m width due to the first mode shape. Thus, the principle tensile stress distribution was mainly localized around the vaults that have bigger span. The main cracking occurred two sides of the three vaults, which have the bigger spans within ten spans. These three vaults showed 42% cracking on these three vaults (Figure 5.64).

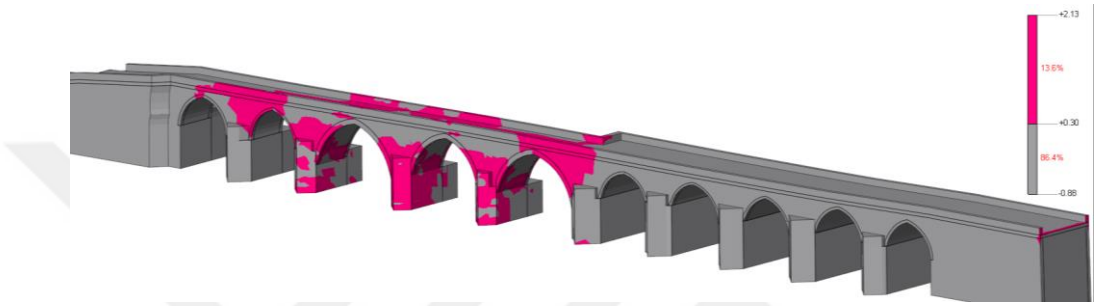

Figure 5.63 : Principle tensile stresses after last converged load-step (pink: ≥0.3MPa, Grey:<0.3MPa), upstream.

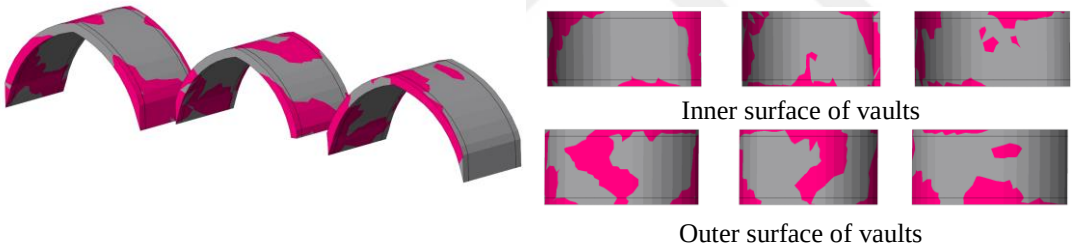

Figure 5.64 : Principle tensile stresses of the vaults after last converged load-step (pink: ≥0.3MPa, Grey:<0.3MPa).

At the last convergence step, 24.6% of the Malabadi Bridge was exceed the tensile strength of 0.3MPa (Figure 5.65 and Figure 5.66).

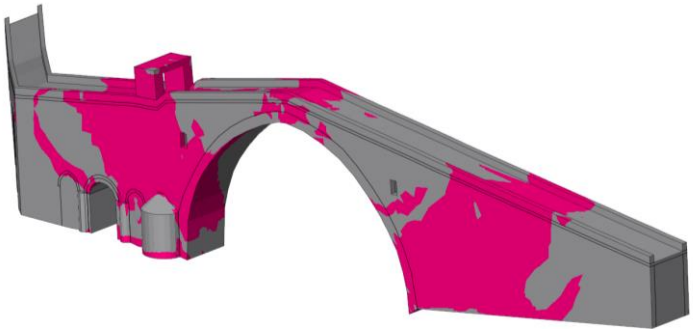

Figure 5.65 : Principle tensile stresses after last converged load-step (pink: ≥0.3MPa, Grey:<0.3MPa), downstream.

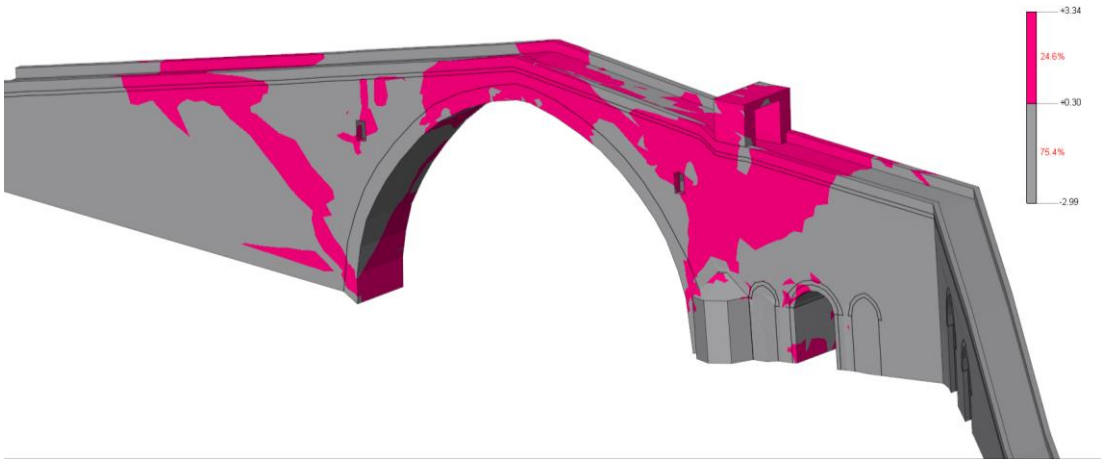

Figure 5.66 : Principle tensile stresses after last converged load-step (pink: ≥0.3MPa, Grey:<0.3MPa), upstream.

The main cracking occurred two sides of the part with maximum span. The gate of bridge also was damaged. The maximum span showed 57% cracking on the maximum span (Figure 5.67). At the level of key stone, almost all stones were passed the 0.3MPa of tensile strength. Therefore, tensile cracking was occurred at the key stones (Figure 5.67). The bridge has not symmetric geometry so the principle stress distribution is not completely symmetric. Papaz Bridge was cracked around 15.6% (Figure 5.68). The main cracking was observed on the spandrel wall of upstream. The short span near the both side of the middle maximum span cracked partially. The vault with brick was passed the threshold for tensile strength merely as seen in figure 5.69. The bridge is symmetric. Thus, observed principle stress distribution was symmetric.

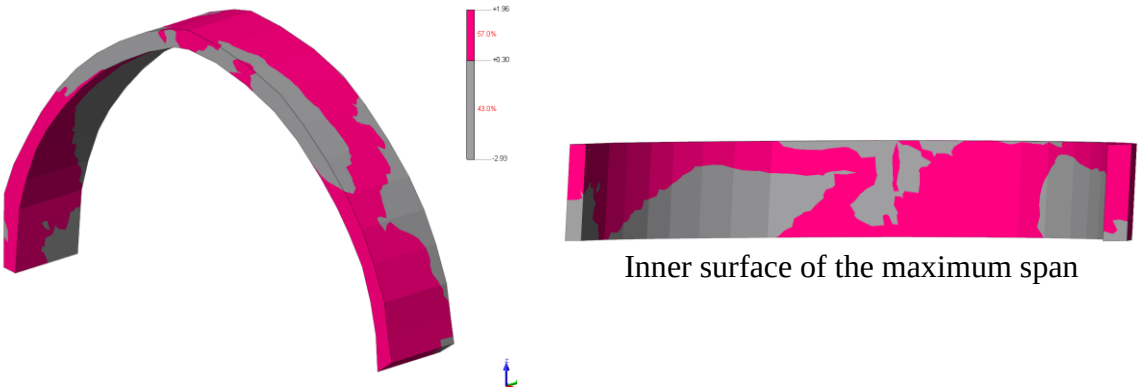

Figure 5.67 : Principle tensile stresses of the vaults after last converged load-step (pink:≥0.3MPa, Grey:<0.3MPa).

Sinanli-Alpullu Bridge was cracked around 19.5% (Figure 5.70). The main cracking was located around the spandrel wall both sides of middle span. The short span near

the both side of the middle maximum span gave tensile crossed cracking. Main three vaults showed 39.2% cracking. The possible locations of the cracking can be seen in figure 5.71.

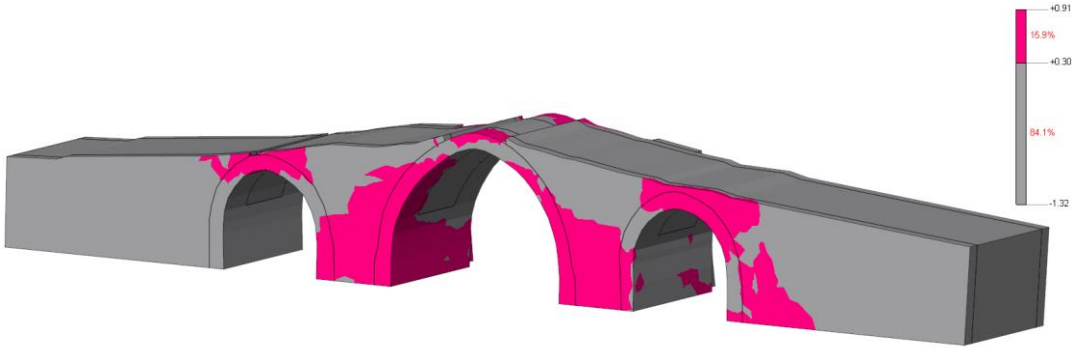

Figure 5.68 : Principle tensile stresses after last converged load-step (pink: ≥0.3MPa, Grey :< 0.3MPa).

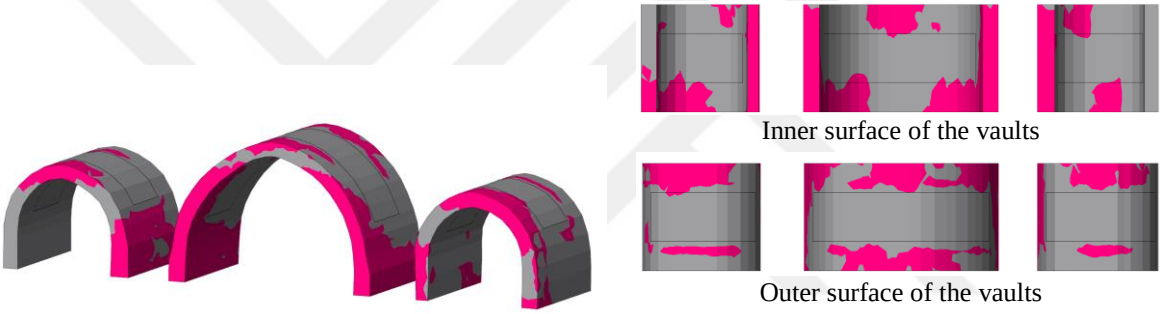

Figure 5.69 : Principle tensile stresses of the vaults after last converged load-step (pink: ≥0.3MPa, Grey:< 0.3MPa).

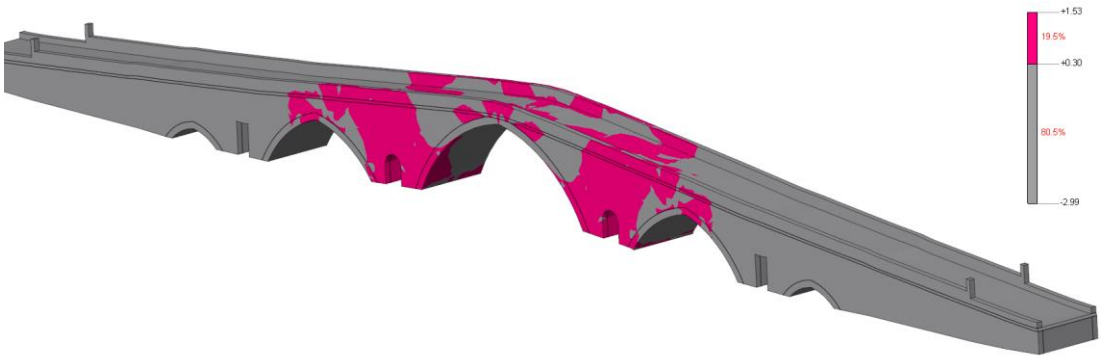

Figure 5.70 : Principle tensile stresses after last converged load-step (pink: ≥0.3MPa, Grey:<0.3MPa).

Obtained drift ratio from the last convergence step of pushover analysis was discussed according to the geometric properties of bridge. The assessment of geometrical properties was done with maximum capacity of drift ratio obtained from pushover analysis versus geometric dimensions. In figure 5.72, span and rise dimensions of the

maximum span of selected bridges were compared with the maximum capacity of drift ratio.

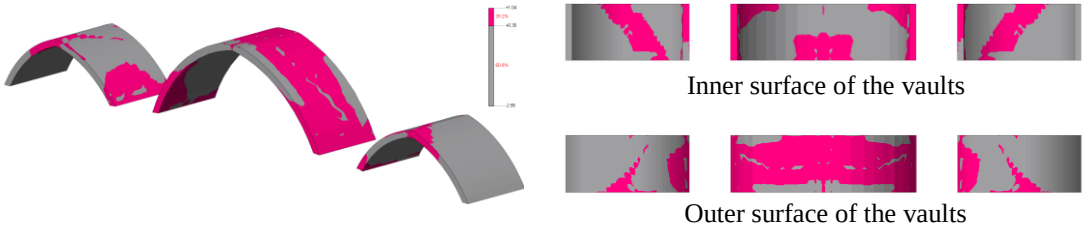

Figure 5.71 : Principle tensile stresses of the vaults after last converged load-step (pink: ≥0.3MPa, Grey:<0.3MPa).

The span, rise and thickness of the arches are directly proportional to the maximum drift ratio capacity (Figure 5.73). Span, rise and thickness parameters have been considered simultaneously to design of the arch bridges. Rise and thickness of the arch depend on the span. The width of the bridge also affects the drift ratio of selected bridges.

Applied force was stable for selected bridges, and with the stable force, which is 0.14g, drift ratios of selected bridges are given in figure 5.74. According to the obtained results, the Malabadi Bridge, which has the biggest span dimensions within selected bridges, gave the maximum drift ratio. Although the applied force was the same for selected bridge, the results in good agreement with increase of span due to the different weight of the selected bridges.

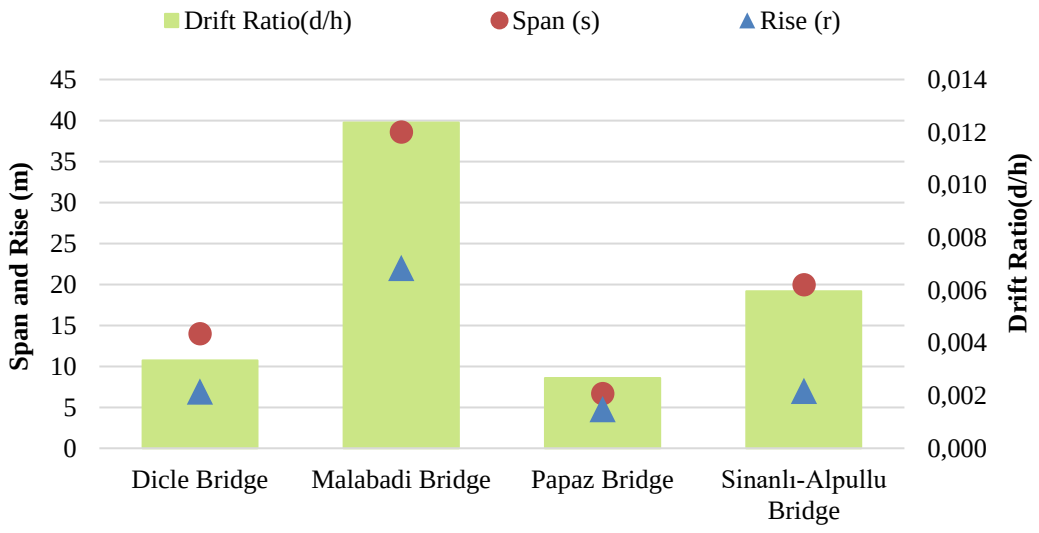

Figure 5.72 : Drift ratio vs span and rise dimensions of maximum span at the last convergence step of pushover analysis for selected bridges.

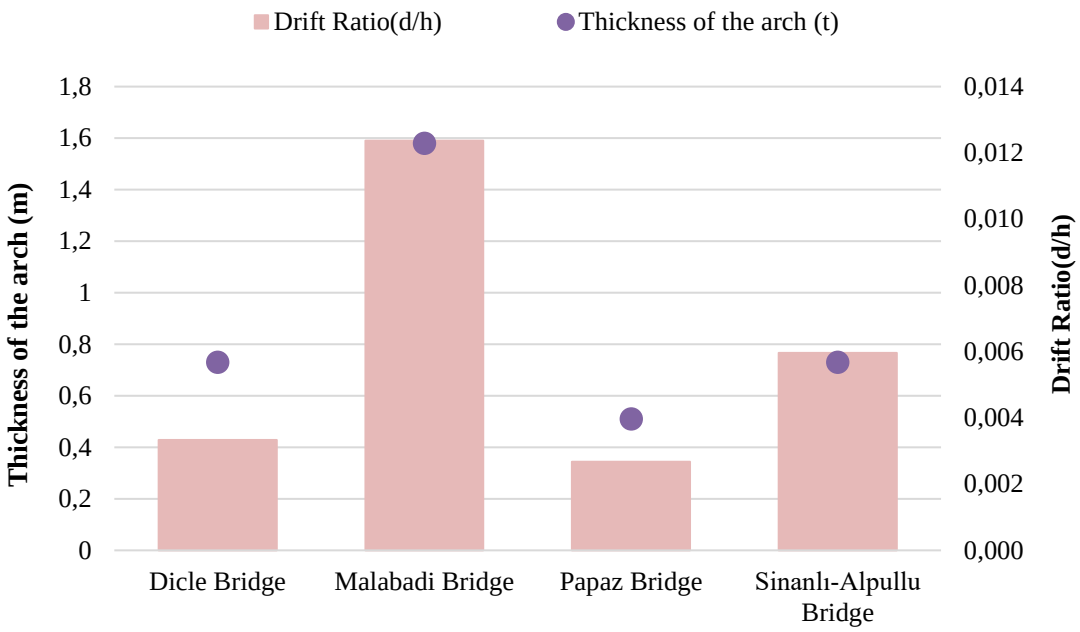

Figure 5.73 : Drift ratio vs thickness of the arch maximum span at the last convergence step of pushover analysis for selected bridges.

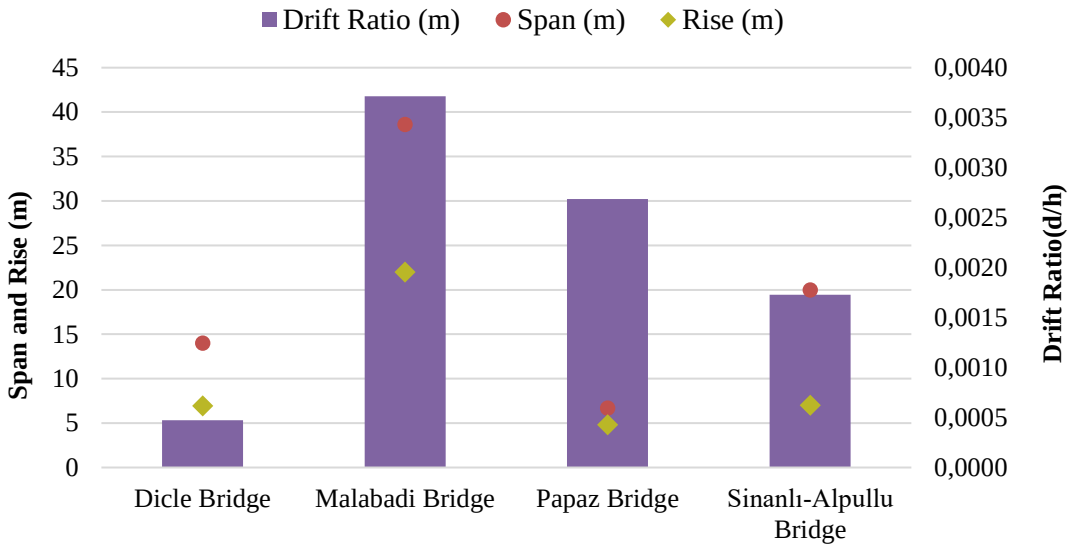

Figure 5.74 : Drift ratio vs span and rise dimensions of maximum span with same loading for selected bridges.

5.3 Nonlinear Dynamic Analysis

The FE model and material properties are the same with the nonlinear static analysis. Nonlinear dynamic analysis was conducted with real ground motion records. Nonlinear dynamic analysis gives more accurate results comparing to other seismic assessment methods (FEMA 440, 2005).

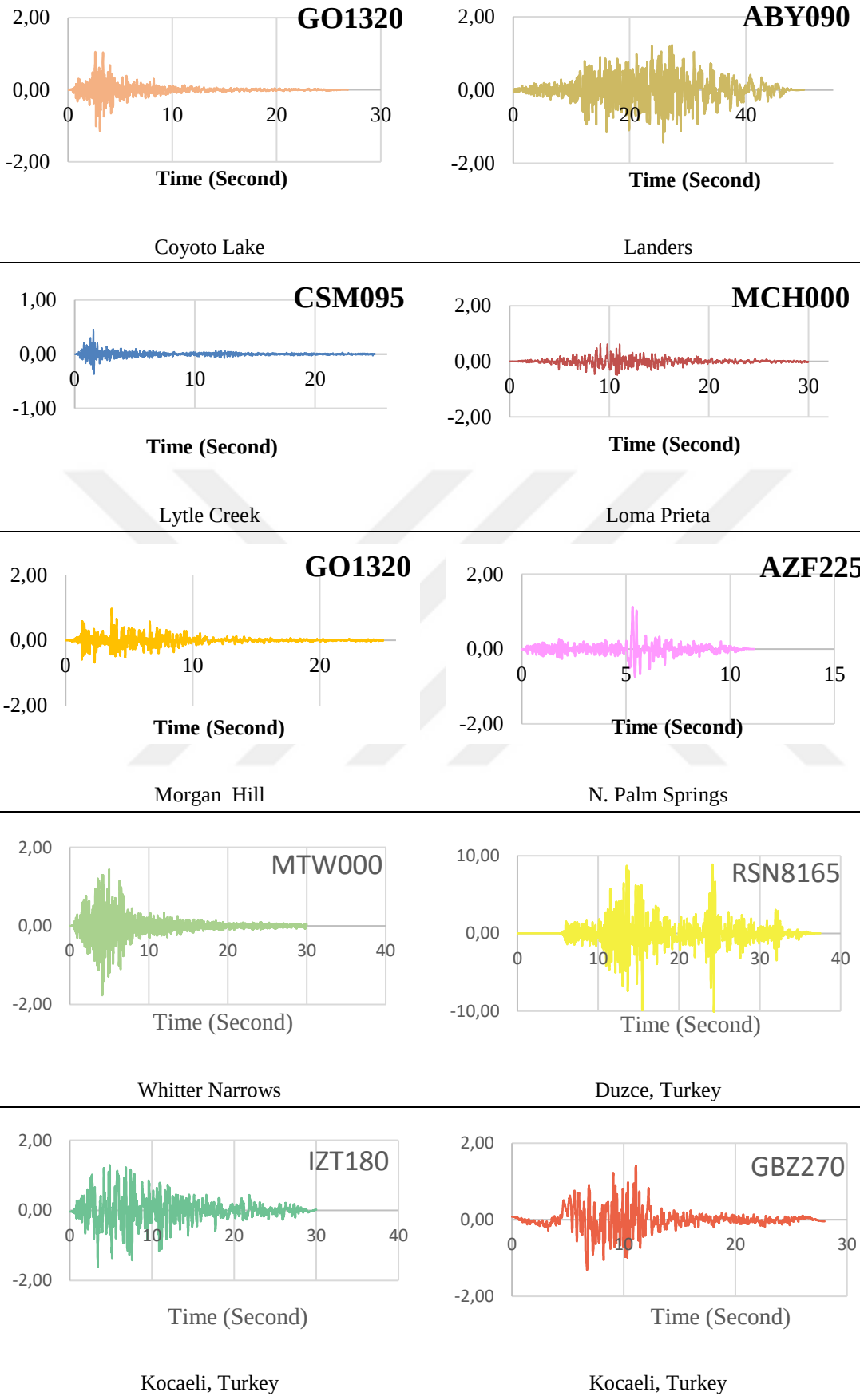

Figure 5.75 : Selected ground motion records graph, vertical axis shows acceleration (m/sec^2), and horizontal axis shows time (second).

According to the Turkish Seismic Code, in linear and nonlinear analysis, at least seven ground motion records have to be assessed to use average of the response quantities as the design value. Within the scope of the time history analyses, ten ground motion records were applied on selected bridges. Ten ground motion records for soil class A were given in figure 5.75. These ground motion records were applied in transversal direction (Y) of selected bridges. Obtained ratio of maximum base shear force to weight versus ratio of maximum displacement to height of the bridge were discussed. The displacements-time curve with ten ground motions are given in between figure 5.76 to figure 5.79 for selected bridges. Within ten ground motions, Duzce, Turkey earthquake has the maximum peak ground acceleration. The displacement obtained with Duzce, Turkey earthquake is the maximum comparing to other earthquakes as expected. The maximum displacement (top of the maximum span) obtained in nonlinear analysis of Dicle Bridge is 48mm and the corresponding acceleration is 0.001g (Figure 5.76).

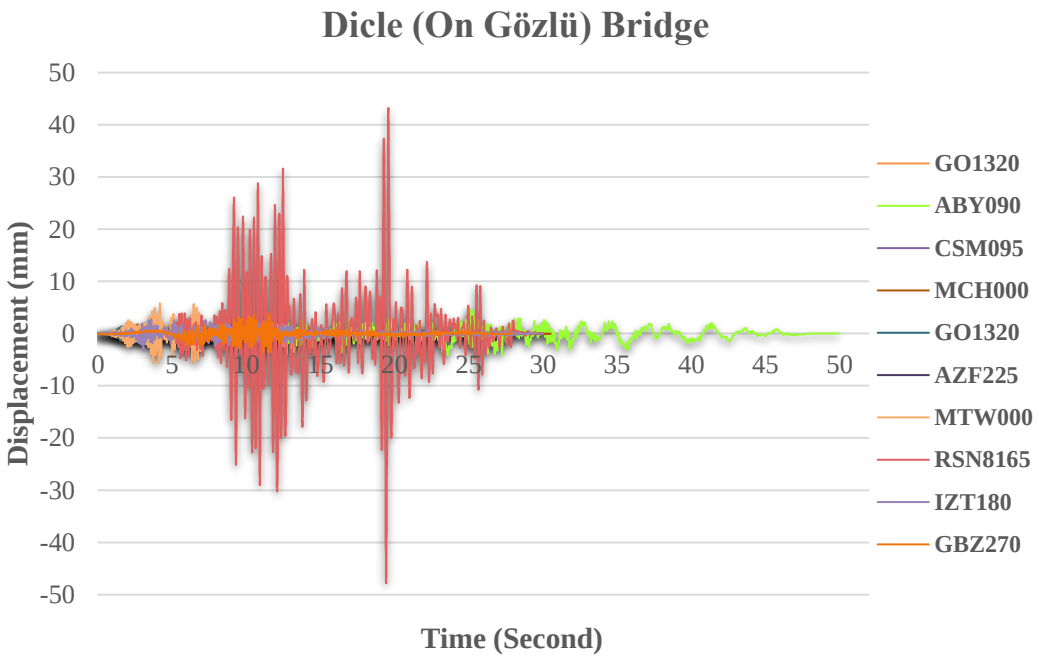

Figure 5.76 : Time-history of displacement of Dicle Bridge for nonlinear dynamic analyses of ten ground motion records.

The maximum displacement (top of the maximum span) obtained in nonlinear analysis of Malabadi Bridge is 79.9mm and the corresponding acceleration is 0.01g in Duzce, Turkey accelogram (Figure 5.77). The maximum displacement obtained in nonlinear

analysis of Papaz Bridge is 3.8mm and the corresponding acceleration is 0.002g with Lander accelerogram (Figure 5.78).

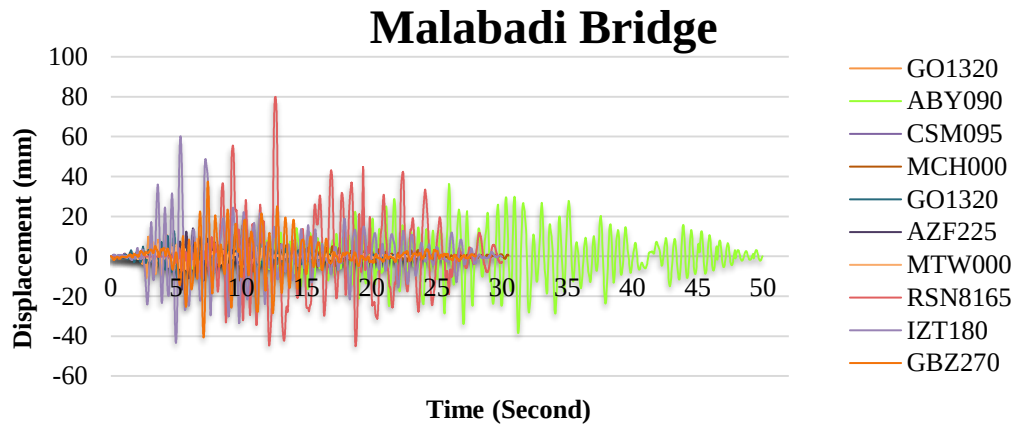

Figure 5.77 : Time-history of displacement of Malabadi Bridge for nonlinear dynamic analyses of ten ground motion records.

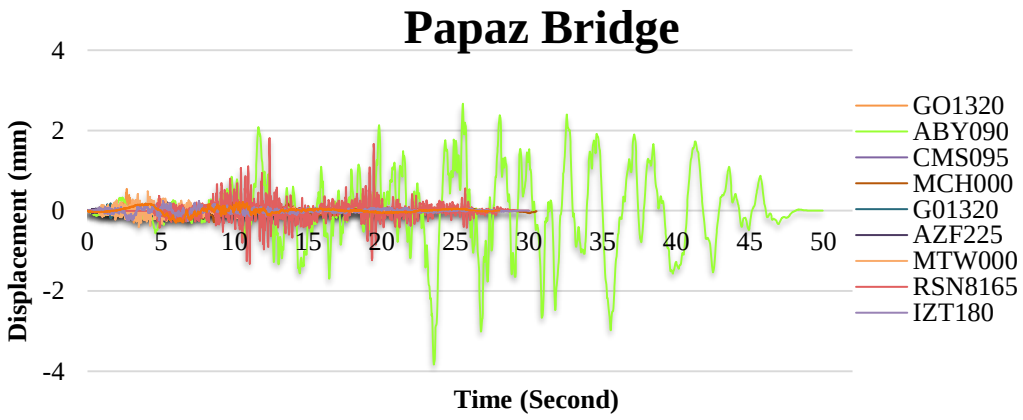

Figure 5.78 : Time-history of displacement of Papaz Bridge for nonlinear dynamic analyses of ten ground motion records.

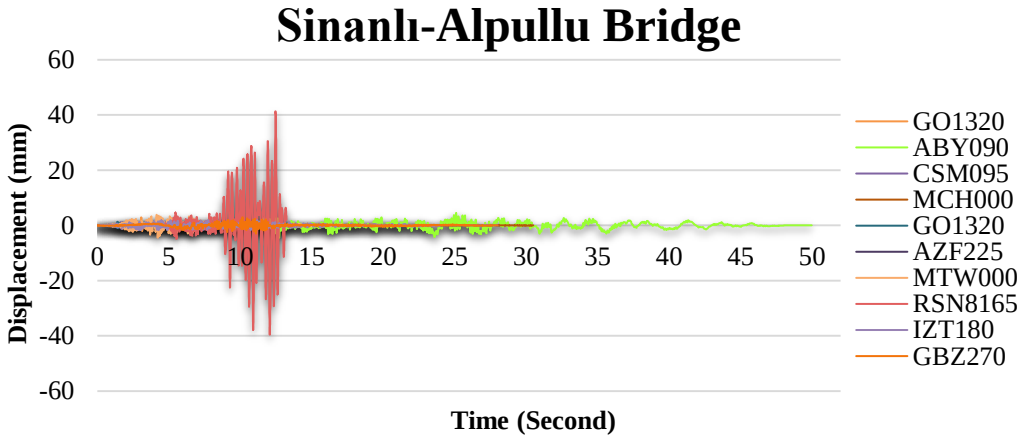

Figure 5.79 : Time-history of displacement of Sinanli-Alpullu Bridge for nonlinear dynamic analyses of ten ground motion records.

The nonlinear analysis of Sinanli-Alpullu Bridge along the transversal direction (Y) stops after 13.24 seconds in Duzce, Turkey accelerogram (Figure 5.79). Duzce, Turkey earthquake has significant increase of the acceleration from 4 seconds to 15 seconds as shown in accelerogram. The maximum displacement of 42mm occurred at 12.4 seconds. The maximum base shear and displacement values are given in figure 5.80 to 5.83 for selected bridges. Dicle and Malabadi Bridges have similar weights. Dicle Bridge is more rigid comparing to Malabadi Bridge. In figure 5.80, Dicle Bridge gave the maximum displacement of 48 mm with Duzce earthquake with 200000kN base shear, however; in figure 5.81, Malabadi Bridge gave the maximum displacement of 80mm with Duzce earthquake with 110000kN. The reason is that Dicle Bridge has smaller spans than Malabadi Bridge. Besides, Dicle Bridge has stiff piers.

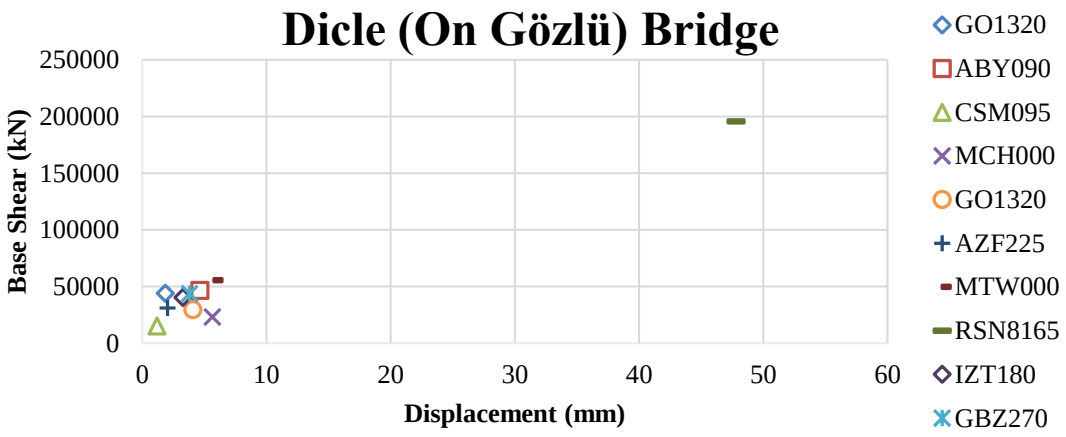

Figure 5.80 : Results of nonlinear dynamic analyses of Dicle (On Gozlu) Bridge under ten ground motion records.

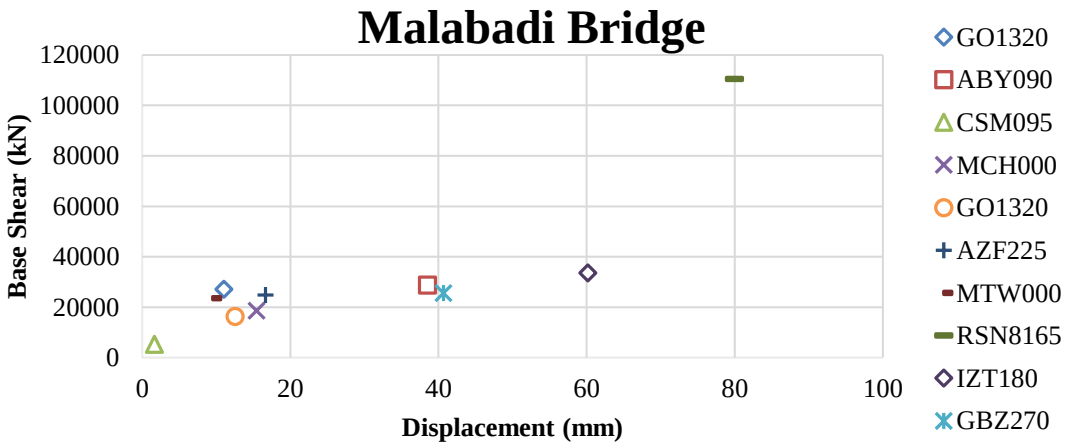

Figure 5.81 : Results of nonlinear dynamic analyses of Malabadi Bridge under ten ground motion records.

Behavior of the Papaz Bridge can be seen in figure 5.82. Papaz Bridge has the smallest span and length within selected bridges. Thus, obtained displacements versus base shear reached up to the maximum value of 3.8mm in Lander earthquake. Sinanli-Alpullu bridges showed its maximum displacement of 41.3mm in Duzce accelerogram as seen in Figure 5.83.

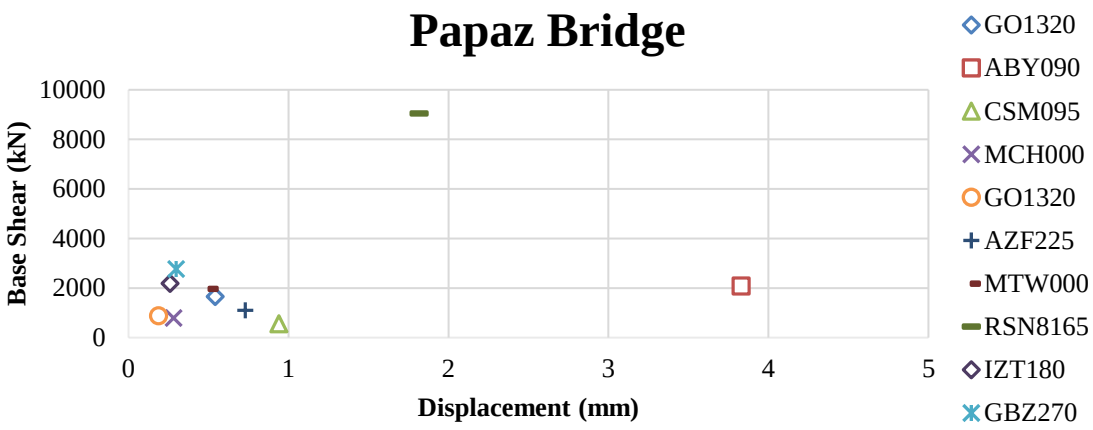

Figure 5.82 : Results of nonlinear dynamic analyses of Papaz Bridge under ten ground motion records.

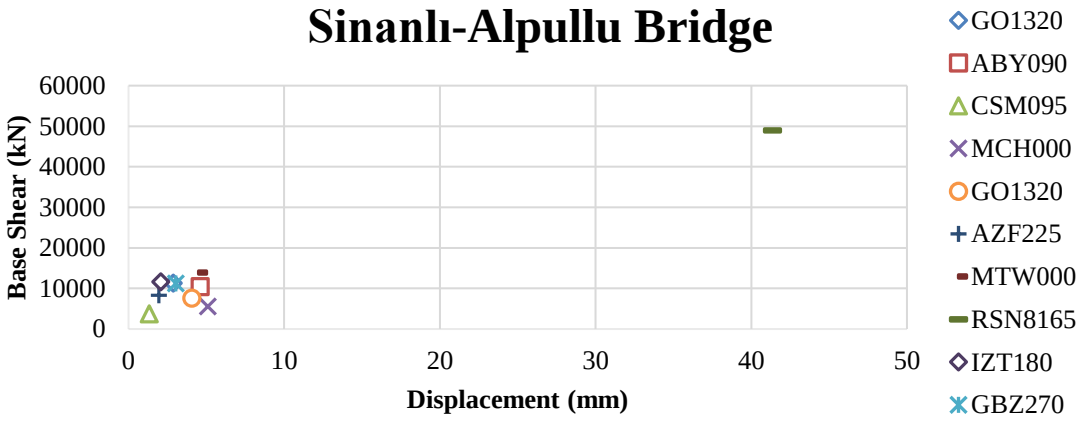

Figure 5.83 : Results of nonlinear dynamic analyses of Sinanlı-Alpullu Bridge under ten ground motion records.

Nonlinear dynamic analyses for selected ten ground motion records and nonlinear static (pushover) analysis results were compared for selected bridges between in figure 5.84 to figure 5.87.

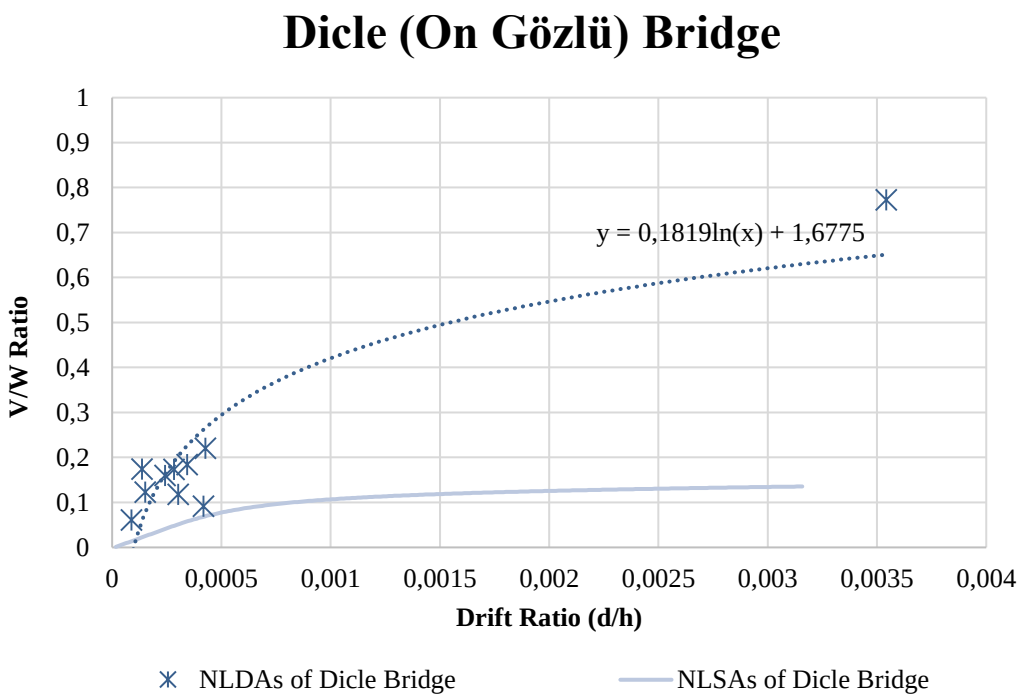

Figure 5.84 : Comparison of nonlinear static and dynamic analyses of Dicle (On Gozlu) Bridge.

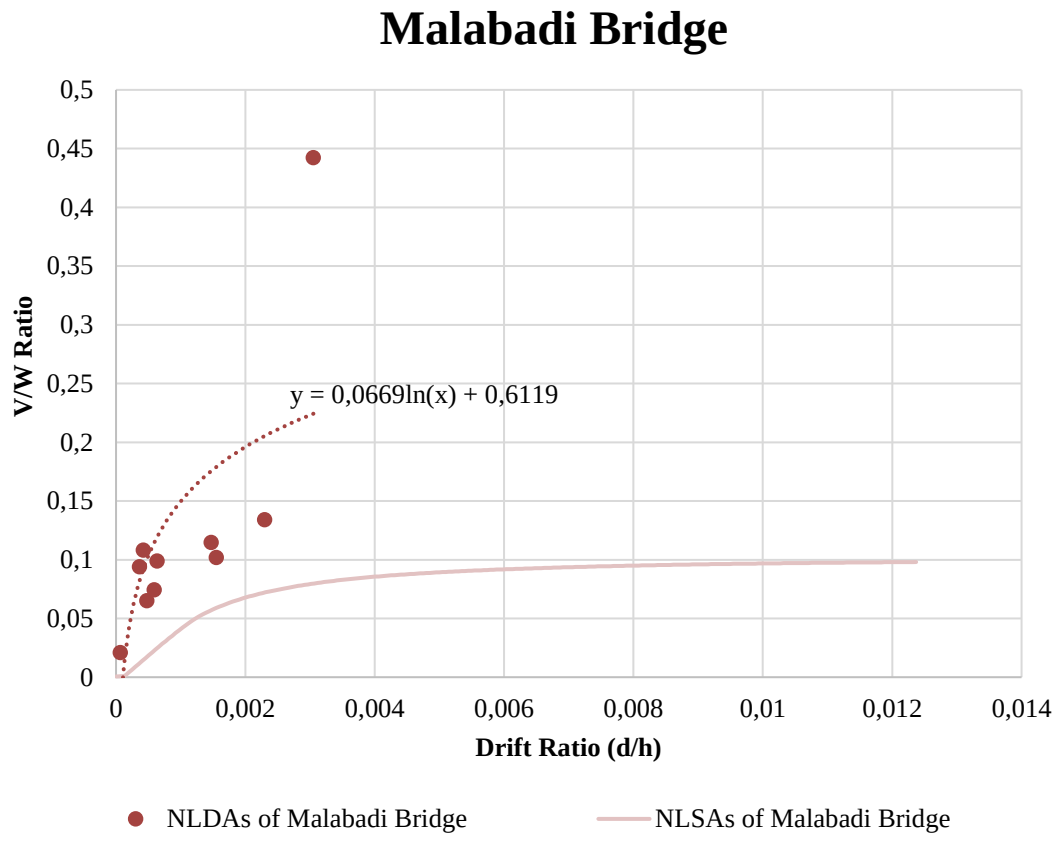

Figure 5.85 : Comparison of nonlinear static and dynamic analyses of Malabadi Bridge.

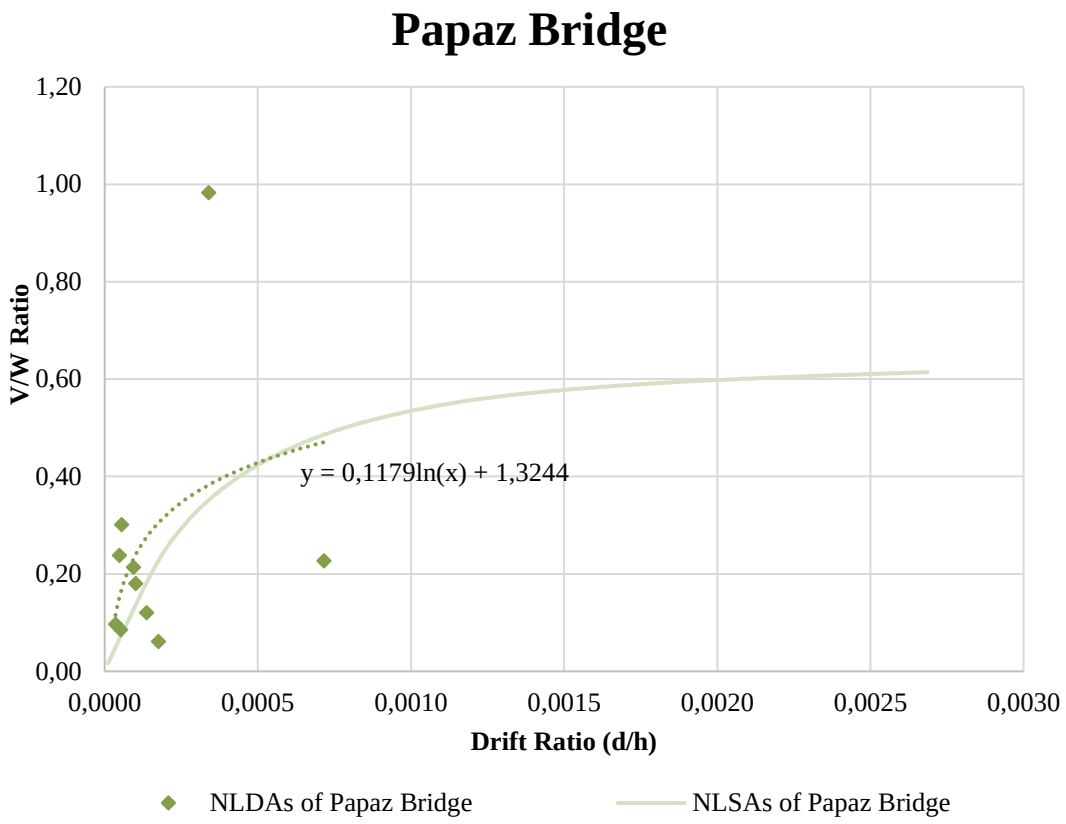

Figure 5.86 : Comparison of nonlinear static and dynamic analyses of Papaz Bridge.

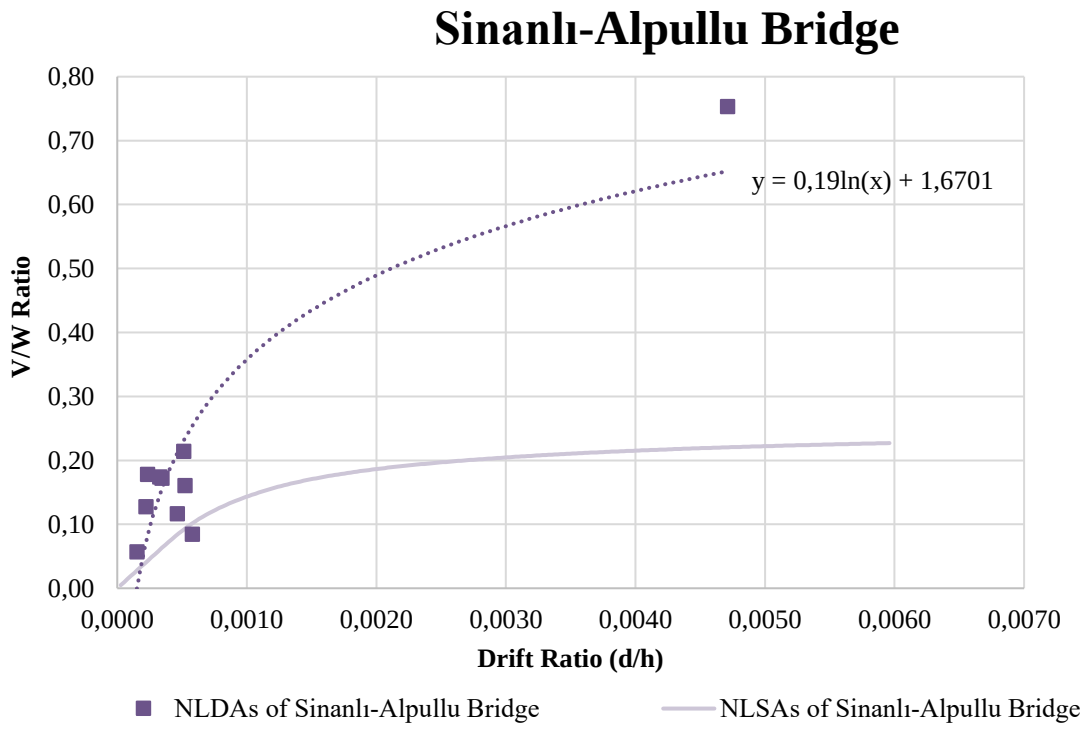

Figure 5.87 : Comparison of nonlinear static and dynamic analyses of Sinanli-Alpullu Bridge.

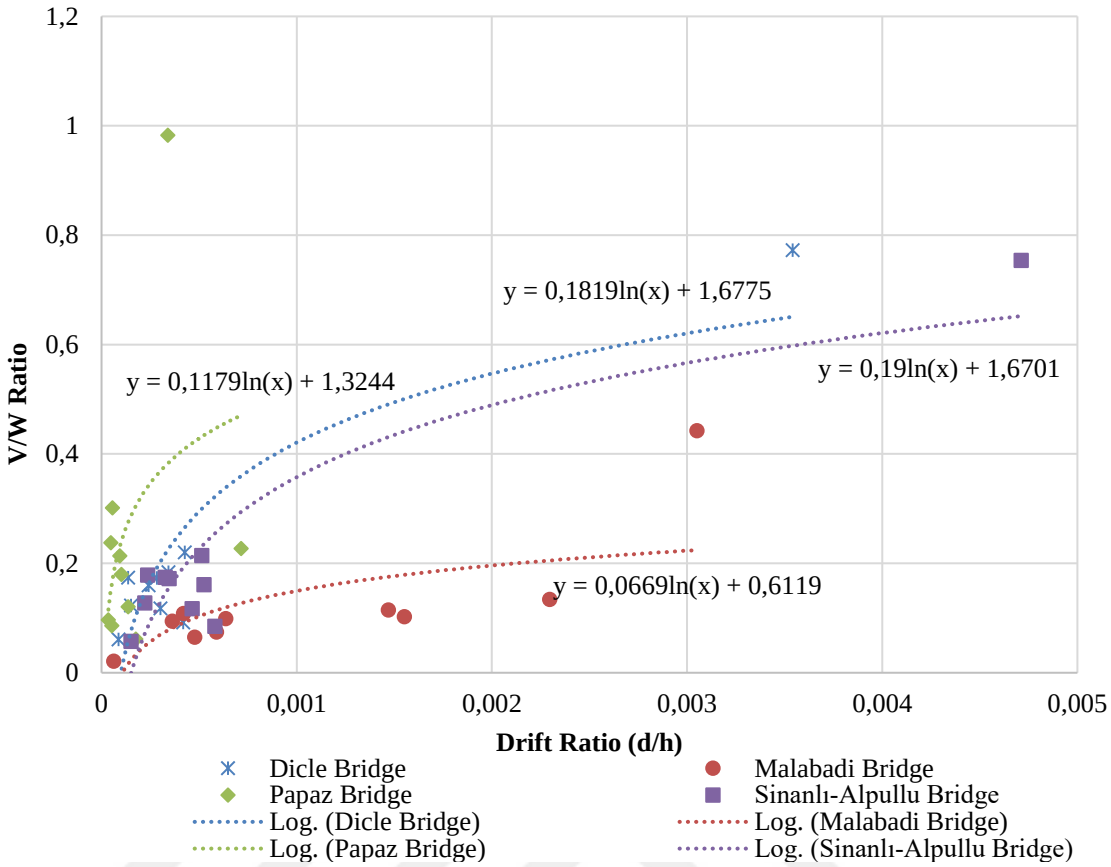

Figure 5.88 : Results of nonlinear dynamic analyses for selected bridges.

6. CONCLUSIONS

The research determines:

- the influence of the modelling which were created by using fine and coarse meshes. By increasing the mesh size and number of sub domain element for 3D models, the results of structural linear, modal and structural response spectrum analyses were compared for both models and discussed. Geometries of selected bridges were introduced in DIANA FX+ software.
- the significance of geometric properties on the load capacity of bridges. With same material and boundary conditions, selected bridges were analyzed under same assumptions. Geometry was selected as only variable. Geometric properties such as span, rise, and thickness of the arch were compared for selected bridges to understand the effect on the obtained results.
- the correspondence of the results obtained from nonlinear static and nonlinear dynamic analyses.

The major findings are:

- Obtained mode shapes of the selected bridges with 2 different modelling approaches were the same.
- Selected bridges gave the nearly same results for structural linear analysis under G+Q load case for fine and coarse meshes. The decrease of the element size mainly affected the time of analyses and computational effort.
- The difference between mode frequencies of selected bridges with fine and coarse meshes fluctuated between in 1% to 8%. The minimum difference was obtained for Malabadi Bridge and the maximum difference was obtained for Sinanlı-Alpullu Bridge.
- The difference of the stress distribution obtained from response spectrum analyses, which were carried out according to the Turkish seismic code in X and Y directions for selected bridges, was obtained no more than 5% for Dicle,

Malabadi and Papaz Bridges. However, the Sinanlı- Alpullu Bridge gave the 13% difference for vertical stress distribution (SZZ).

- The maximum displacements in X and Y directions under G+Q+Ex and G+Q+Ey load cases were obtained nearly the same for both fine and coarse meshes.
- According to the obtained pushover curves, Papaz Bridge needs more force than the other bridges to show same drift ratio with the other selected bridges. The reason of that the effect of geometry of the Papaz Bridge.
- The increase of the span, rise and thickness resulted in the increase of the drift ratio. These all parameters are related with each other in analytical design in past.
- Under the same V/W ratio, the cracking of the selected bridges and vaults with maximum and minimum span was maximum and minimum, respectively. Papaz Bridge gave the minimum cracking, and Malabadi Bridge gave the maximum cracking. Papaz Bridge has the smallest span in selected bridges and Malabadi Bridge has the maximum span. The span dimensions are directly related with the results obtained from nonlinear static analyses.
- The width of the bridges causes to increase or decrease the rigidity in transversal direction. This parameter has the influence on drift ratio of selected bridges. However, the effect of width is not meaningful when it is taken into account only. It should be associated with length and height of the bridge.
- In nonlinear dynamic analyses, as expected, within ten ground motion records, Duzce record which has maximum peak ground acceleration between selected ground motion records, gave the maximum drift ratio for selected bridges.
- Pushover curves and ground motion records did not match with each other. Only Papaz Bridge gave the approximately same curves for both nonlinear static and dynamic analysis. The main reason of that the mass participation of the first mode shape, which was used for the static analysis, is more than the other bridges. Obtained first mode shapes of selected bridges were localized around some parts of the bridges due to their length. But, Papaz Bridge has symmetric geometry and the distribution of the first mode shape also was

symmetric for whole bridges. To conduct nonlinear static analysis, mode than one mode shape should be taken account to obtain more accurate results for masonry.

The suggestions for further research:

- The Finite element model can be created by using interface elements between different structural elements of the bridge to obtain results that are more realistic.
- Mesh dimensions should be investigated by creating different models with different mesh sizes. Also, nonlinear material models and material properties should be obtained from laboratory and in situ tests to decide the most accurate models with appropriate nonlinear material model.
- The nonlinear dynamic analyses can be performed under more ground motion records for different soil classes.
- Material model should be changed, and nonlinear analyses should be discussed in detail with different models.
- Nonlinear static analysis should be performed by using more than one mode shape to take account into the higher mass participating ratio.

REFERENCES

Alfaiate, J. and Gallardo, A. (2001). Numerical simulations of a full scale load test on a stone masonry arch bridge. *Historical Constructions*, (739-748).

Aoki, T., Sabia, D., Rivella, D. and Komiyama, T. (2007). Structural Characterization of a Stone Arch Bridge by Experimental Tests and Numerical Model Updating. *International Journal of Architectural Heritage*, 1(3), pp.227-250.

Bayraktar, A., Altunışık, A., Birinci, F., Sevim, B. and Türker, T. (2010). Finite-Element Analysis and Vibration Testing of a Two-Span Masonry Arch Bridge. *J. Perform. Constr. Facil.*, 24(1), pp.46-52.

Bayraktar, A., Altunışık, A., Sevim, B. and Türker, T. (2009). Karaman Köprüsünün Sonlu Eleman Model İyileştirmesi. *IMO teknik dergi*, pp.4675-4700.

Bayraktar, A., Altunışık, A. C., Türker, T., ve Sevim, B. (2007). Tarihi Köprülerin Deprem Davranışına Sonlu Eleman Model İyileştirilmesinin Etkisi, *Sixth National Conference on Earthquake Engineering*, Istanbul, Turkey.

Behnamfar, F. and Afshari, M. (2013). Collapse Analysis and Strengthening of Stone Arch Bridges against Earthquake. *International Journal of Architectural Heritage*, 7(1), pp.1-25.

Bergamo, O., Campione, G., Donadello, S. and Russo, G. (2015). In-situ NDT testing procedure as an integral part of failure analysis of historical masonry arch bridges. *Engineering Failure Analysis*, 57, pp.31-55.

Bjurström, H. and Lasell, J. (2009). *Capacity assessment of a single span arch bridge with backfill-A case study of the Glomman Bridge*. Master's Thesis. Royal Institute of Technology (KTH).

Boothby, T., Yurianto, Y. and Ece Erdogmus, E. (2005). Experimental Replication of Masonry Arch Bridge Spandrel Wall Collapse. *TMS Journal*, 1(12), pp.37-46.

Cai, Y. (2011). *Detailed numerical stimulation of experiments on masonry arch bridges by using 3D FE*. Master's Thesis. Universida degli Studi di Padova, Universitat Politecnica de Catalunya.

Cappini, A., Stagnitto, G., Pederzani, A., Rossi, C. and Rossi, P. (2010). Structural analysis and strengthening intervention of the multi-span stone masonry bridge of Ribellasca, between Italy and Switzerland. In: *6th International Conference on Arch Bridges*.

Croci, G. (1998). *The conservation and structural restoration of architectural heritage*. Southampton, UK: Computational Mechanics Publications.

Costa, C.; Ribeiro, D.; Arêde, A. & Calçada, R.: Experimental and numerical assessment of the modal parameters of Côa railway bridge. *Proceedings of the 7th International Conference on Arch Bridges (ARCH'13)*. University of Zagreb, Trogir-Split, 2013.

Dellbecq, J. M. (1982). "Masonry bridges-stability evaluation", Structure s Dept., 46 Ave. Aristide Briand, 92223 Gagneux, SETRA, France, June.

DeJong, M. (2009). *Seismic Assessment Strategies for Masonry Structures*. Doctor of Philosophy in Architecture. Massachusetts Institute of Technology.

Diaz, J., Romera, L. and Hernandez, S. (2007). Non-linear finite element analysis and limit analysis comparison of the Caaveiro stone arch bridge. *Structural studies, repairs and maintenance of heritage architecture*, pp.555-566.

Dulinska, J. (2010). Evaluation of Dynamic Characteristics of Masonry Arch Bridges: Linking Full-Scale Experiment and FEM Modeling. AMR, 133-134, pp.605-610.

Fanning, P. and Boothby, T. (2001). Three-dimensional modelling and full-scale testing of stone arch bridges. *Computers & Structures*, 79(29-30), pp.2645-2662.

Fanning, P., Boothby, T. and Roberts, B. (2001). Longitudinal and transverse effects in masonry arch assessment. *Construction and Building Materials*, 15(1), pp.51-60.

FEMA 440, 2005. *Improvement of nonlinear static seismic analysis procedures.* Washington DC: Federal Emergency Management Agency.

Frunzio, G., Monaco, M. and Gesualdo, A. (2001). 3D F.E.M. analysis of a Roman arch bridge. *Historical Constructions*, pp.591-598.

Fuente J.V., Fernandez R., Albert V.(2010). Brick masonry elastic modulus determination using the numerical simulation and experiments of sonic wave propagation, *Simulation in NDT Workshop*, September, 2010.

Gencturk, B., Kilic, S., Erdik, M. and Pinho, R. (2007). Assessment of Stone Arch Bridges under Static Loading Using Analytical Techniques. New Horizons and Better Practices.

Harvey, B. (1986). Testing times for Arches. *New Scientists Arch Stand The Test of Time*, 1508.

Hatzigeorgiou, G., Teodorakopoulos, D., Beskos, D. and Sfakianakis, M. (1999). Static and Dynamic Analysis of the Arta Bridge by Finite Elements. *Architecture and Civil Engineering*, 2(1), pp.41-51.

Heyman, J. (1982). *The masonry arch. Chichester: E. Horwood*.

Heyman, J. (1995). *The stone skeleton. Cambridge*: Cambridge University Press.

Heyman, J. (1996). *Arches, vaults, and buttresses*. Aldershot, Hampshire, Great Britain: Variorum.

Historic Documentation Company, Inc., (2009). Historic Stone Highway Culverts in New Hampshire Asset Management Manual. Historic Stone Highway Culverts in New Hampshire Asset Management Manual. Portsmouth: *Historic Documentation Company*, pp.1-64.

Holmström, K. (2010). *On engineering methods for assessment of load capacity of stone arch bridges*. Master's thesis. Chalmers University of Technology.

International Council on Monuments and Charts (ICOMOS), (1964). *International Charter for The Conservation and Restoration of Monuments and Sites (The Venice Charter 1964)*. Venice: IInd International Congress of Architects and Technicians of Historic Monuments.

Invernizzi, S., Lacidogna, G., Manuello, A. and Carpinteri, A. (2010). AE Monitoring and Numerical Simulation of a Two-span Model Masonry Arch Bridge Subjected to Pier Scour. *Strain*, 47, pp.158-169.

Jun, S., Fumin, W. and Kang, S. (2015). Failure Modes Analysis of Stone Arch Bridges. *TOCIEJ*, 9(1), pp.442-449.

Karayolları Genel Müdürlüğü, Sanat Tarihi Şube Başkanlığı, Tarihi Köprüler, Ankara, Turkey.

Karaveziroglou, M., Stavrakakis, E., Lazarides, P., Liolios, A., Giannopoulou, M., Roukounis, Y. and Yeroyianni, M. (2001). A comparative analysis of some historical stone arch bridges in Greece by two new numerical approaches. *Historical Constructions*, pp.749-756.

Kindij, A., Ivanković, A. and Vasilj, M. (2014). Adjustment of small-span masonry arch bridges to present-day demands. *Journal of the Croatian Association of Civil Engineers*, 66, pp.37-49.

Kishi, Y., Nozaka, K. and Izuno, K. (2016). Dynamic behavior of multi-span masonry arch bridge using different stiffness in tension and compression. In: *8th International Conference on Structural Dynamics. Leuven*, pp.1267-1272.

Kiyono, J., Furukawa, A. and Toki, K. (2008). Seismic Assessment of Stone Arched Bridges. In: *World Conference on Earthquake Engineering*. Lisboa.

Korkmaz, K., Zabin, P., Çarhoğlu, A. And Nuhoğlu, A. (2013). Seismic Behavior Investigation of Arc Stone Bridges: Timisvat Bridge Case. *Journal of Advanced Technology Sciences*, 2(1), pp.66-75.

Köseoğlu, G. (2011). Investigation of A Damaged Historical Mosque With Finite Element Analysis. Master's thesis. Middle East Technical University.

León,, J. and Espejo,, S. (2007). Load test to collapse on the masonry arch bridge at Urnieta Javier. In: *5th International Conference on Arch Bridges*. pp.969-977.

Lolias, Y. (2016). *Structural Behaviour of Segmental Arch Structures.* Undergraduate Thesis. Charles Darwin University.

Lourenco, P. (1994). *Analysis of Masonry Structures with Interface Elements Theory and Applications*. Ph. D. Delft University of Technology.

Lourenço, P., Hunegn, T., Medeiros, P. and Peixinho, N. (2010). Testing and analysis of masonry arches subjected to iMPact loads. In: *6th International Conference on Arch Bridges*. pp.603-610.

Lubowiecka, I., Arias, P., Riveiro, B. and Solla, M. (2011). Multidisciplinary approach to the assessment of historic structures based on the case of a masonry bridge in Galicia (Spain). *Computers & Structures*, 89(17-18), pp.1615-1627.

Mabon, L. (2002). Assessment, strengthening and preservation of masonry structures for continued use in today's infrastructure. In: *International Association for Bridge and Structural Engineering Conference*.

Manie, J. (2009). DIANA – Finite Element Analysis User's Manual rel. 9.3, TNO DIANA BV Schoemakerstraat 97, 2628 VK Delft, The Netherlands.

Nagarajan, T., Viswanathan, S., Ravi, S., Srinivas, V. and Narayanan, P. (2014). Experimental Approach to Investigate the Behaviour of Brick Masonry for Different Mortar Ratios. In: *International Conference on Advances in Engineering and Technology*. Singapore, pp.586-592.

NG, K. (1999). *Analysis of masonry arch bridges*. PhD. Napier University.

Nobile, L. and Bartolomeo, V. (2014). Methods for the Assessment of Historical Masonry Arches. In: *Proceedings of the 5th European Conference of Civil Engineering.* pp.160-167.

Pela , L., Aprile, A. and Benedetti, A. (2009). Seismic assessment of masonry arch bridges. Engineering Structures, 31(8), pp.1777-1788.

Pina-Henriques, J., Lourenço, P. and Krakowiak, K. (2005). Modelling of Masonry Creep and Damage J. In: International Conference on Fracture. Italy.

Rafiee, A., Vinches, M. and Bohatier, C. (2008). Application of the NSCD method to analyze the dynamic behaviour of stone arched structures. *International Journal of Solids and Structures*, 45(25-26), pp.6269-6283.

Raj, S., Srinivas, V. and Sakaria, P. (2014). Failure Behaviour of Masonry Arch Bridges using Finite Element Analysis. *International Journal of Emerging Technology and Advanced Engineering*, 4(11), pp.125-130.

Sayın, E., Karaton, M., Yön, B. and Calayır, Y. (2011). Tarihi Uzunok Köprüsünün Yapı Zemin Etkileşimi Dikkate Alınarak Doğrusal Olmayan Dinamik Analizi. In: 1. *Türkiye Deprem Mühendisliği ve Sismoloji Konferansı*. Ankara, pp.1-8.

Scheibmeir, E. (2012). *Nonlinear Seismic Analysis of a Masonry Arch Bridge*. Master's Thesis. Universitat Politecnica de Catalunya.

Sevim, B., Bayraktar, A., Altunışık, A., Atamtürktür, S. and Birinci, F. (2010). Assessment of nonlinear seismic performance of a restored historical arch bridge using ambient vibrations. *Nonlinear Dynamics*, 63(4), pp.755-770.

Srinivas, V., Sasmal, S., Ramanjaneyulu, K. and Ravisankar, K. (2014). Performance Evaluation of a Stone Masonry Arch Railway Bridge under Increased Axle Loads. *J. Perform. Constr. Facil.*, 28(2), pp.363-375.

Stablon, T., Sellier, A., Domede, N., Plu, B. and Dieleman, L. (2011). A numerical tool for masonry arch bridges assessment Thomas. In: *9th World Congress on Railway Research*.

The Specification for Buildings to be Built in Seismic Zones (Turkish Seismic Code,2007), Amended on: 3.5.2007, Official Gazette No.26511, Ministry of Public Works and Settlement Government of Republic of Turkey

TNO DIANA BV (2014). *DIANA Finite Element Analysis User Manuals*. Delph: Nederlandse Organisatie voor toegepast-natuurwetenschappelijk onderzoek.

Tecchio, G., Porto, F., Zampieri, P., Modena, C. and Bettio, C. (2012). Static and seismic retrofit of masonry arch bridges: case studies. *Bridge Maintenance, Safety, Management, Resilience and Sustainability*, pp.1094-1098.

Toker, S. and Ünay, A. (2004). Mathematical Modeling and Finite Element Analysis Of Masonry Arch Bridges. *Gazi University Journal of Science*, 17(2), pp.129-139.

Ural, A. (2005). Tarihi Kemer Köprülerin Sonlu Elemanlar Methoduyla Analizi. In: *Deprem Sempozyumu*, pp.408-413.

Ural, A., Oruç, Ş., Doğangün, A. and Tuluk, Ö. (2008). Turkish historical arch bridges and their deteriorations and failures. *Engineering Failure Analysis*, 15(1-2), pp.43-53.

Xul, Z., Lu, X., Guan, H., Lu, X. and Ren, A. (2013). Progressive-Collapse Simulation and Critical Region Identification of a Stone Arch Bridge. *J. Perform. Constr. Facil*., 27(1), pp.43-52.

Yan, Y. (1991). *Progressive failure analysis of masonry arch bridges*. PhD. The University of Wollongong.

Url-1 :https://yandex.com.tr/kullan/panorama-live?short_url=CVTm7IJu , Accessed: 09- Apr- 2016.

Url-2. **:**https://yandex.com.tr/kullan/panorama-live?short_url=CVT5NS4s, Accessed: 10-Apr-2016

Url-3. **:**http://peer.berkeley.edu/ , Accessed: 15-Apr-2016.

CURRICULUM VITAE

Name Surname : **Ayşegül DEMİR**

Place and Date of Birth : **Erzurum, 23/09/1990**

E-Mail : **demirayse@itu.edu.tr**

EDUCATION :

- **B.Sc.** : 2013, Dokuz Eylül University, Engineering Faculty, Civil Engineering
- **B.Sc.** : 2013, Dokuz Eylül University, Engineering Faculty, Environmental Engineering

PROFESSIONAL EXPERIENCE AND REWARDS:

- -

PUBLICATIONS, PRESENTATIONS AND PATENTS ON THE THESIS:

- -